UNIVERSIDAD DE CHILE
Facultad de Ciencias Físicas y Matemáticas
Departamento de Ingeniería Civil

SPATIOTEMPORAL FEATURES OF NATURAL CONVECTION

TESIS PARA OPTAR EL GRADO DE DOCTOR EN
CIENCIAS DE LA INGENIERÍA MENCIÓN FLUIDODINÁMICA

CHRISTIAN FELIPE IHLE BASCUÑÁN

PROFESOR GUÍA:
Yarko Niño Campos

MIEMBROS DE LA COMISIÓN:
Stuart Bruce Dalziel
Aldo Tamburrino Tavantzis
Peter Anthony Davies
Álvaro Valencia Musalem

Santiago de Chile
Enero 2011

RESUMEN DE TESIS
PARA OPTAR AL GRADO DE DOCTOR EN CIENCIAS DE LA INGENIERÍA MENCIÓN FLUIDODINÁMICA
POR: CHRISTIAN IHLE BASCUÑÁN
FECHA: 7 DE ENERO DE 2011
PROF. GUIA: YARKO NIÑO

Esta tesis, consistente en una recopilación de artículos de investigación originales autocontenidos, se ocupa del estudio de los mecanismos físicos que explican algunas características de la dinámica de convección térmica con aplicación a convección penetrativa, frecuentemente observada en lagos y reservorios chilenos. Este fenómeno consiste en la aparición de un campo de flujo derivado del enfriamiento superficial de una masa de de fluido donde potencialmente puede existir una estratificación de densidad previa. Si bien este problema ha sido extensivamente estudiado empleando experimentos de pequeña escala (desde 1 mm hasta unos pocos centímetros), no es el caso para sistemas naturales de mayor tamaño, donde los flujos son comúnmente turbulentos y la dinámica asociada está además acoplada con perturbaciones espaciotemporales, incluyendo temperatura ambiente y vientos locales. El presente trabajo se ocupa de algunas de estas interrogantes, incluyendo las condiciones requeridas para la aparición de convección penetrativa bajo condiciones de borde térmicas que dependen del tiempo y suponiendo ausencia de viento. Primero, se consideró el caso más simple de un enfriamiento superficial repentino, modelado como una capa horizontal infinita, inicialmente en reposo, de fluido de Boussinesq. La siguiente fase de este estudio consistió en la elaboración de un modelo teórico simplificado, propuesto como una base para dar cuenta de la estabilidad de sistemas de pequeña escala frente a patrones de forzamiento térmico sinusoidales, buscando así un símil al efecto de enfriamiento vespertino o nocturno en lagos en los casos donde además hay turbulencia media nula antes del comienzo del flujo convectivo. Un segundo aspecto de este trabajo de tesis fue el estudio del efecto de la presencia de fuentes y sumideros térmicos cercanos. Para condiciones débiles de calentamiento y enfriamiento, se ha encontrado que el estudio de esta configuración es equivalente al estudio de la interacción entre plumas térmicas y corrientes de densidad en régimen laminar.

Se ha perseguido los objetivos mencionados empleando una combinación de métodos, incluyendo simulaciones numéricas, técnicas analíticas de perturbación para el estudio de la estabilidad de los sistemas referidos modelados a través de las ecuaciones de Navier-Stokes y energía, además de la realización de experimentos. En este último caso, se propone una técnica de medición simultánea de los campos vectoriales de velocidad (usando PIV) y gradiente de densidad (usando schlieren sintético). La naturaleza inherentemente delicada de los experimentos llevados a cabo hizo necesario el desarrollo de sistemas de control ad-hoc. Como resultado de estas actividades, ha sido posible vincular las propiedades del fluido con parámetros adimensionales (incluyendo los números de Prandtl y Rayleigh), para dar cuenta de los tiempos de inicio de convección y frecuencia de forzamiento térmico en la superficie (entre otros). Del estudio de inhomogeneidades espaciotemporales, se encontró que las plumas térmicas bidimensionales laminares pueden sobrevivir el impacto con una corriente de gravedad modificando, sin embargo, su posición original.

Abstract

This thesis, consisting of a series of self-contained research articles, is devoted to the study of physical mechanisms allowing to explain some characteristics of the dynamics of thermal convection with application to penetrative convection, frequently observed in Chilean lakes and reservoirs. This phenomenon consists of the appearance of a flow field derived from the surface cooling of a fluid enclosure in systems where an existing background density stratification is possibly present. Although it has been extensively studied using small-scale experiments (from 1 mm to few centimetres), it is not the case for large, natural systems, where flows are commonly fully turbulent and associated phenomena is often coupled with spatiotemporal disturbances, including ambient temperature, and local winds. The present work deals with some related questions, including the conditions required for the appearance of penetrative convection under time-dependent thermal boundary conditions. First, it was considered the simpler case of a sudden decrease of surface temperature, modelled as a infinite horizontal Boussinesq fluid layer with no initial velocity vector field. The next phase of this study consisted of the construction of a simplified theoretical model, proposed as a base to account for the stability of small-scale lakes and reservoirs in front of a sinusoidally-varying forcing thermal pattern, thus mimicking the effect of evening or overnight cooling in fluid systems where zero-mean-flow turbulence exist, as is the case of many lakes. A second aspect of this thesis work was the study of the effect of the presence of nearby thermal heat and sources. For weak heating and cooling, this was found to be equivalent to study the interaction of laminar thermal plumes and gravity currents.

The aforementioned objectives have been pursued using a combination of techniques, including direct numerical simulations, analytic perturbation techniques for the study of the stability of the referred systems using Navier-Stokes and energy equations, and experiments. In the latter case, a new observation technique, based on colour separation concepts, was proposed to simultaneously measure velocity (using PIV) and density gradient (using synthetic schlieren) vector fields. The inherently delicate nature of experiments made it necessary to develop ad-hoc control systems. As an outcome of the referred activities, it was possible to link flow properties with nondimensional parameters (including Prandtl and Rayleigh numbers) accounting for convection onset times and thermal forcing frequency (among others). From the study of spatial thermal inhomogeneities, it was found that two-dimensional, laminar thermal plumes can withstand an impelling gravity current, though displaced from their original position.

We are like sailors who on the open sea must reconstruct their ship but are never able to start afresh from the bottom.

Otto Neurath (1882-1945)

Acknowledgements

I would like to thank my supervisor, Prof. Yarko Niño, whose guidance, support and constant encouragement was crucial for the successful completion of my studies and thesis work. Thanks to my co-supervisor, Dr. Stuart Dalziel, for his tutelage and guidance, and for showing me how interesting and fun experiments in fluids can be. I would like to extend my acknowledgements to GK Batchelor Laboratory personnel, particularly David Page-Croft and John Milton for their valuable cooperation during experiment preparation. Thanks to Prof. Aldo Tamburrino for his patience and support during the final stage of my thesis work.

I gratefully acknowledge the different institutions that provided the funding to my work: Universidad de Chile (Faculty Scholarship), CONICYT (Doctoral Scholarship), MECESUP (MECE program for Higher Education), FONDECYT (Projs. 1040494 and 1080617) and GK Batchelor Laboratory, Department of Applied Mathematics and Theoretical Physics, University of Cambridge.

Quisiera agradecer a mis colegas y amigos Santiago Montserrat, Cristián Godoy, Carlos Reiher, Sergio Quijada, Wernher Brevis, Nastja Bethke, Andrew Lawrie, Abigail Nye, Andrea Maffioli y Jeroen Hazewinkel, quienes hicieron tan grato como estimulante mi paso por el programa. Gracias a mis amigos Claudio Albornoz, Jorge Rosales y Robert Fromm (q.e.p.d.) por su apoyo permanente e incondicional. Gracias a mis padres y hermanos por su cariño y compañía.

Quedo en deuda para siempre con mi esposa Daniela, mi fuente de inspiración, sin cuya infinita paciencia, energía y amor no habría llegado hasta aquí.

Contents

List of Figures

List of Tables

Chapter 1

Introduction

When an initially quiescent horizontal Boussinesq fluid layer is heated from below (or cooled from above), a vertical density gradient is induced. After heating at the bottom a 1 mm-depth cell with wax in it, the French physicist Henri Bénard (Bénard, 1900; Drazin & Reid, 1981) discovered that under certain heating conditions, hexagonal flow patterns formed. He interpreted these patterns as convective flow strctures, named Bénard convection after him. Minimal conditions for the formation of such a flow structure were analysed in the seminal paper of Rayleigh (1916, with over 586 cites in the scientific literature), who, as a first approximation assumed first-order disturbances in an infinitely wide fluid enclosure to neglect boundary effects. In his work, he found a formal relation between the exponential growth of disturbances and a balance between buoyancy driven by the density contrast induced by heating and the effects of thermal diffusion (or the concentration of a passive scalar) and viscosity, which are inherent properties of the fluid. Flow structures similar to those corresponding to Bénard experiments can be found over and over again in a countless number of situations in nature, as well as in industry. They are often the prelude of complex momentum and mass exchange processes. In the industry, an area of active research is flow control in nuclear reactors (Liaqat & Baytas, 2001), crystallization processes (Worster, 2001), the conception of heat exchangers in hydrocarbon processing (Gebhart *et al.*, 1988) and the design of buildings optimised for low energy consumption due to heating systems (Linden, 1999). In nature, large scale convective structures are ubiquitous in the planetary boundary layer (Stull, 1988), the ocean (Marshall & Schott, 1999; Maxworthy, 1997), lakes and reservoirs (Imberger & Patterson, 1990; Jonas *et al.*, 2003; Wüest & Lorke, 2003), magma and liquid metal flows occurring near the earth inner core (Griffiths, 2000), the sun and several planets in the solar system (Majumder & Yuen, 2004; Veronis, 1963).

The need to elucidate the impact of different initial and boundary conditions on the sta-

bility of systems where Bénard convection can occur has motivated numerous research investigations, including the effect of different initial thermal stratifications (Chandrasekhar, 1961; Jeffreys, 1928; Low, 1929; Pellew & Southwell, 1940; Rayleigh, 1916; Reid & Harris, 1958; Sparrow *et al.*, 1964; Sutton, 1950) and the result of disturbances during transient heating conditions (Currie, 1967; Foster, 1965*a*, 1968; Goldstein, 1959; Homsy, 1973; Kim *et al.*, 1999, 2008, 2002; Lick, 1965; Morton, 1957; Neitzel, 1982; Yang & Choi, 2002*a*). Aspects of non-linear dynamics of this type of flow, both from the point of view of transition to turbulence (Busse, 1978), as well as in the case of fully developed turbulence have been revised in greater detail during the last two decades (Chavanne *et al.*, 2001; Siggia, 1994), partly because of advances in computer hardware (Moin & Mahesh, 1998; Pope, 2000). In turbulent flow in closed containers, main elements driving convective flows are plumes, the thermal boundary layer adjacent to where heating or cooling is applied, and the central region Grossmann & Lohse (2000); Kadanoff (2001). Plume is defined as a non-linear convective flow driven by an instability driven on the thermal boundary layer (Turner, 1969). In particular, flows induced by this mechanism have a remarkable impact on mixing processes in density-stratified fluids present in natural systems. Even biological variables such as oxygenation and eutrophication strongly depend on them (Fernando, 1991; Imberger & Patterson, 1990; Martin *et al.*, 1999; Svendsen, 1997).

Nature offers many non-ideal situations where convective flows occur mixed with several other effects, including spatiotemporal variations in heat flux. Examples are unusually distributed atmospheric convective patterns due to vegetation, introducing local variations in sensible heat and moisture (Grossman *et al.*, 2004). In polar areas, the re-freezing of narrow channels, also know as leads, induce the formation of plume-like elongated structures. Their existence have a significative effect on the energy balance along with the biological activity in the ocean(Morison *et al.*, 1992). This kind of flow structure, often modelled as two-dimensional plumes, are close enough to interact among each other (Ching *et al.*, 1996). A different consequence of a spatial heterogeneity in heat flux is the interaction between plumes and thermally-induced gravity currents. The latter can appear when exists a locally cooler zone at the bottom of an enclosure. Their properties depend of fluid properties, the slope of the surface where they grow, and existing the density contrast (Benjamin, 1968; Simpson, 1997; Turner, 1973), and they behaviour can be significantly affected in the presence of a density-stratified background (Ungarish & Huppert, 2002).

The objective of this thesis work is to study some spatiotemporal features in thermal convection. The present document is the compilation of a series of related research papers. First of them deals with the link between time and the onset of convection. When the surface temperature of a large reservoir drops below its initial (steady) level, an enhanced mixing appears at specified times (Imberger & Patterson, 1990; Jonas *et al.*, 2003). In this

work a model based on linear stability analysis for convection onset times is proposed, both for the case of a sudden cooling (chapter 2), and the more realistic condition of sinusoidal cooling (chapter 3). Also, in chapter 4, using linear and non-linear stability analysis, critical conditions for the existence of convective patterns when no heat exchange whatsoever exists between the layer of fluid and its bottom were explored. Some numerical simulations are given on the appendix A.1, while the effect of an initial background stratification is referred to in the conference paper enclosed in appendix A.2. On the other hand, with the purpose of studying the generation of laminar plumes and their interaction with thermally-induced gravity currents, a new experimental methodology was developed to simultaneously observe velocity and temperature fields (chapter 5).

Chapter 2

The onset of nonpenetrative convection in a suddenly cooled layer of fluid

This chapter is published as research paper, authored by Christian Ihle and Yarko Niño, in *International Journal of Heat and Mass Transfer*, volume 49 (2006), pp. 1442–1451.

Abstract

Conditions for the onset of nonpenetrative convection in a horizontal Boussinesq fluid layer subject to a step change in temperature are studied using propagation theory. A wide range of Prandtl numbers and two different kinematic boundary conditions are considered. It is shown that for high Rayleigh numbers, critical conditions for the onset of convective motion reproduce exactly those for the unsteady Rayleigh-Bénard instability. Present results extend those of previous research and show a tendency of the rigid-rigid and free-rigid critical curves to converge for low Prandtl numbers. Comparison between present and previously reported results on critical conditions for the onset of instabilities and onset time using different methods yields good agreement on a middle to high Prandtl number range. A ratio of 10 between experimentally measured and theoretically predicted onset times is suggested for stress-free bounded systems.

Keywords: Buoyancy-driven instability, critical time, nonpenetrative convection, Prandtl number, propagation theory, Rayleigh number, isothermal heating.

Nomenclature

a_s, b_s	coefficients of Eqs. (2.10) and (2.11), respectively, $s = 1, \ldots, 5$ (integer), or ∞
(a_x, a_y)	dimensionless horizontal wavevector
a	dimensionless horizontal wavenumber, $\sqrt{a_x^2 + a_y^2}$
C	concentration [kmol/m^3] or designation of constant value
C_p	specific heat of the fluid at constant pressure [J kg^{-1} K^{-1}]
D	mass diffusion coefficient [m^2/s]
$\mathrm{D}(\cdot)$	ordinary derivative with respect to ζ, $\mathrm{d}(\cdot)/\mathrm{d}\zeta$
$\partial_{\chi(\psi)}(\cdot)$	partial derivative, $\partial(\cdot)/\partial\chi$ or $\partial^2(\cdot)/\partial\chi\psi$
DP	deep pool acronym
$\mathbf{g}$	gravity vector (pointing in the direction of z axis) [m s^{-2}]
k	thermal conductivity of the fluid [W m^{-1}K^{-1}]
L	depth of the fluid layer [m]
Pr	Prandtl number, $\nu\alpha^{-1}$
r	slope of the geometrical sequence to extrapolate critical Ra_τ values
t	time (dimensionless if no superscript)
$\mathbf{u}$	velocity, (u, v, w) (dimensional or not depending on the superscript. w is ζ-dependent if no superscript is present)
Ra	Rayleigh number, $g\beta(\theta^*_{\max} - \theta^*_{\min})L^3\nu^{-1}\alpha^{-1}$
Ra_τ	τ-dependent Rayleigh number, $\tau^{3/2}\mathrm{Ra}$
TBL	thermal boundary layer acronym
(x, y, z)	Cartesian coordinates (dimensionless if no superscript is present)

Greek letters

α	thermal diffusivity of the fluid [m^2 s^{-1}]
β	thermal expansion coefficient [K^{-1}]
λ	relative difference coefficient, $\max_\zeta\{100 \times \lvert 1 - \theta_0/\theta_{0_{\mathrm{DP}}}\rvert\}$
δ_θ	dimensionless thermal penetration depth
Δ	laplacian operator (dimensional or not depending on the superscript)
Δ_1	horizontal laplacian operator (dimensional or not depending on the superscript)
γ	concentration coefficient of expansion [kg/kmol]
ζ	self-similar vertical coordinate, $z/\sqrt{t}$
θ	temperature (self-similar if no superscript, otherwise dimensional or dimensionless)
ν	kinematic viscosity of the fluid [m^2 s^{-1}]

σ	temporal growth rate for disturbances
τ	definition for time in the self-similar framework, $\tau = t$

Subscripts

0	base state
1	disturbance, or correlative assignment to constant
2–5	correlative assignment to constant
b	bulk
c	critical state
DP	deep pool assumption: ζ-only dependence
linear	linear boundary forcing
∞	infinite Prandtl number
m	experimental detection
min	minimal condition
max	maximal condition
u	thermal advection dominance over pure diffusivity
step	step boundary forcing
τ	τ-dependent variable: $\Gamma_\tau \equiv \tau^\phi \Gamma$

Superscripts

$*$	dimensional length, temperature, time, velocity or differential operator
$\sim$	dimensionless temperature, velocity or differential operator
–	root-mean-square

2.1 Introduction

Nonpenetrative convection is defined by Adrian (1986) as the unstable flow field that derives from the existence of a fluid layer heated from below (or cooled from above) with adiabatic top (or bottom if cooled from above), resembling Bénard convection (Rayleigh, 1916). This thermal boundary condition precludes the existence of a steady flow regime. Nonpenetrative convection represents a reasonable assumption in a variety of physical problems, that range from ventilation and air conditioning (like, for instance, cold storage rooms and warehouses with poor insulation from one side) to earth sciences, particularly regarding the dynamics of the planetary boundary layer (Stull, 1988). In this paper,

the attention is focused on the study of conditions for the onset of impulsively generated nonpenetrative convection. Here, the base state of the system to be perturbed, at difference from the one that gives rise to Bénard convection (Drazin & Reid, 1981), is unsteady due to the existence of a thermally diffusive state whose temporal rate of change is high at the very beginning of the evolution. Hence, a stability model able to deal with this difficulty is to be considered.

After early approaches to the analysis of the stability of unsteady systems (e.g. 'frozen time' and 'quasi-static' models, reviewed by Gresho & Sani (1971) and Homsy (1973), respectively), the study of the onset of manifest convection in high Rayleigh number fluid layers impulsively heated or cooled began with Foster (1965*b*), who used an initial value technique, so-called 'amplification model', which considers a transient evolution of the base state. In this case, disturbances that cause the onset of convection are assumed to occur only initially. The major drawback of this method is that determination of amplification requires the knowledge of amplitudes of initial disturbances, for all the wavelengths present on the eigenfunction expansion. As this is impossible, Foster's approach consisted of a heuristic procedure that combined the assumption of several disturbance patterns along with experimental observations (Foster, 1969). Using a different approach, Jhaveri & Homsy (1982) and Kim & Kim (1986) used random forcing functions to solve an initial value problem to find the onset times, both for step and ramp-heated systems of high Rayleigh numbers, suggesting a definition of the onset time as that corresponding to a certain excess of the computed Nusselt number with respect to the purely conductive one.

More recently, Kim *et al.* (1999) studied the impulsively driven Rayleigh-Bénard problem with initial stratification, using the method called by these authors 'propagation theory' (Choi *et al.*, 1988; Kang & Choi, 1997; Kim *et al.*, 1996). Its basis lies on the assumption that most of the disturbances are confined within the thermal penetration depth, which is considered as a length scale, leading to the transformation of the linearized equations into self-similar forms. In more recent contributions, Chung *et al.* (2004) and Choi *et al.* (2004*d*) suggest new definitions for onset times, taking into account nonlinear effects that come from the numerical simulation of the unsteady Rayleigh-Bénard problem and compare them with results obtained using propagation theory. In the latter work, the influence of initial stratification on the distribution of the mentioned time scales is analyzed.

In an experimental context, Spangenberg & Rowland (1961) studied the onset of evaporative convection using Schlieren photography techniques, while Foster (1965*a*), by means of radiometry, showed that surface temperature in suddenly cooled evaporative systems evolves in a linear fashion. Plevan & Quinn (1966), Blair & Quinn (1969) and later Tan & Thorpe (1992), measured onset times in non-evaporative systems whose stability depends on the concentration of gases into water. Their results, in the context of the present re-

search, are commented in Section 2.4. Goldstein & Volino (1995), studied the onset of convection on a thick fluid layer heated impulsively from below. Their work presents also an extensive review of literature focused on the transient features of natural convection.

In this paper, propagation theory was the chosen stability method to assess the onset of nonpenetrative convective motion. For high thermal perturbations, it is shown that this phenomenon behaves the same as the onset of unsteady Rayleigh-Bénard convection. This result allows for a side by side comparison of present computations with numerical and experimental results reported in the context of the latter problem. Some new findings in that regard are presented and discussed as well.

2.2 Problem description

An initially quiescent horizontal fluid layer, well mixed at temperature $\theta^* = \theta^*_{\max}$, infinite on its horizontal dimension but finite, with height L, on the vertical axis z^*, is suddenly cooled, by dropping its surface temperature, at time $t^* = 0$ and $z^* = 0$, to $\theta^* = \theta^*_{\min}$. Surface is to be kept at this lower temperature for $t^* > 0$ (Fig. 2.1).

For high enough temperature step: $\delta\theta^* = \theta^*_{\max} - \theta^*_{\min}$, a buoyancy-driven circulation is induced. This problem can be modeled using continuity, Navier-Stokes and energy equations on a Boussinesq fluid, with no heat sources present. Surface tension effects in the free-rigid case are neglected in the present study. This assumption is reasonable in the present context, as shown experimentally by Davenport & King (1974) in the case of linearly heated deep reservoirs. Scales to be used are L to form dimensionless coordinates (x, y, and z), $L^2\alpha^{-1}$ to form dimensionless time, t, αL^{-1} to form dimensionless velocity base state and perturbations, $(\tilde{u}_0, \tilde{v}_0, \tilde{w}_0)$ and $(\tilde{u}_1, \tilde{v}_1, \tilde{w}_1)$, respectively. $\nu\alpha g^{-1}\beta^{-1}L^{-3}$, to form dimensionless temperature perturbation, $\tilde{\theta}_1$, whereas the dimensionless base temperature, $\tilde{\theta}_0$, is scaled to range between 0 and 1: $\tilde{\theta}_0 = (\theta^*_0 - \theta^*_{\min})(\theta^*_{\max} - \theta^*_{\min})^{-1}$. α, ν and β are the thermal diffusivity, kinematic viscosity, and thermal expansion coefficient of the fluid, respectively. g is the magnitude of the gravity vector, which points in the same direction of the z axis. In the latter expressions, the subscript 0 refers to the base state and 1 to the perturbed one.

A first order expansion for the dimensionless temperature and velocity is considered, with the form $\tilde{\theta} = \tilde{\theta}_0 - \tilde{\theta}_1$, and $\tilde{\mathbf{u}} = \tilde{\mathbf{u}}_0 + \tilde{\mathbf{u}}_1 = \tilde{\mathbf{u}}_1 = (\tilde{u}_1, \tilde{v}_1, \tilde{w}_1)$, respectively. The minus sign on the expansion for temperature means that positive perturbations have a cooling effect. The base state is that of a horizontally infinite, quiescent fluid layer. Neglecting second order terms, the following set of equations is obtained for the vertical velocity and

temperature perturbations:

$$\left(\frac{1}{\mathrm{Pr}}\partial_t - \tilde{\Delta}\right)\tilde{\Delta}\tilde{w}_1 = \tilde{\Delta}_1\tilde{\theta}_1 \tag{2.1a}$$

$$\partial_t\tilde{\theta}_1 - \mathrm{Ra}\,\tilde{w}_1\partial_z\tilde{\theta}_0 = \tilde{\Delta}\tilde{\theta}_1, \tag{2.1b}$$

where $\mathrm{Pr} = \nu\alpha^{-1}$ corresponds to the Prandtl number and $\mathrm{Ra} = g\beta(\theta^*_{\max} - \theta^*_{\min})L^3\nu^{-1}\alpha^{-1}$ corresponds to a Rayleigh number based on the overall temperature step, $\tilde{\Delta} \equiv \partial_{xx} + \partial_{yy} + \partial_{zz}$ and $\tilde{\Delta}_1 \equiv \tilde{\Delta} - \partial_{zz}$, provided the dimensionless equation for the base state is satisfied:

$$\partial_t\tilde{\theta}_0 = \partial_{zz}\tilde{\theta}_0 \tag{2.2a}$$

$$\tilde{\theta}_0(t=0,z) = 1, \quad \tilde{\theta}_0(t>0,z=0) = \partial_z\tilde{\theta}_0(t\geq 0, z=1) = 0. \tag{2.2b}$$

The derivation of stability equations using propagation theory is analogous to that of Kang & Choi (1997) and Yang & Choi (2002*a*). Hence, only the essential steps are given here. In propagation theory it is stated that, for the case of thermal convection in systems where instabilities are confined mainly into the thermal boundary layer (TBL), a balance between viscous and buoyant forces can be made, such that it is possible to scale dimensionless vertical velocity perturbations with time as $|\tilde{w}_1\tilde{\theta}_1^{-1}| \sim \delta_\theta^2$, where $\delta_\theta \propto \sqrt{t}$ is the dimensionless thermal penetration depth. From the latter relation and dimensional analysis it can also be inferred that (Yang & Choi, 2002*a*):

$$\left[\tilde{\theta}_1(z,t), \tilde{w}_1(z,t)\right] = \left[t^n\theta_1\left(z/\sqrt{t}\right), t^{n+1}w_1\left(z/\sqrt{t}\right)\right], \tag{2.3}$$

where n is a parameter. Now, stability equations are represented in a new coordinate system defined as $\left(t, \zeta = z/\sqrt{t}\right)$, instead of (t,z), while $\tilde{\theta}_1$ and $\tilde{w}_1$ turn to θ_1 and w_1 in the newly defined system. To avoid confusion, t will be defined as τ. The present criterion for the setting of n is to find the lowest possible onset times from the characteristic problem. To this purpose, it must be set to zero (Yang & Choi, 2002*a*). Additionally, Choi *et al.* (2004*d*) and Chung *et al.* (2004) argue that this condition can be also derived from the assumption that the onset time occurs when the growth rates of the root-mean-square values of the base state temperature and of the temperature perturbations are equal. In the context of a system with an imposed heat flux, the latter assumption leads to a different n value of 1/2 (Choi *et al.*, 2004*a*,*b*).

Eqs. (2.1) are cyclic in the horizontal plane. Then, modes with wavenumbers a_x and a_y for the x and y axis, respectively, are considered. Introducing (2.3)$\times \exp[\mathrm{i}(a_x x + a_y y)]$ in the latter system, noting that $\partial_\tau(\cdot) = -\zeta(2\tau)^{-1}\partial_\zeta(\cdot)$ and that $\partial_z(\cdot) = \tau^{-1/2}\partial_\zeta(\cdot)$, the

set of stability equations to be solved is:

$$\left[\left(\mathrm{D}^2 - a_\tau^2\right)^2 + \frac{1}{2\mathrm{Pr}}\left(\zeta\mathrm{D}^3 - a_\tau^2\zeta\mathrm{D} + 2a_\tau^2\right)\right] w_1 - a_\tau^2\theta_1 = 0 \tag{2.4a}$$

$$\left(\mathrm{D}^2 + \frac{1}{2}\zeta\mathrm{D} - a_\tau^2\right)\theta_1 + w_1\mathrm{Ra}_\tau\mathrm{D}\theta_0 = 0, \tag{2.4b}$$

where $\mathrm{D}^n(\cdot) = \mathrm{d}^n(\cdot)/\mathrm{d}\zeta^n$, $a_\tau = \tau^{1/2}\sqrt{a_x^2 + a_y^2}$ and $\mathrm{Ra}_\tau = \tau^{3/2}\mathrm{Ra}$.

The scaling assumed here, which considers the hypothesis that disturbances are confined mainly into a thermal penetration depth, makes Eqs. (2.4) valid for small values of time only. In this case, the base state for temperature, θ_0, can be expressed as a function exclusively of ζ. This kind of system, representative of a thermally semi-infinite one, is commonly named 'deep pool' system (the acronym DP will be adopted hereafter). Its TBL is small compared with the thickness of the fluid layer.

For large values of τ, when equations are not self-similar anymore, it has been shown (Kim *et al.*, 2002; Yang & Choi, 2002*a*) that eigenvalues for (2.4) can still be found. In those works, it was also shown that asymptotic convergence in time to results obtained with the frozen time model is achieved. However, the validity at intermediate values of time of the thermal scaling proposed here is not clear. Regarding this topic, an analysis on the validity of this model, in the context of nonpenetrative convection, is being presently prepared (Ihle & Niño, 2005). For the system with no-slip top and bottom surfaces (named herein as the rigid-rigid case), boundary conditions for the perturbed quantities are:

$$\theta_1 = w_1 = \mathrm{D}w_1 = 0 \quad \text{in } \zeta = 0 \tag{2.5a}$$

$$\mathrm{D}\theta_1 = w_1 = \mathrm{D}w_1 = 0 \quad \text{in } \zeta = 1/\sqrt{\tau}. \tag{2.5b}$$

In the case with stress-free top and no-slip bottom (defined also as the free-rigid case), boundary conditions which are to be applied to Eqs. (2.4) are:

$$\theta_1 = w_1 = \mathrm{D}^2w_1 = 0 \quad \text{in } \zeta = 0 \tag{2.6a}$$

$$\mathrm{D}\theta_1 = w_1 = \mathrm{D}w_1 = 0 \quad \text{in } \zeta = 1/\sqrt{\tau}. \tag{2.6b}$$

The marginal stability problem to be considered is to solve: $\min_{a_\tau} \mathrm{Ra}_\tau$, where a_τ and Ra_τ satisfy (2.4), with boundary conditions (2.5) or (2.6), in the rigid-rigid and free-rigid cases, respectively. This procedure is to be applied to the self-similar system, valid for small values of time. Under this condition, the present definition of the Rayleigh number is the same as the one used in the classical Rayleigh-Bénard problem, based on the temperature difference between the top and bottom horizontal boundaries, since here, the

bottom boundary holds its higher temperature throughout the whole lapse of time during which the present stability model is valid.

2.3 Solution method

Eqs. (2.4) and the boundary conditions (2.5) and (2.6) are homogeneous. Then, the value of $\mathrm{D}^2 w_1(0)$ and $\mathrm{D}w_1(0)$ can be assigned arbitrarily in the rigid-rigid and free-rigid cases, respectively (Kang & Choi, 1997; Kim *et al.*, 2002). To solve the problem posed in the previous section, a solver based on the shooting method using a fourth order Runge-Kutta numerical integration formula was implemented. Convergence to minima was achieved using a Newton-Raphson scheme. Validation of the numerical implementation was done by analyzing the classical rigid-rigid Rayleigh-Bénard problem with a step change in the bottom temperature (Kim *et al.*, 1999), using Eqs. (2.4). Monotonic, albeit slow convergence for increasing time, close to the well known value of the critical Rayleigh number of 1708 was found for different Prandtl numbers. This result numerically checks the classic result for the steady state problem, which states that the onset of the Rayleigh-Bénard instability does not depend on the Prandtl number (Drazin & Reid, 1981). This statement is recalled expressing (2.4) in the (z,t) space, re-scaling w_1 and θ_1 and their derivatives to $\tilde{w}_1$ and $\tilde{\theta}_1$ *via* (2.3), and taking the limit when $\tau \to \infty$. The resulting equations are $\left(\partial_{zz} - a^2\right)^2 \tilde{w}_1 = a^2 \tilde{\theta}_1$ and $\left(\partial_{zz} - a^2\right) \tilde{\theta}_1 + \tilde{w}_1 \mathrm{Ra} = 0$, regardless of the value of Prandtl number, for which no assumption has been made but to be positive. Now, as the resulting expressions are only functions of z, it is noted that the latter equations also correspond to the linearized stability system obtained assuming an exponential growth rate, $\exp \sigma t$, with a critical stability condition $\sigma = 0$ (Yang & Choi, 2002*a*). This approach corresponds to the 'marginal state' variation of the frozen time model (Gresho & Sani, 1971). With this set of equations, the computed critical Rayleigh number and its associated wavenumber are 1707.7618 and 3.11632, respectively, in agreement with the pair $(1707.765, 3.12)$ proposed by Sparrow *et al.* (1964) and $(1707.7618, 3.11635)$, computed by Mizushima (1995).

In numerical terms, the DP system assumption means that the outer boundary to be considered goes to infinite. To reproduce this fact into the computation of eigenvalues prior to the minimization process, the extrapolation procedure described by Chen *et al.* (1983) for critical Ra_τ numbers was used. Roughly, this approach is based on the observation that different $\mathrm{Ra}_{\tau n}$ numbers, obtained for different outer depths ζ_n, decrease approximately as a geometrical sequence. Then, the asymptotic Rayleigh number can be computed as $\mathrm{Ra}_\tau^0 \approx \mathrm{Ra}_{\tau n}^0 + r(\mathrm{Ra}_{\tau n}^0 - \mathrm{Ra}_{\tau n-1}^0)/(1-r)$, where r is the slope of the approximately logarithmic line obtained using different pairs $(\zeta_n, \mathrm{Ra}_{\tau n})$.

2.4 Results and discussion

2.4.1 Base state solutions

The base state solution can be calculated using Laplace transforms, which yields equation (2.7). This approach has the advantage of producing a series with faster convergence than that obtained through Fourier decomposition.

$$\theta_0(\zeta,\tau) = 1 + \sum_{n\geq 0}(-1)^{n+1}\left\{\operatorname{erfc}\left[\frac{n}{\sqrt{\tau}}+\frac{\zeta}{2}\right] + \operatorname{erfc}\left[\frac{n+1}{\sqrt{\tau}}-\frac{\zeta}{2}\right]\right\} \tag{2.7}$$

The DP solution can be readily obtained solving (2.2) on a semi-infinite domain:

$$\theta_{0\mathrm{DP}}(\zeta) = \operatorname{erf}(\zeta/2)\,. \tag{2.8}$$

For values of τ lower or close to 0.01 very small relative differences between equations (2.7) and (2.8) are observed. Computing the latter as $\lambda = \max_\zeta\{100\times|1-\theta_0/\theta_{0\mathrm{DP}}|\}$, for $\tau = 0.005$, 0.007, 0.01, 0.02 and 0.05, $\lambda < 10^{-12}$, 10^{-12}, 10^{-10}, 10^{-4} and 0.1, respectively.

2.4.2 Comparison with the unsteady Rayleigh-Bénard problem

The deduction of the nonpenetrative stability problem in the light of the propagation model yields an interesting similitude with the unsteady Rayleigh-Bénard problem studied by Kim *et al.* (1999). Eqs. (2.4a) and (2.4b) have the same analytical expression than those corresponding to the latter work. The only difference between them is the thermal condition imposed at the boundary away from the step change in temperature (named herein as the outer boundary). In the present problem, the boundary condition $\lim_{\zeta\to\infty}\mathrm{D}\theta_1 = 0$ is imposed, while in Kim *et al.* (1999), $\lim_{\zeta\to\infty}\theta_1 = 0$ is imposed instead, representing the existence of an isothermal outer boundary. It can be shown, however, that both types of outer boundary condition must be satisfied simultaneously in both problems. For fixed Rayleigh and Prandtl numbers, an onset time τ_c exists such that $\theta_1 = 0$ for $\tau < \tau_c = \tau_c(\mathrm{Pr},\mathrm{Ra})$ (i.e., the system does not experience convection before the onset time). On the other hand, the similarity condition inherent to the present propagation model imposes the scaling $\delta_\theta \sim \sqrt{\tau} \ll 1$ ($\tau \lll 1$) for the thermal penetration depth, and the boundary condition $\mathrm{D}\theta_1(1/\sqrt{\tau}) = 0$. Then, considering, as stated previously, that the perturbations are mainly confined within the TBL, and assuming continuity of the temperature disturbance, necessarily $\theta_1(1/\sqrt{\tau}) = 0$, which is a mere consequence of the small penetration depth occurring at small times. As this holds for arbitrarily small onset times (and, consequently, arbitrarily large values of the Rayleigh number), if $\lim_{\zeta\to\infty}\mathrm{D}\theta_1 = 0$,

then $\lim_{\zeta\to\infty}\theta_1 = 0$. Consequently, both problems, the impulsively isothermally heated Rayleigh-Bénard and the present nonpenetrative convection, are equivalent, provided the existence of a Rayleigh number range that support the deep-pool assumption.

Another interesting feature of the eigensystem (2.4) is that its eigenvalues are insensitive to the type of outer boundary condition considered, free or rigid, as can be verified with arguments similar to those of the previous paragraph. Hence, according to the propagation model, for high Rayleigh numbers the only boundary that matters to eigenvalues (both in the thermal and kinematic sense) is the one subjected to the impulsive change on temperature. This conclusion agrees with that of Foster (1965*b*), who noticed that motion was 'decoupled from the bottom', analyzing the problem of a surface-stress-free fluid layer subject to a step change in temperature, using the amplification model. Another consequence of this conclusion is that the free-rigid results to be presented here should be valid for the free-free and free-rigid variations of the Rayleigh-Bénard convection. The same applies, of course, to the free-free nonpenetrative convection problem, which offers a reasonable approximation to systems where a nearly stress-free, strong and stable density interface exists between two rather homogeneous layers of fluid. The latter, so-called 'thermocline' (Imberger & Patterson, 1990), is commonly found in lakes and reservoirs.

2.4.3 Solution of the eigenvalue problem

As $\tau \leq 0.01$ (which is bonded to the assumption of a highly supercritical system) must hold to keep the self similarity of the base state, a lower bound to valid Rayleigh numbers is imposed:

$$\mathrm{Ra}(\mathrm{Pr}) \geq \mathrm{Ra}_{\min}(\mathrm{Pr}) = \frac{\mathrm{Ra}_\tau(\mathrm{Pr})}{0.01^{3/2}} \tag{2.9}$$

Despite the existence of Kim *et al.* (1999) results for the impulsively heated Rayleigh-Bénard problem, whose mathematical posing fully coincides with that of the present nonpenetrative convection problem as discussed in previous section, the eigenvalues for the rigid-rigid case were re-calculated here to serve as an additional validation of the numerical results obtained. Differences on computed values of Ra_τ were found only for $\mathrm{Pr} = 100$, and even in that case they were not higher than about 1%. In the case of the a_τ computed values, a difference (of about 10%) was found for $\mathrm{Pr} = 1$. The latter are indicative of an apparent error on Kim et al.'s (Kim *et al.*, 1999) solution. Table 2.1 shows the minimum $(a_\tau, \mathrm{Ra}_\tau)$ eigenvalues computed for the DP system for a range of Prandtl numbers and the corresponding values of the minimum valid Rayleigh number, given by (2.9).

Results for the DP free-rigid case, which have not been previously reported in the context of the present problem and method, are shown in Fig. 2.2. The Ra_τ parameter varies exponentially for $\mathrm{Pr} \leq 1$ and is virtually constant for values of $\mathrm{Pr} > 1000$. The

same trend occurs for the rigid-rigid case, as previously commented by Kim *et al.* (1999, 2002). Considering comments on Section 2.4.2, present data extend the results reported in the former work and are new to the nonpenetrative problem context. The following correlations, valid for $0.01 \leq \mathrm{Pr} \leq 1000$, can be used to predict the onset time and the most unstable mode in the case of the DP system, for the free-rigid or rigid-rigid cases, with an error bound of 2%:

$$\tau_c = a_1 \left[a_2 + \left(\frac{a_3}{\mathrm{Pr}} \right)^{a_4} \right]^{a_5} \mathrm{Ra}^{-2/3} \tag{2.10}$$

$$a_c = \left(b_1 + b_2 \,\mathrm{erf} \left[\left(\frac{b_3}{\mathrm{Pr}} \right)^{b_4} \right]^{b_5} \right) \tau_c^{-1/2} \tag{2.11}$$

Corresponding values of the parameters a_j are given on Table 2.2. For higher values of the Prandtl number ($\mathrm{Pr} > 1000$), $\tau_c = a_\infty \mathrm{Ra}^{-2/3}$ and $a_c = b_\infty \tau_c^{-1/2}$ replace (2.10) and (2.11), respectively. Here, $a_\infty = 7.531$ and 4.207, $b_\infty = 0.533$ and 0.317, for the rigid-rigid and free-rigid cases, respectively.

The amplitude functions corresponding to the results in Table 2.1 are represented in Fig. 2.3. Here, a TBL can be defined as the ζ value for which the base temperature reaches a value of 0.99. This limiting condition is depicted in Fig. 2.3 with a vertical line. With this definition, the latter figure shows a tendency of the amplitude curves to displace out of the TBL with increasing Prandtl number. The same trend was previously observed by Kang & Choi (1997) in the DP system associated with the Bénard-Marangoni convection.

For Prandtl numbers greater than about one, it is found that vertical velocity disturbances reach depths that exceed by a factor close to 2 the thermal penetration depth. The increasing of the penetration of disturbances with Prandtl number means that the higher the latter parameter, the deeper is the layer where disturbances exist (Fig. 2.3). At the same time, as the Prandtl number increases, the system becomes less stable as shown by the monotonically decreasing marginal stability curves of the upper panel of Fig. 2.2.

An interesting feature of the eigenfunctions is that only for medium to large Prandtl numbers (greater that about 10) the asymptotic decay of the disturbances with depth in the case of the free-rigid case is noticeably slower than in the rigid-rigid case (Fig. 2.3). This trend is consistent with the separation between the stability curves for different boundary conditions depicted in Fig. 2.2 (upper panel), which appears to be minimum for low Prandtl numbers and maximum in the infinite Prandtl number case. As some liquid metals, like mercury, have very low Prandtl numbers (~ 0.025 at room temperature), present results suggest a way to avoid the kinematic effect of the boundary condition in laboratory experiments with a proper choice of the fluid.

Computed critical wavenumbers exhibit slight variations with the Prandtl number, for

values of this parameter lower than about 0.1 and larger than about 10 (Fig. 2.2, lower panel). In the intermediate range ($0.1 < \mathrm{Pr} < 10$), however, they present rather steep change rates with Pr. As the onset of convection is marked by the formation of regular cells, within the intermediate Pr range those disturbances should be rather more sensitive to small spatial variations in fluid properties than in the low and high Pr cases. Consequently, it is believed that this factor may influence to some extent the reproducibility of experiments and possibly explain in part the large dispersion in the horizontal wavelengths experimentally obtained by Foster (1969, Fig. 4).

Present results have some differences with respect to previous numerical calculations using other other approaches to the stability analysis. In particular, in the amplification model (Foster, 1965*b*) an amplification factor, built upon the normalized RMS of the disturbance of the vertical velocity field, is defined as $\bar{w}(t) = [\int_0^1 \tilde{w}_1^2(z,t)\,\mathrm{d}z / \int_0^1 \tilde{w}_1^2(z,0)\,\mathrm{d}z]^{1/2}$, where $\tilde{w}_1(z,0)$ represents the initial disturbance condition, which has been commonly chosen as white noise with equal amplitude coefficients (see Foster, 1965*b*; Gresho & Sani, 1971; Mahler *et al.*, 1968). When $\bar{w}(t)$ grows beyond some predefined factor, the corresponding time is marked as the onset time. In this context, different thresholds for $\bar{w}$ induce the estimation of different times. Such need for a definition of limiting conditions precludes a straightforward comparison between results coming from different methods and care should be taken. The onset time predicted by the present method is analyzed in more detail next.

2.4.4 Analysis of onset time

To assess the onset time, commonly three classes of characteristic times are considered. The first corresponds to that which comes indirectly from the eigensystem (2.4a)–(2.4b), τ_c. The second one is that which marks the thermal dominance of advection over diffusion, τ_u. Finally, the third one is that at which fluid motion or temperature increase can be experimentally detected, τ_m. It is likely that the better the experiment, the closer is τ_m to τ_u since normally scalar change sensing is used. Experimental verification of τ_c seems to be more difficult, as it marks the beginning of convection, with a very small amplitude fluid motion (Choi *et al.*, 2004*d*; Chung *et al.*, 2004; Davenport & King, 1974; Foster, 1969; Yang & Choi, 2002*a*). On the other hand, there must be a lapse of time when velocities are small enough to make the advective term in the energy equation negligible compared with the diffusive one (Elder, 1969), that is $0 < w_1^* \partial_{z^*} \tilde{\theta} \ll \alpha \tilde{\Delta} \tilde{\theta}$ for τ such that $\tau_c < \tau < \tau_u$. Then, τ_c must always be lower that τ_u.

In the case of results for the rigid-rigid case, Kim *et al.* (1999) supported the conjecture of Foster (1969) about the existence of a scaling factor of about 4, between time τ_c coming

from eigenvalue calculations and time τ_m corresponding to observations of convective motion. To this purpose, they used the propagation model with the temperature step change setup and compared their theoretical results with the experimental ones by Ueda *et al.* (1984). Further comparisons were later reported by the same research group (see Choi *et al.*, 2004*d*; Kim *et al.*, 2002, and references therein) for large Prandtl numbers.

For the free-rigid case, theoretical results using the amplification model are given by Foster (1965*b*) for step and ramp changes in surface temperature with an isothermal bottom and some Ra-Pr combinations. However, no experimental results were available to validate the former case. Also in a theoretical framework, for $\mathrm{Pr} = 7$ and free-free conditions, defining the onset time, τ_u, from a Nusselt number departure of 1% above the conductive state, Jhaveri & Homsy (1982), found that $\tau_u \sim \mathrm{Ra}^{-2/3}$ (named hereafter as the $-2/3$ power law), and also that $a_c \sim \mathrm{Ra}^{1/3}$, showing that the latter relations hold for $\mathrm{Ra} \geq 30 \times (27/4)\pi^4 \approx 2 \times 10^4$, which is close to the corresponding lower limit of this parameter proposed in Table 2.1. From their data and onset time definition (considered herein as being representative of τ_u), the value $\mathrm{Ra}\,\tau_u^{3/2} \approx 350$ is obtained. This value is greater than the critical $\mathrm{Ra}_\tau = 12.68 = \mathrm{Ra}\,\tau_c^{3/2}$ obtained from Table 2.1, thus giving a value of the ratio $\tau_u/\tau_c = (350/12.68)^{2/3} \approx 9.1$.

In Fig. 2.4 (right panel), results from both the present propagation theory and the amplification model (Foster (1965*b*)) for different Prandtl numbers and $\mathrm{Ra} = 10^6$ are shown. It can be seen that for the free-rigid case both models differ on computed onset times by a factor close to 5, when $\bar{w} = 10$ is used as an amplification factor, and the Prandtl number is greater than about 10. For lower values of Pr, the propagation model yields higher onset times than the ones found using the amplification model. It is noteworthy that the best amplification ratios for the rigid-rigid experiment by Foster (1969) were found between $\bar{w} = 10^3$ and 10^8 (the latter theoretical calculations were previously reported by Foster (1968)). Taking these results into account, it can be concluded that the tuned amplification factor can also be understood as a measure of the disturbance level that a system can afford just before the onset of convection. Wavenumbers were calculated with the present model using the data for $\mathrm{Pr} = 7$ shown in Table 2.1, i.e., $a_\tau = 0.447 = a_c\sqrt{\tau_c}$. Fig. 2.4 (left panel) shows good agreement between present computations of the critical wavenumber a_c and those of Foster (1965*b*) for Rayleigh numbers higher than about 10^5, verifying the 1/3 power law scaling previously noted.

Experimental data for the free-rigid unsteady Rayleigh-Bénard case have been reported by Spangenberg & Rowland (1961) and Foster (1965*a*), but a step in surface temperature was not obtained since evaporative cooling was the dominant effect. An approximate piecewise linear cooling on top was found experimentally. Using infrared radiometry to record surface layer temperature, the latter author compared his results with those obtained by

the former, checking them against calculations made with the amplification model (Foster, 1965*b*). Good correspondence with this theory was found, however, due to the linear evolution of temperature on the top boundary, the experimental results fitted better a $-2/5$ exponent, instead of the $-2/3$ power law expected for the step change case. Table I of Foster (1965*a*) lists several results for the onset time given combinations of Prandtl and Rayleigh numbers. That table also includes results from Spangenberg & Rowland (1961). This data set agree well with amplification model calculations by Foster (1965*b*) using amplification factors between 10 and 100, showing that computed values of the onset times for low amplification and linear cooling describe well the onset of evaporative convection, as previously mentioned. On the other hand, the latter measurements yield times that differ in approximately three orders of magnitude with the present propagation theory results. Differences appear to reside solely on the different applicable power laws, with $\tau_{c\,\mathrm{step}}/\tau_{c\,\mathrm{linear}} \sim 10^{-3}$ in the range of Ra values analyzed, since for the step cooled system $\mathrm{Ra}\,\tau_c^{3/2} = C_1$ (constant), while in the linearly cooled one the scaling is rather $\mathrm{Ra}\,\tau_c^{5/2} = C_2$ (constant).

In the case of convection induced by gas absorption with free-rigid boundaries, defining a Rayleigh number based on a concentration step, $\mathrm{Ra} = g\gamma(C - C_b)L^3D^{-1}\nu^{-1}$ (γ, C, C_b and D are the concentration coefficient of expansion, equilibrium and bulk concentration of solute and mass diffusion coefficient, respectively), along with the time scale L^2/D, Plevan and Quinn's data (Plevan & Quinn, 1966) yield measured dimensionless onset times $\tau_m \approx 2.1\times10^{-3}$ for carbon dioxide in water and $\tau_m \approx 1.3\times10^{-4}$ for sulphur dioxide in water. Although $\mathrm{Pr} \approx 6.25$ in both cases, differences may come partly from the better solubility of the latter gas in water (Blair & Quinn, 1969). Corresponding time ratios, compared with that obtained from Eq. (2.10), are $\tau_m/\tau_c \approx 11$ and 13.1, respectively. Similarly, Blair & Quinn (1969) found $\mathrm{Ra}\,\tau_m^{3/2} \approx 300$ for sulphur dioxide in water. Using data from Table 2.1, time ratios are $\tau_m/\tau_c \approx 8.2$, 10.3 and 10.6, for Prandtl numbers of 7, 100, and 1 000, respectively. In both works, $\mathrm{Ra} \gtrsim 10^6$. Unfortunately, it is impossible to build similar relations with the experimental setup information from Tan & Thorpe (1992), since no liquid layer thickness was specified in that paper. On the other hand, in the latter work, an alternative temporal and depth-dependent version of the Rayleigh number is proposed, along with a theoretical model where the solution of $\mathrm{Ra}(z^*, t^*) = z^{*4}g\gamma\mu^{-1}D^{-1}\mathrm{d}C/\mathrm{d}z^*$ is maximized with respect to z^*, finding the length scale $L(t^*) = 2\sqrt{2Dt^*}$. The corresponding onset time is computed using the critical Rayleigh number in Bénard convection on a steady, horizontally infinite domain with free-rigid boundaries (Chandrasekhar, 1961) on the expression for the maximum $\mathrm{Ra}(z^*, t^*)$. From Tan & Thorpe (1992) data, the latter was found to be on the order of 1 000. Using $\mathrm{Ra}(z^*, t^*)$ and $L(t^*)$ as the corresponding Rayleigh number and length scale, yields time ratios τ_m/τ_c close to 4, but their definitions

are not analogous to the present Rayleigh number and length scale. Consequently, except for Tan and Thorpe's data (Tan & Thorpe, 1992), which provides no clue, all the revised references support the present estimation of a time ratio τ_m/τ_c on the order of 10, rather that 4, for the free-rigid system.

2.5 Concluding remarks

A stability analysis using propagation theory has been conducted to predict the factors that rule the temporal dependence of the onset of nonpenetrative convection in an initially isothermal Boussinesq fluid. It was shown that for the DP system, or, in other words, for high thermal disturbances, which are defined in terms of Rayleigh numbers that exceed a certain minimum for given Prandtl numbers (Table 2.1), the study of nonpenetrative convection equates conceptually and numerically the unsteady Rayleigh-Bénard convection. An extension of previously reported results for the rigid-rigid system using propagation theory (Kim *et al.*, 1999) has been proposed for free-rigid boundary conditions. As several works have reported the study of the onset of unsteady Rayleigh-Bénard convection, a comparison of their results obtained with different methods, with those obtained using the present linear model was made. For Rayleigh and Prandtl numbers within the limits of the present theory, good agreement was found between present results and theoretical ones obtained with the amplification model (Foster, 1965*b*) and the stochastic method (Jhaveri & Homsy, 1982). General agreement on the validity of the scaling $\tau_c \sim \mathrm{Ra}^{-2/3}$ was found. On the other hand, numerical evidence along with experimental data, suggest that the lag between theoretical onset times (τ_c) and detected ones (τ_u or τ_m) is dominated at least by two conditions, namely, the kinematic boundary condition on the side where the heat flow (or temperature change) is imposed, and the way heating (or cooling) is applied in time. It is argued that, at difference from the theoretical determination of τ_c or τ_u, recording of τ_m depends in great extent on the experiment configuration and technological limitations. In particular, present results suggest that for medium to large Prandtl numbers (greater than about 1) and a top (if cooled from above) stress-free boundary, an onset time relation of $\tau_m/\tau_c \sim 10$ rather than 4 (previously proposed for the rigid-rigid system), seems to fit the available data reasonably well. Given these results, it is concluded that the latter values of the τ_m/τ_c ratio are particular cases of a more complex function that should take into account, at least, boundary conditions for the prediction of the onset of convective motion from the experimental knowledge of changes in scalar fields.

Ackgnowledgments

The authors gratefully acknowledge support from the Chilean National Commission for Scientific and Technological Research, CONICYT, the Department of Civil Engineering of the University of Chile, and Fondecyt Project No. 1040494.

Table 2.1: Critical $(a_\tau, \mathrm{Ra}_\tau)$ parameters found for the DP system, as a function of Prandtl number. The fourth and fifth columns (labelled as KCC99) show the critical numbers found for the transient Rayleigh-Bénard problem studied by Kim *et al.* (1999). Columns 6 and 9 show the minimum Rayleigh numbers that guarantee that the DP assumption is valid both for the rigid-rigid and for the free-rigid system, respectively.

	Rigid-rigid					Free-rigid		
	Present work		KCC99					
Pr	a_τ	Ra_τ	a_τ	Ra_τ	$\mathrm{Ra}_{\mathrm{min}}$	a_τ	Ra_τ	$\mathrm{Ra}_{\mathrm{min}}$
0.01	0.824	1799.06	0.82	1799.1	1.80×10^6	0.809	1675.92	1.68×10^6
0.1	0.813	219.10	0.81	219.1	2.19×10^5	0.766	180.98	1.81×10^5
0.71	0.725	53.56	—	—	5.36×10^4	0.637	36.58	3.66×10^4
1	0.702	44.81	0.63	44.81	4.48×10^4	0.607	29.36	2.94×10^4
7	0.589	24.73	—	—	2.47×10^4	0.447	12.68	1.27×10^4
100	0.538	20.97	0.54	20.70	2.10×10^4	0.337	9.01	9.01×10^3
1000	0.533	20.70	0.53	20.69	2.07×10^4	0.320	8.67	8.67×10^3
∞	0.533	20.67	0.53	20.67	2.07×10^4	0.317	8.63	8.63×10^3

Table 2.2: Parameters a_j and b_j of Eqs. (2.10) and (2.11) for the rigid-rigid (RR) and free-rigid (FR) conditions.

	a_j		b_j	
j	RR	FR	RR	FR
1	9.8371	5.9017	0.5291	0.3066
2	1.9022	1.3279	0.2923	0.5002
3	2.0867	2.5505	0.6329	1.1196
4	0.8502	0.7730	0.3347	0.1971
5	1.1421	1.3132	2.0924	3.2267

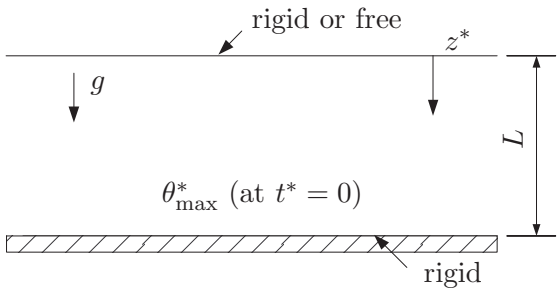

Figure 2.1: Problem configuration. z^* axis points downward.

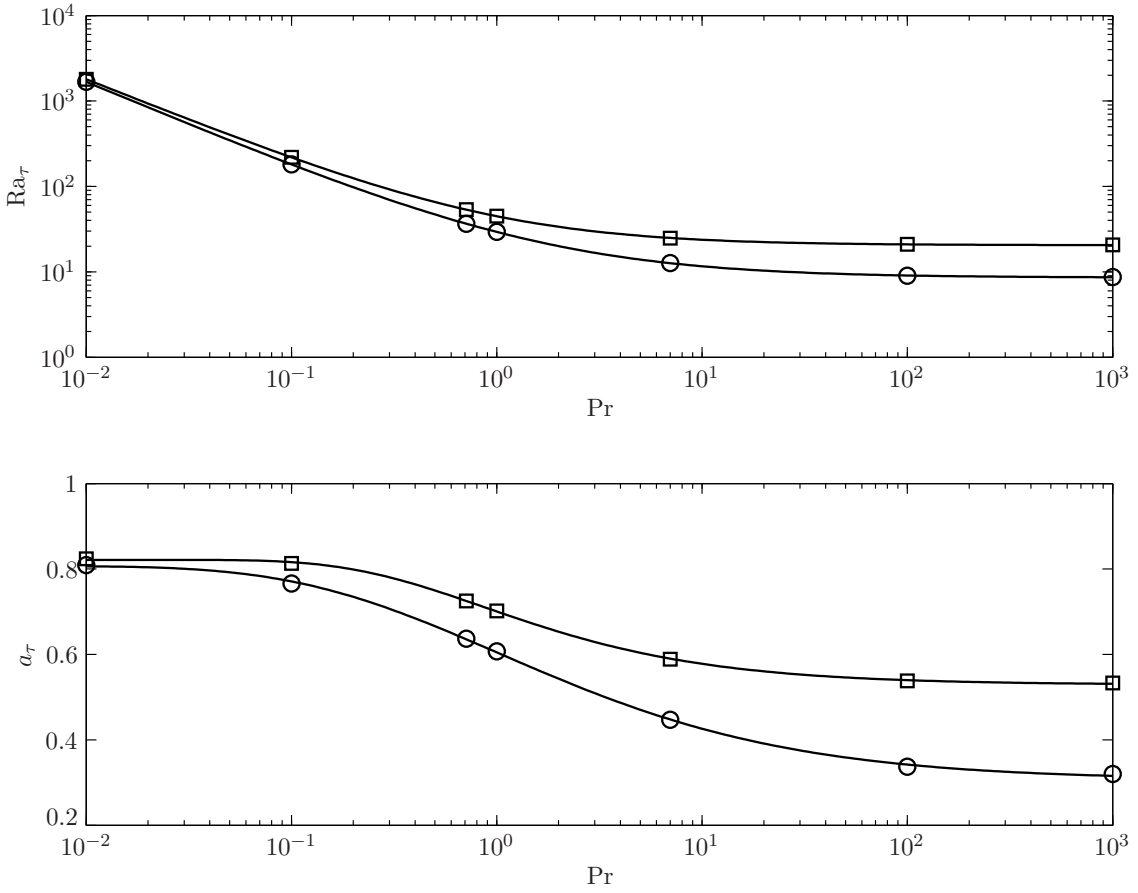

Figure 2.2: Upper panel: effect of the Prandtl number on Ra_τ for the rigid-rigid and rigid-free cases. Lower panel: effect of the Prandtl number on the wavenumber of the fastest growing horizontal mode, a_c. Symbols represent calculated points, corresponding to Table 2.1: squares for the rigid-rigid case and circles for the free-rigid case. Curves represent interpolated results using the models given by Eqs. (2.10), and (2.11) and parameter sets given by Table 2.2.

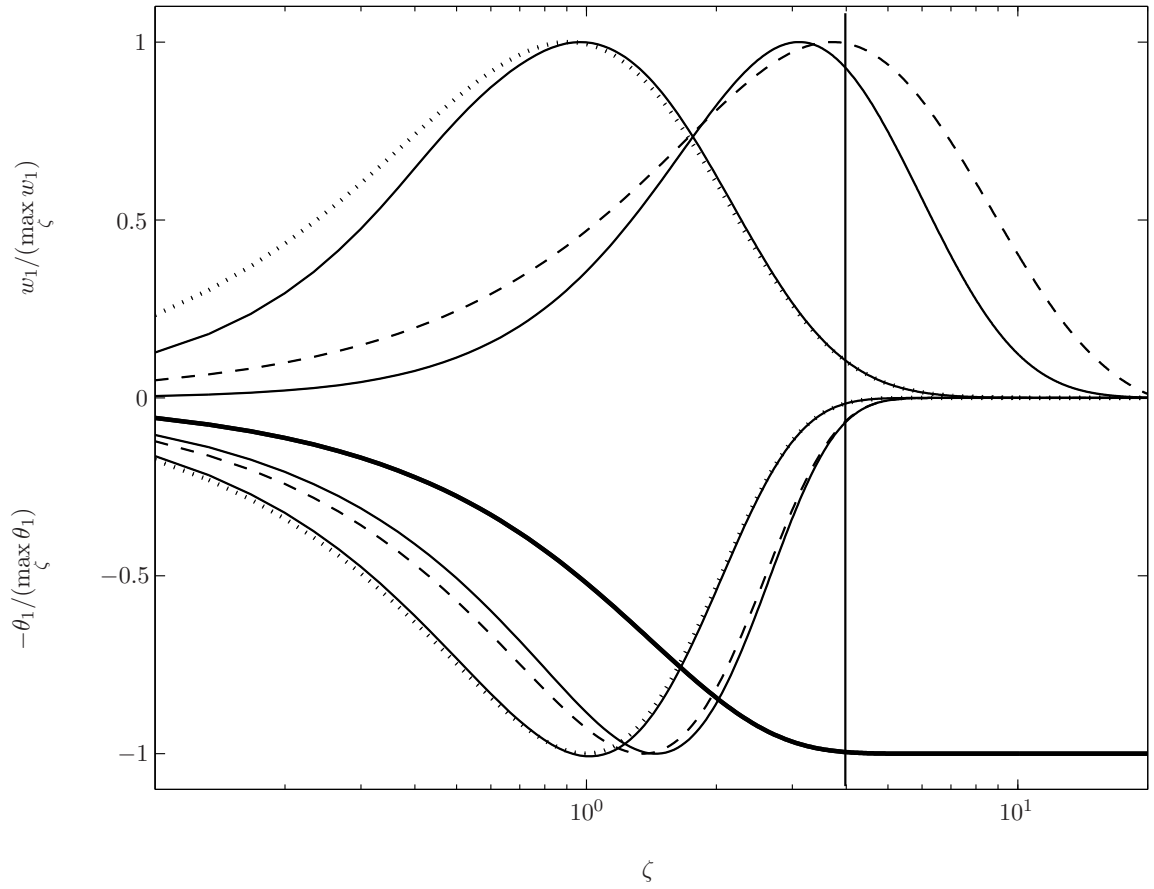

Figure 2.3: Normalized amplitude functions for (minus) temperature and vertical velocity disturbances (lower and upper half, respectively). Solid lines represent the rigid-rigid case in both sets. From left to right, the latter curves show computed results for $\mathrm{Pr} = 0.01$ and $\mathrm{Pr} \to \infty$. The dotted and dashed curves represent the free-rigid case for $\mathrm{Pr} = 0.01$ and $\mathrm{Pr} \to \infty$, respectively. The bold monotonic curve exhibits (minus) the base state temperature, given by (2.8).

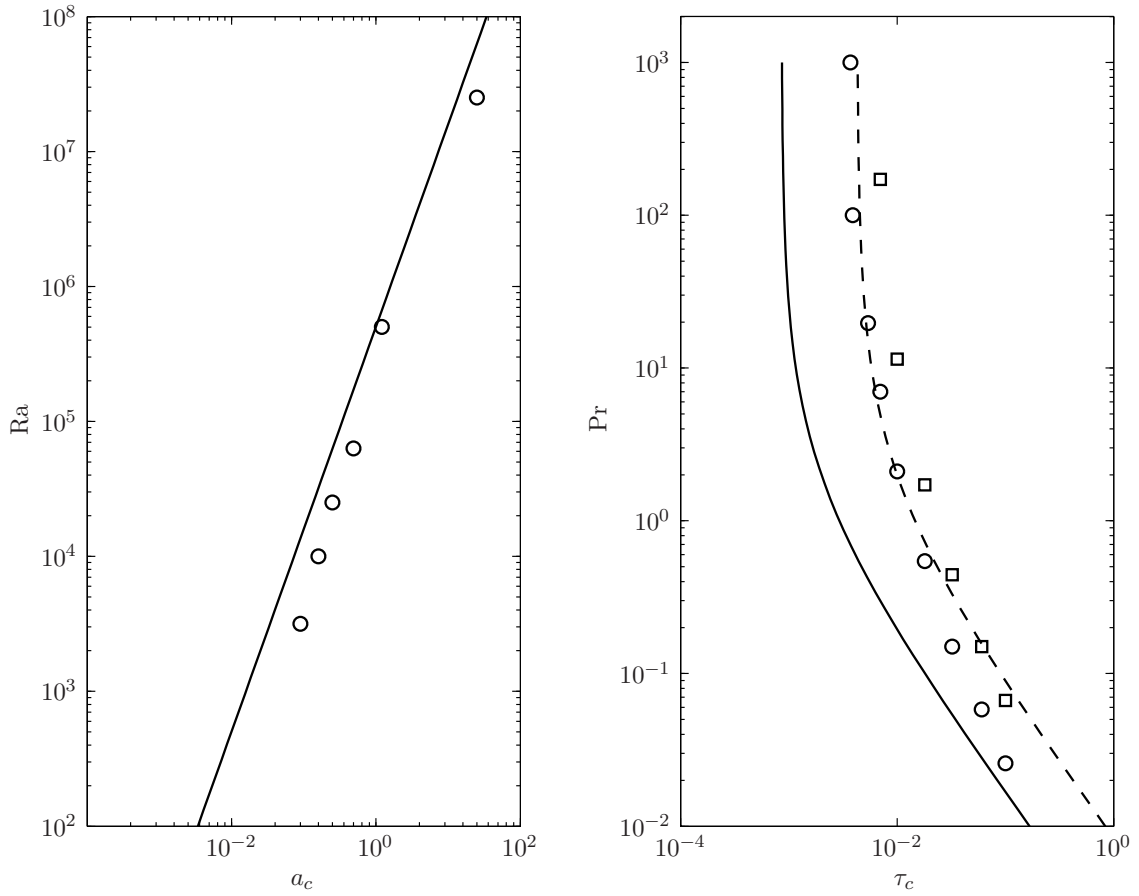

Figure 2.4: Left panel: comparison between critical wavenumbers computed using the present propagation model (solid line) and the ones reported by Foster (1965*b*) (circles), for the free-rigid case, step change in temperature, with Pr = 7. Right panel: Critical time as a function of Prandtl number; comparison between results obtained using propagation and amplification models with Ra = 10^6. Solid line represents results obtained with the present propagation model, while the dashed line shows the latter predictions amplified by a factor of 5. Circles represent results from Foster (1965*b*), using an amplification factor $\bar{w} = 10$; squares represent equivalent results with $\bar{w} = 100$.

Chapter 3

The onset of thermal convection increasing the temperature sinusoidally

This chapter, authored by Christian Ihle and Yarko Niño, is in the form of research article, on its final stage of preparation to be submitted to *Environmental Fluid Mechanics*.

Abstract

A theoretical model, based on linear stability analysis, is proposed to predict the onset of natural convection in lakes and reservoirs due to night time cooling. To such purpose, the system was modelled as a initially quiescent deep Boussinesq fluid reservoir, whose boundary temperature changes sinusoidally. From scaling analysis, it is found that critical onset times for convection are proportional to $R^{-2/7}$, where R is a Rayleigh number including fluid properties and forcing frequency, whereas the proportionality constant is a function of fluid properties. Results were compared with lake field data obtained in a recent campaign and with a previous work. Present model predictions differ with field observations by a relatively constant factor.

3.1 Introduction

Temperature is a relevant variable in lake and reservoir dynamics. Commonly, the daily evolution of the density profile of a relatively thin layer near the surface depends on diurnal heating and nocturnal cooling (Imberger & Patterson, 1990). In the latter case, it is the turbulent process known as penetrative convection (Adrian, 1986) that which enhances mixing and thus breaks the weak stratification formed during daytime. The study of such process is largely justified by its influence on water quality, as well as on ecology issues (e.g. Spigel & Imberger, 1987; Wehde *et al.*, 2001), where accelerated eutrophication, associated with elevated phytoplankton production as a consequence of high nutrients inputs to a lake (Wetzel, 2001) is a major anthropogenic environmental problem. The hydrodynamics of the system is the main agent affecting the distribution of these nutrients in the lake and therefore, meteorological forcing acting on the underlying physics may have a major effect on the biochemistry and, ultimately, on the water quality of the system.

In natural systems, the external forcing due to heating depends on the coupling of a daily and a seasonal time scale. Regarding the surface layer buildup, the former is often dominant. Implications of nocturnal cooling can be commensurate with those of wind, and thus of induced surface and internal waves, where such cooling process is well described as sinusoidal. Nonetheless, the enhancement of turbulent kinetic energy resulting from cooling does not start at the very beginning of the cooling process, as anticipated by related, theoretical studies (for instance, Goldstein & Volino, 1995; Homsy, 1973, and references therein) and suggested by field observations (Jonas *et al.*, 2003).

A heated 40×15×20 cm perspex tank filled with water, initially at 19.5°C, was used to account for a preliminary experimental verification for convection. The heater was a brass plate connected to a Haake C heat bath. The latter has a built-in controller. Temperature of the plate was modified sinusoidally, fixing a semi-period of 55 min and an overall temperature difference of 6.8°C. The tank bottom temperature was measured using a K-type thermocouple. The flow was seeded with 90–110 μm Pliolite. Convective motion was exposed using a 4 mm thick light sheet generated with a 1 kW photographic lamp and captured using a Jai CVM4+CL digital video camera with a 50 mm f0.95 Vortex lens mounted, at a refresh rate of 4 frames per second. The criterion employed to decide on the onset time for convection was to detect a rapid increase of the root-mean square of the computed velocity field using a PIV algorithm (Dalziel *et al.*, 2000). A noticeable increase of the kinetic energy was only observed after about 350 s, nearly 10.5% of half a heating cycle. This sub-daily time-dependence is not directly addressed in present one-dimensional models, where the nocturnal mixing is used to assume a complete mixing of the surface layer (Gal *et al.*, 2003).

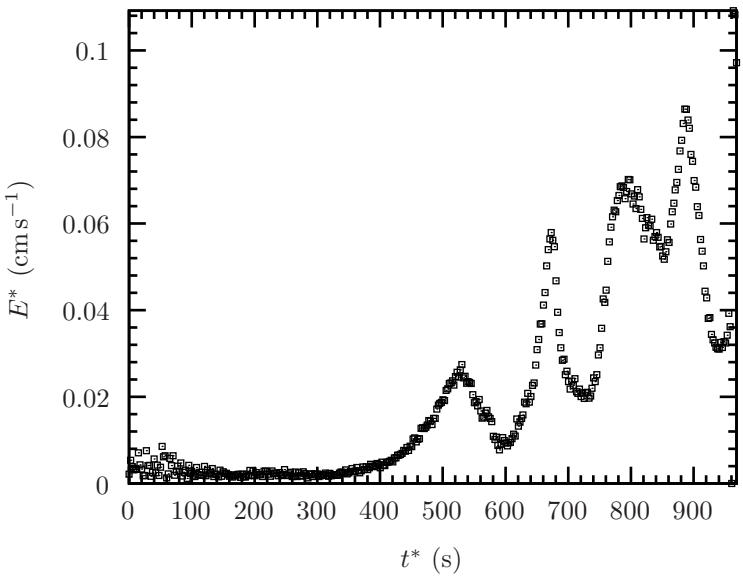

Figure 3.1: RMS of the kinetic energy of a 2D flow slice exposed using PIV, computed as $E^* = \left(\langle u^{*2}\rangle + \langle v^{*2}\rangle\right)^{1/2}$, where brackets denote spatial averaging.

Although a significant amount of works have been devoted to the study of the stability of periodically forced systems, both from the point of view of temperature and gravity modulation, emphasis has been given to the role of frequency on the growth of disturbances (Davis, 1976; Dowden, 1981; Orr & Kelly, 1999). Differently, in the present case, given the dimensions of the natural systems that are intended to be modelled, even for temperature amplitudes as small as 0.1 K, convection starts at each cycle, and thus, to the purposes of the present paper, the determination of minimal dimensionless parameters to get convection is not important. Moreover, as in most of the cases disturbances propagate within a thin layer near the surface, overall reservoir depth is not a relevant variable, and a semi-infinite geometry is a better approximation. Given that hypothesis, the present paper proposes a way of estimating critical times for disturbances growth in a sinusoidally, thermally forced system. An approach based on a linear stability analysis of the governing equations is considered to such purpose.

3.2 Problem description

An initially quiescent horizontal Boussinesq fluid layer, well mixed at temperature $\theta^* = \theta^*_{\min}$, infinite on its horizontal dimension and semi infinite on the vertical axis, z^*, is heated by increasing the boundary temperature, at time $t^* = 0$ and $z^* = 0$, to $\theta^* = \theta^*_{\max}$ sinusoidally:

$$\frac{\tilde{\theta}^*_0(t^* > 0, z^* = 0)}{\Delta\theta^*} = \frac{1}{2}\left[1 - \cos\left(\frac{2\pi}{T}t^*\right)\right]. \tag{3.1}$$

Here, $\Delta\theta^* = \theta^*_{\max} - \theta^*_{\min}$ is the temperature amplitude and T is the forcing period. $\omega = 2\pi/T$ is the corresponding angular frequency and its reciprocal naturally appears as time scale of the problem. For the purposes of the present work, only the effect of the first forcing cycle is relevant: it is not the intent of the present work to assess the effect of the forcing frequency over more than one cycle (Davis, 1976, presents a review on this topic).

From the point of view of Rayleigh's analysis it turns out, from writing a Rayleigh number based on a length scale equal to the depth of the fluid layer, that a very deep reservoir will always evolve to convection in the presence of first order disturbances, no matter the strength of the buoyancy force applied. However, such motion becomes manifest only from a certain time on, where it is apparent that also fluid properties and the forcing frequency play a role. At time t^*, when convection is about to start, buoyancy marginally balances viscosity:

$$g\alpha\Theta^* \sim \frac{\mu}{\rho_0}\frac{W^*}{\delta^{*2}} \sim \frac{\mu}{\rho_0\delta^* t^*}. \tag{3.2}$$

where $\Theta^*(t^*)$ and $\delta^*(t^*)$ are a time-dependent characteristic temperature and length scales, μ is the dynamic viscosity of the fluid and ρ_0 its reference density. In the third term, the velocity W^* was written in terms of a length and time scale as $W^* \sim \delta^*/t^*$.

This problem can be modelled using continuity, Navier-Stokes and energy equations, with no heat sources present. Surface tension effects are neglected in the present study. This assumption is reasonable in the present context, as shown experimentally by Davenport & King (1974) in the case of linearly heated deep reservoirs. As prior the onset of convection heat transfer is diffusive, length and velocity scales can be written using the thermal diffusivity κ along with ω as $(\kappa/\omega)^{1/2}$ and $(\kappa\omega)^{1/2}$, respectively.

It is intuitive that if thermal forcing is stronger or the forcing frequency is larger, convection will start earlier. Expressing the boundary condition (3.1) in terms of a MacLaurin cosine expansion, it turns out that instabilities becomes manifest quickly, then the following balance is valid:

$$\frac{\Theta^*}{\Delta\theta^*} \approx \frac{\omega^2 t^2}{4}, \tag{3.3}$$

otherwise, more terms in the MacLaurin cosine expansion need to be considered.

The balance (3.2) holds right before convection becomes manifest. From the point of view of the temperature evolution, a suitable length scale would be that corresponding to the temperature diffusion process, where $\delta^* \sim (\kappa t^*)^{1/2}$ or, in dimensionless terms,

$$\delta \sim t^{1/2}. \tag{3.4}$$

Using (3.3) and (3.4) in (3.2) yields

$$Rt^{7/2} \sim 1, \tag{3.5}$$

with

$$R = \frac{g\alpha(\theta^*_{\max} - \theta^*_{\min})\kappa^{1/2}}{\nu\omega^{3/2}}, \tag{3.6}$$

where $\nu = \mu/\rho_0$ is the kinematic viscosity. An estimation of onset times can be derived from (3.5). However the prefactor for $R^{-2/7}$, which can possibly depend on fluid properties, should be found either numerically or experimentally. For step-forced systems, such coefficients have been found in the past in terms of ad-hoc Rayleigh numbers (see Ihle & Niño, 2006*b*, and references therein). At difference, to the knowledge of the authors, this is the first work where such objective is pursued in sinusoidally forced systems.

To the purpose of determining onset times, or, equivalently, the proportionality constant in (3.5), propagation theory is used. Such approach, based on similarity considerations on the linearised Navier-Stokes and energy equations, has the advantage of giving fluid property-dependent results. However, one of its limitations is the requirement of a self-similar evolution prior the onset of instability. Fortunately, this restriction is not a strong one for the context where this paper was mainly focused to, namely, the onset of convection in medium to large-scale natural systems, as is discussed in Section 3.4.

3.3 Solution method

Using the length and velocity scales mentioned in the previous section, the dimensionless coordinates are denoted as x, y, and z. A linear stability analysis is the base of present method. Corresponding dimensionless velocity base state and perturbations are defined as $(\tilde{u}_0, \tilde{v}_0, \tilde{w}_0)$ and $(\tilde{u}_1, \tilde{v}_1, \tilde{w}_1)$, respectively. The dimensionless base temperature is scaled to range between 0 and 1: $\tilde{\theta}_0 = (\theta^*_0 - \theta^*_{\min})(\theta^*_{\max} - \theta^*_{\min})^{-1}$ and the corresponding perturbation, $\tilde{\theta}_1$, is scaled by $\nu\omega^{3/2}g^{-1}\alpha^{-1}\kappa^{-1/2}$. In the latter expressions, the subscript 0 refers to the base state and 1 to the perturbed one.

A first order expansion of the dimensionless temperature and velocity are expressed as $\tilde{\theta} = \tilde{\theta}_0 + \tilde{\theta}_1$, and $\tilde{\mathbf{u}} = \tilde{\mathbf{u}}_0 + \tilde{\mathbf{u}}_1 = \tilde{\mathbf{u}}_1 = (\tilde{u}_1, \tilde{v}_1, \tilde{w}_1)$, respectively. The base state is that

of a horizontally infinite, vertically infinite, quiescent fluid layer. Neglecting second order terms, the following set of equations is obtained for the vertical velocity and temperature perturbations:

$$\left(\frac{1}{\mathrm{Pr}}\frac{\partial}{\partial t} - \tilde{\Delta}\right)\tilde{\Delta}\tilde{w}_1 = \tilde{\Delta}_h\tilde{\theta}_1 \tag{3.7a}$$

$$\frac{\partial\tilde{\theta}_1}{\partial t} - R\,\tilde{w}_1\frac{\partial\tilde{\theta}_0}{\partial z} = \tilde{\Delta}\tilde{\theta}_1, \tag{3.7b}$$

where $\tilde{\Delta} \equiv \partial^2/\partial x^2 + \partial^2/\partial y^2 + \partial^2/\partial z^2$ and $\tilde{\Delta}_h \equiv \tilde{\Delta} - \partial^2/\partial z^2$, provided the dimensionless equation for the base state is satisfied:

$$\frac{\partial\tilde{\theta}_0}{\partial t} = \frac{\partial^2\tilde{\theta}_0}{\partial z^2} \tag{3.8a}$$

$$\tilde{\theta}_0(t=0,z) = 0, \tag{3.8b}$$

$$\tilde{\theta}_0(t>0,z=0) = \frac{1}{2}[1-\cos(t)], \tag{3.8c}$$

$$\frac{\partial\tilde{\theta}_0}{\partial z}(t\geq 0, z\to\infty) = 0. \tag{3.8d}$$

Equations (3.7) pose a non-separable problem. Both $\tilde{w}_1$ and $\tilde{\theta}_1$ are functions of time. Part of this time-dependency corresponds to the determination of the times when the latter eigenfunctions will start to grow. The quasistatic hypothesis, which forces a separability assumption in (3.7)[1], states that such growth is exponential, and gives no hint of a characteristic time to mark the onset of convection. Not relying on this assumption, the amplification model (Gresho & Sani, 1971, and references therein) uses series based on separable, non-exponential terms, solving numerically for each of them. However, they strongly depend on the initial conditions and thus add some degree of ambiguity to results. More recently, a new approach has been proposed (Riaz *et al.*, 2006), based on the combination of a similarity space for disturbances (e.g., Yang & Choi, 2002*a*), and an ad-hoc eigenfunction expansion (Foster, 1965*a*; Robinson, 1976), to find onset time predictions largely independent of the initial conditions, thus improving such major drawback in the amplification model.

In the present work, the principles of propagation theory are considered. In such approach (Kang & Choi, 1997; Yang & Choi, 2002*a*) it is stated that, for the case of thermal convection in systems where instabilities are confined mainly into the thermal boundary layer (TBL), a balance between viscous dissipation and buoyancy occurs just at

[1]Although equations are non-separable, eigenvalues R can be found nevertheless.

the onset of convection implying, from (3.7), that

$$\left|\frac{\tilde{w}_1}{\tilde{\theta}_1}\right| \sim \delta^2, \tag{3.9}$$

In particular, (3.9) implies that the scaling $\psi(t)\tilde{w}_1 \sim \psi(t)t\tilde{\theta}_1$ is true if $\psi(t) \neq 0$. The solution of the problem (3.8) can be expressed semi-analytically as

$$\tilde{\theta}_0(z,t) = \frac{1}{2}\sum_{j=1}^{\infty}(-1)^{j+1}\mathrm{i}^{4j}\,\mathrm{erfc}\left(\frac{z}{2\sqrt{t}}\right), \tag{3.10}$$

with $h(x \mid k) = \mathrm{i}^k\,\mathrm{erfc}(x)$, the k^{th} integral of the complementary error function:

$$\mathrm{i}^k\,\mathrm{erfc}(x) = \begin{cases} \dfrac{2}{\sqrt{\pi}}\displaystyle\int_x^{\infty}\mathrm{e}^{-t^2}\mathrm{d}t & \text{if } k = 0 \\ \displaystyle\int_x^{\infty}\mathrm{i}^{k-1}\,\mathrm{erfc}(t)\mathrm{d}t & \text{if } k > 0, \end{cases} \tag{3.11}$$

with $\mathrm{i}^{-1}\,\mathrm{erfc}(x) \equiv 2\pi^{-1/2}\mathrm{e}^{-x^2}$ (Abramowitz & Stegun, 1965). It is noted that (3.10) does not consider the approximation (3.3).

For small values of time, (3.10) is well-described by the first term of the MacLaurin expansion previously mentioned, suggesting that if convection sets in early enough, $\tilde{\theta}_0 \approx t^2 h(z/\sqrt{t} \mid 4) \equiv t^2\theta_0(\zeta = z/\sqrt{t})$. Supposing that disturbances behave similarly in the limit of the onset of convection leads to the scaling $\psi(t) \sim t^n$, where n is a parameter. Therefore,

$$\left[\tilde{\theta}_1\left(z,t\right), \tilde{w}_1\left(z,t\right)\right] = \left[t^n\theta_1(\zeta), t^{n+1}w_1(\zeta)\right], \tag{3.12}$$

Stability equations can be thus expressed in a new coordinate system defined as (t,ζ), instead of (t,z), where the tildes were dropped to stand for the newly defined variables. To avoid confusion, t will be defined as τ. Eqs. (3.7) are cyclic in the horizontal plane and then, modes with wavenumbers a_x and a_y for the x and y axis, respectively, are considered. Introducing (3.12)$\times\exp[\mathrm{i}(a_x x + a_y y)]$ in (3.7), noting that $\partial(\cdot)/\partial\tau = -\zeta(2\tau)^{-1}\partial(\cdot)/\partial\zeta$ and that $\partial(\cdot)/\partial z = \tau^{-1/2}\partial(\cdot)/\partial\zeta$, the set of stability equations to be solved is:

$$\left\{\left(\mathrm{D}^2 - a_\tau^2\right)^2 + \frac{1}{2\mathrm{Pr}}\left[\zeta\mathrm{D}^3 - 2n\mathrm{D}^2 - a_\tau^2\zeta\mathrm{D} + 2(n+1)a_\tau^2\right]\right\}w_1 - a_\tau^2\theta_1 = 0 \tag{3.13a}$$

$$\left(\mathrm{D}^2 + \frac{1}{2}\zeta\mathrm{D} - a_\tau^2 - n\right)\theta_1 - w_1 R_\tau \mathrm{D}\theta_0 = 0, \tag{3.13b}$$

where $\mathrm{D}^k(\cdot) = \mathrm{d}^k(\cdot)/\mathrm{d}\zeta^k$, $a_\tau = \tau^{1/2}\sqrt{a_x^2 + a_y^2}$ and $R_\tau = \tau^{7/2}R$, provided $\mathrm{D}\theta_0 = -4\mathrm{i}^3\,\mathrm{erfc}(\zeta/2)$. Boundary conditions for disturbances depend of the kind of thermal and kinematic condi-

tions to be applied. The present model aims to reproduce Dirichlet boundary condition for temperature, along with stress free and no-slip kinematic conditions. On the outer boundary, corresponding to the limit $\zeta \to \infty$, no heat exchange should occur and the velocity field should asymptotically decay. In the case of a no-slip boundary

$$\theta_1 = w_1 = \mathrm{D}w_1 = 0 \text{ in } \zeta = 0 \tag{3.14a}$$

$$\mathrm{D}\theta_0 = w_1 = \mathrm{D}w_1 = 0 \text{ when } \zeta \to \infty \tag{3.14b}$$

For the second case studied, consisting of an inner stress-free boundary condition,

$$\theta_1 = w_1 = \mathrm{D}^2 w_1 = 0 \text{ in } \zeta = 0 \tag{3.15a}$$

$$\mathrm{D}\theta_0 = w_1 = \mathrm{D}w_1 = 0 \text{ when } \zeta \to \infty \tag{3.15b}$$

The present criterion for the setting of n is to find the lowest possible onset times provided the optimisation problem

$$R_{\tau,c}(n) = \min_{a_\tau} R_\tau(n), \tag{3.16}$$

where $R_\tau(n)$ is an eigenvalue of (3.13). Computations show that R_τ is a monotonically increasing function of n and, moreover, $R_\tau(0) \leq R_\tau(n)$ for $n \geq 0$, in agreement with previous results (Kim *et al.*, 2002; Yang & Choi, 2002*a*). For the purposes of onset time computations n was set to zero. A different path for the definition of a value of n would be to adjust it to make the growth rate of the base state and that of the first order disturbances equal. In the case of an imposed step heat flux, this leads to $n = 1/2$ (Choi *et al.*, 2004*a*,*b*). Anyhow, results are weakly dependent on such choice.

Equations (3.13) along with the boundary conditions (3.14) or (3.15) are homogeneous. The solution method used to find optimal eigenvalues consists of an implementation of the shooting method in combination with a Newton-Raphson scheme, corresponding to that adopted in Ihle & Niño (2006*b*), where also its corresponding validation and comparison against known results is given. The base state was computed efficiently expressing the integrals of the complementary error functions in terms of Confluent Hypergeometric functions of the first kind (Airey & Webb, 1918) as (Abramowitz & Stegun, 1965):

$$\mathrm{i}^k \operatorname{erfc}(x) = \mathrm{e}^{-x^2} \left[\frac{1}{2^k \Gamma\left(\frac{k}{2}+1\right)} M\left(\frac{k+1}{2}, \frac{1}{2}, x^2\right) - \frac{x}{2^{k-1}\Gamma\left(\frac{k+1}{2}\right)} M\left(\frac{k}{2}+1, \frac{3}{2}, x^2\right) \right], \tag{3.17}$$

Table 3.1: Critical time for the series expansion (3.10) to require at any position ζ more than one term to achieve a prescribed relative tolerance $\epsilon = |\tilde{\theta_0}^{(n+1)}/\tilde{\theta_0}^{(n)}|$, where $\tilde{\theta_0}^{(n)}$ is the nth term of (3.10).

ϵ	10^{-5}	5×10^{-5}	10^{-4}	5×10^{-4}	10^{-3}	3×10^{-3}
τ	0.043	0.10	0.16	0.39	0.56	0.99

where

$$M(k, m, x) = \sum_{j=0}^{\infty} \frac{(k)_j}{(m)_j} \frac{x^j}{j!}, \tag{3.18}$$

with

$$(\gamma)_j = \begin{cases} 1 & \text{if } j = 0 \\ \prod_{i=1}^{j} [\gamma + i - 1] & \text{if } j \geq 1 \end{cases} \tag{3.19}$$

and $\Gamma(x) = \int_0^\infty t^{x-1} \mathrm{e}^{-t} \mathrm{d}t$. This expression is specially more efficient than the recursive definition (3.11), for large values of k and x.

3.4 Results and discussion

On considering the solution of the base state (3.10), a relatively strong hypothesis is the truncation of the cosine series of the boundary condition (3.8c), resulting on a separable form, consisting of a product of a power of time and a function of ζ, a requisite to derive the linear similarity system (3.13). Considering two or more terms on the expansion (3.10) departs from such separability condition. Therefore, a restriction of this linear approach is time through the spatial derivative of the base state. Table 3.1 shows the relative difference between the truncated expansion for the boundary condition and that assumed herein. For instance, to achieve a relative tolerance in (3.10) lower than or equal to 10^{-4} with only the first term of the expansion, dimensionless time can be as large as 0.16 to preserve the validity of the self-similar system (3.13).

Figure 3.2 shows the eigenfunctions that result from (3.13) along with (3.14) and (3.15). Such disturbance curves result to penetrate deeper increasing the Prandtl number. As this number increases, the fluid, relatively more viscous, exhibits steeper temperature gradients, and thus tend to evolve more quickly to convection than when the retarding role of thermal diffusivity is more efficient. However, as the system will evolve to convection anyhow, times for the onset of convection are finite regardless the Prandtl number. Indeed,

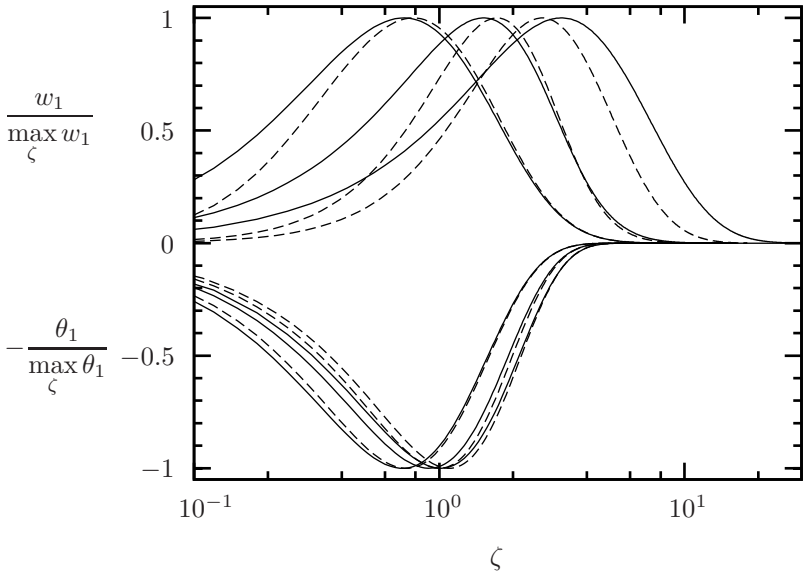

Figure 3.2: Normalized eigenfunctions resulting from the numerical integration of (3.13). Upper curves represent the vertical velocity disturbance while the bottom ones (minus) temperature disturbances. Solid lines represent the stress-free case in both sets, while dashed ones the no-slip kinematic boundary condition. In both cases, from left to right, computed results correspond to $\mathrm{Pr} = 0.01$, $\mathrm{Pr} = 1$ and $\mathrm{Pr} \to \infty$.

what the Prandtl number changes is not actually the absolute Rayleigh numbers necessary to find convection, but only growth rates, given a previous supercritical condition. On its original formulation, the energy method, conceived to define a boundary for global stability, yields critical conditions regarding solely on a limiting value of time and a Rayleigh number (Homsy, 1973; Joseph, 1966). Recently, Kim *et al.* (2008) have proposed a similar approach, introducing an explicit Prandtl-number dependence for the transient Rayleigh-Bénard problem.

The solution of the optimisation problem (3.16), given $n = 0$ and either a stress-free or no-slip condition, is a set of eigenvalues R_τ along with critical wavenumbers a_τ, both assumed correct whenever the self-similar behaviour is valid. It is observed a tendency to exponential curves for $R_{\tau,c}(\mathrm{Pr})$ as Pr becomes smaller. On the other extreme, where $\mathrm{Pr} \to \infty$, $R_{\tau,c}$ tends to an asymptotic value, equal to 229.77 and 84.51 for the no-slip and stress-free kinematic boundary conditions, respectively. According to present data, critical

Table 3.2: Parameters a_j of Eq. (3.20) for no-slip (R) and stress free (F) kinematic boundary conditions.

	a_j				
j	1	2	3	4	5
R	15.27	9.95	8.87	0.81	1.18
F	12.99	3.75	6.06	0.71	1.44

times can be estimated within a 2% error, for $0.01 \leq \mathrm{Pr} \leq 1000$, as:

$$R\tau^{7/2} = a_1 \left[a_2 + \left(\frac{a_3}{\mathrm{Pr}} \right)^{a_4} \right]^{a_5} \tag{3.20}$$

The corresponding coefficients are shown in Table 3.2. Figure 3.3 shows a plot of (3.20) using such coefficients for both kinematic boundary conditions.

The closest previous resemblance of present results corresponds to the case where a linear, rather than step, heating is applied, as reviewed in Goldstein & Volino (1995) and Ihle & Niño (2006*b*), respectively. Using scaling arguments similar to those employed to deduce (3.5), it can be shown that if $\mathrm{Ra}t^a = C$, imposing temperature and heat linearly imply that $a = 5/2$ and 3, respectively (Kim *et al.*, 2005; Yang & Choi, 2002*a*). It can be also shown that increasing the heat flux sinusoidally yields an exponent $a = 4$. Therefore, present scalings suggest that sinusoidal heating tend to delay the onset of convection in comparison when heating in a linearly and stepwise fashion, an intuitive consequence of the manner of heating.

Some figures can be obtained from the preliminary laboratory experiment referred to in Section 3.1. Considering molecular properties for the viscosity and thermal diffusivity of water with no slip where the temperature was imposed, $R \approx 1.64 \times 10^4$, while the observed/predicted dimensionless critical onset time ratio is $0.33/0.31 \approx 1.1$.

Unfortunately, available field and experimental data for onset times is not copious and, to the knowledge of the authors, no systematic field work has been done so far to the purpose of obtaining the time lag between temperature drop and mixing increase above the thermocline. In a recent field campaign oriented to study the effect of wind on mixing and the production of algae in Villarrica Lake, Chile, wind velocities, atmospheric and water temperature at different depths was obtained (Rozas, 2009). This lake, whose free surface altitude is 230 m.a.s.l., has an ellipsoidal shape with a maximum width (N-S direction) of 11.5 km and a maximum length (E-W direction) of 23.05 km. With a total surface and volume of 176 km^2 and 21 km^3, respectively, it is a 28c-type lake (Hutchinson, 1957;

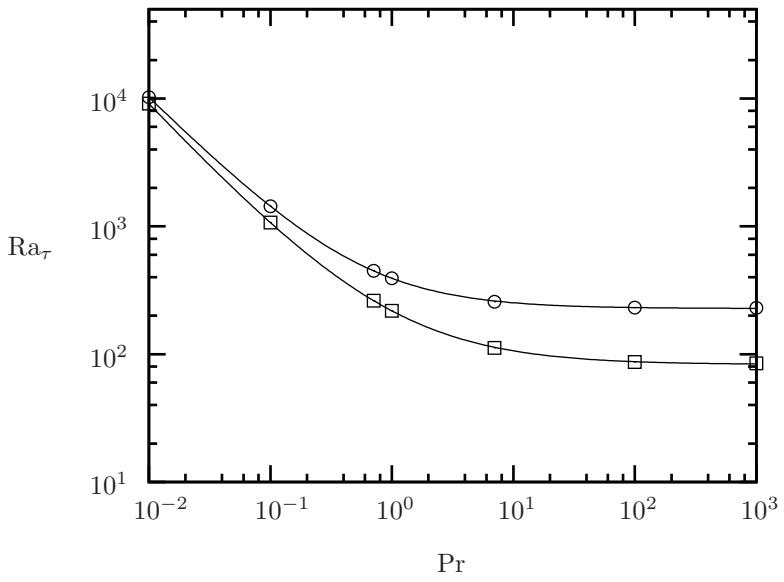

Figure 3.3: Upper panel: effect of the Prandtl number on Ra_τ for the no-slip (upper curve) and stress-free (lower curve) cases. Symbols represent calculated points, corresponding to $\mathrm{Pr} = 0.01$, 0.1, 0.71, 1, 7, 100 and 1000, respectively. Curves represent interpolated results using the models given by Eqs. (3.20) and parameter sets given by Table 3.2.

Rozas, 2009). During winter time, water temperature remains constant close to 10°C. Solar radiation during summer drives surface temperature until about 22.5°C during daytime (Campos *et al.*, 1983). At difference from winter, during summer there is a strong thermal stratification, where a marked thermocline is observed about 20 m depth (Meruane & Garreaud, 2005). During this season, evening and night ambient temperature dips below that of the water surface layer, giving way to penetrative convection (Imberger & Patterson, 1990). On the other hand, daytime (often strong) winds decrease to virtually 0 at midnight. Nightly water surface cooling events drive a daily change on the thermal structure of the column. To assess this effect, in the referred campaign a set of measurements using thermistor probes chains was made. Probes were placed every 2 m in the thermocline, and at larger spacings in the hypolimnion, eventually reaching a maximum depth of 80 m (Rozas, 2009). The meteorological station from where the ambient temperature and wind velocity was measured is located about 5 km South-West the lake. A normalized ambient and temperature surface temperature (0.5 m depth) and wind speed time series is shown in Figure 3.4 for the week between 6th February and 13th February 2009. The decrease on wind speed during nights is manifest. On the other hand, ambient temperatures amplitudes are on the order of 15°C. This makes surface temperatures have maximum amplitudes of about 2°C which, provided the absence of wind, is enough to induce mixing on the column. A typical picture of this process is shown in the water temperature column evolution between 10th and 11th February 2009 (Figure 3.5 with ambient conditions detailed on Table 3.3). During the nightly temperature drop, depicted in Figure 3.4, penetrative convection eases mixing, which is reflected on more uniform temperatures through out the column (11th Feb., 0:00 in Figure 3.5). As ambient temperatures rise, heating diminishes mixing and temperature stratification appears again. Although wind velocities are significant during daytime, kinetic energy transferred to the water column tends to keep it confined to the surface. In turn, the effect of surface cooling is to decrease potential energy in the system, thus deepening the thermocline in this short time scale.

From the results shown above, it is seen that mixing have a significant impact on the temperature distribution where the epilimnion is. An increased level of mixing implies a narrower temperature distribution and thus a smaller standard deviation. It is therefore expected that when maximum mixing occurs, the spatial standard deviation of temperature in the epilimnion should reach a minimum value. Figure 3.6 shows the mean and standard deviation of temperature for depths Z such as $0 \leq Z \leq 20$ m, compared to ambient temperature. It is defined here the minimum of the standard deviation of the epilimnion as a measure of the start of active mixing at diurnal scale. Vertical lines on Figure 3.6 present the surface cooling starting and assumed onset condition. For the case of Villarrica

Lake data analysed, mixing onset times defined this way are between 3.7 and 5.75 hours. Surface water temperature amplitudes are between 0.97 and 1.4°C. Considering a reference turbulent kinematic viscosity $\nu_t = 10^{-4}$ m^{2}s^{-1}, the same value for the turbulent thermal diffusivity and a typical forcing perdiod of 24 h, corresponding Rayleigh numbers as defined in (3.6), are between 4×10^5 and 5.7×10^5. Comparison between measured and estimated onset times using (3.20) are detailed presented in Table 3.4. Corresponding measured vs model onset times differ by factors between 8 and 18. This result somewhat resembles the factor of 10 found in Ihle & Niño (2006*b*) considering laboratory studies in the case of shear-free kinematic conditions and sudden cooling. However, present results are established under a specific onset time definition scheme.

Results can be also compared to those by Jonas *et al.* (2003). In their paper, it is observed a significant turbulent kinetic energy increase close to 3 hours after the maximum solar radiation point (during day 266). In terms of the present, nondimensional variables, this yields $\tau \approx 0.79$. Considering the same turbulent kinematic viscosity and turbulent Prandtl number as in the case of Lake Villarrica, and a reference temperature amplitude corresponding to 0.3°C, yields $R \approx 1.23 \times 10^5$. Using this value in (3.20) for the stress-free boundary condition yields a critical time equal to 0.16, close to 4.8 times too short than that observed in the field. Considering the approach as in Lake Villarrica, i.e., to define the onset times as the time when there is a maximum for mixing or, alternatively from their data, a maximum for the vertical velocity component, the corresponding onset time is about 6 hours after the maximum solar radiation point. Bearing this definition in mind, corresponding measured vs modelled onset times is 9.5, which is commensurate with those obtained from Villarrica Lake.

There are some points to note about present model and their comparison with field data. As eddy viscosity and thermal diffusivity have to be properly measured, present results cannot be considered as conclusive, but suggestive of the possibility to calibrate the model summarized in (3.20). On the other hand, it is noted that in the present stability analysis, it was used a sinusoidal forcing function. In real lakes, such a forcing is periodical but in general not sinusoidal. However, the proposed model can be extended to different periodical functions expressing them using a combination of Fourier modes, thus replacing (3.1) by an expression tractable in a similar manner to that presented herein, to derive in a different base state. This is another element that can be adapted to local conditions.

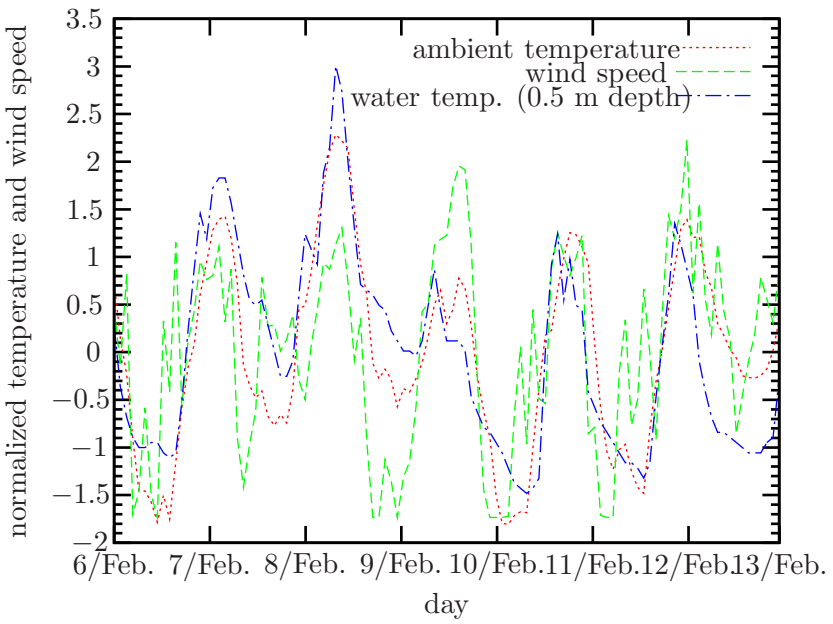

Figure 3.4: Normalized ambient temperature, water at 0.5 m depth temperature and wind speed time series between 6th February and 13th February 2009. Labels in the x-axis corresponds to noon. Variables χ were normalized to $\hat{\chi}$ as $\hat{\chi} = [\chi - \mu_t]/\sigma_t$, where μ_t and σ_t are the time average and standard deviation over the range of days considered. For wind speed, $(\mu_t, \sigma_t) = (1.6, 0.92)\,\mathrm{m\,s^{-1}}$. For ambient and water temperature, $(\mu_t, \sigma_t) = (16.6, 5.25)^\circ\mathrm{C}$ and $(\mu_t, \sigma_t) = (20.6, 0.45)^\circ\mathrm{C}$, respectively.

Table 3.3: Measured wind speed (w_s) and ambient temperatures (T_a) at times corresponding to those analyzed on Figure 3.5.

Date, time	w_s ($\mathrm{m\,s^{-1}}$)	T_a ($^\circ\mathrm{C}$)
10/Feb., 12:00	2.29	17.67
10/Feb., 18:00	3.40	20.69
11/Feb., 0:00	0.01	12.54
11/Feb., 6:00	1.60	7.94
11/Feb., 12:00	1.53	17.63

3.5 Conclusions

A model for the prediction of convective motions in a semi infinite Boussinesq fluid layer heated sinusoidally has been proposed using scaling arguments along with linear stability analysis. The present paper aims to predict onset times in a supercritical system in the

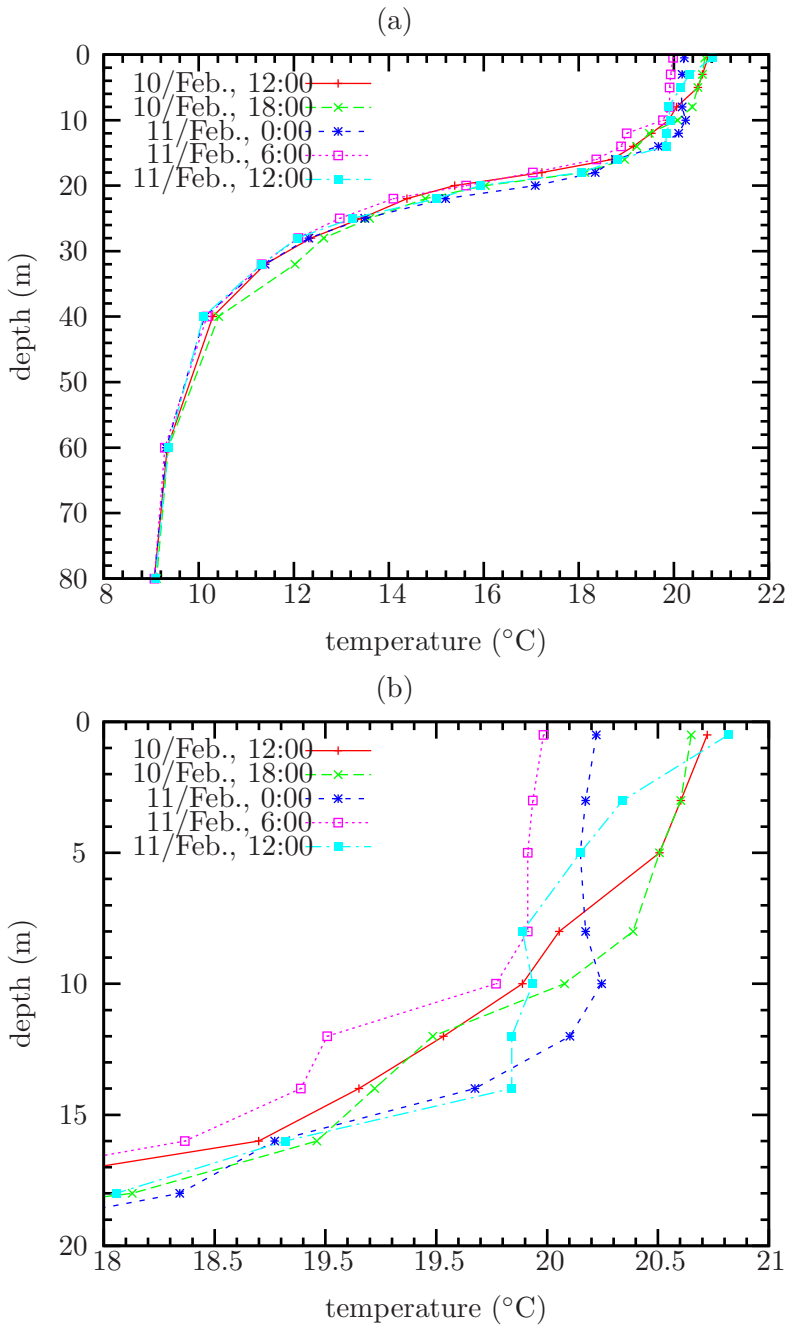

Figure 3.5: Thermistor probe measurements for different times between 10th and 11th February 2009. (a) Full depth, (b) detail of depths near the surface.

sense of Rayleigh-Bénard convection. Using scaling arguments it is suggested that $t \sim R^{-2/7}$, where R is a measure of the relative importance of buoyancy over viscous dissipation

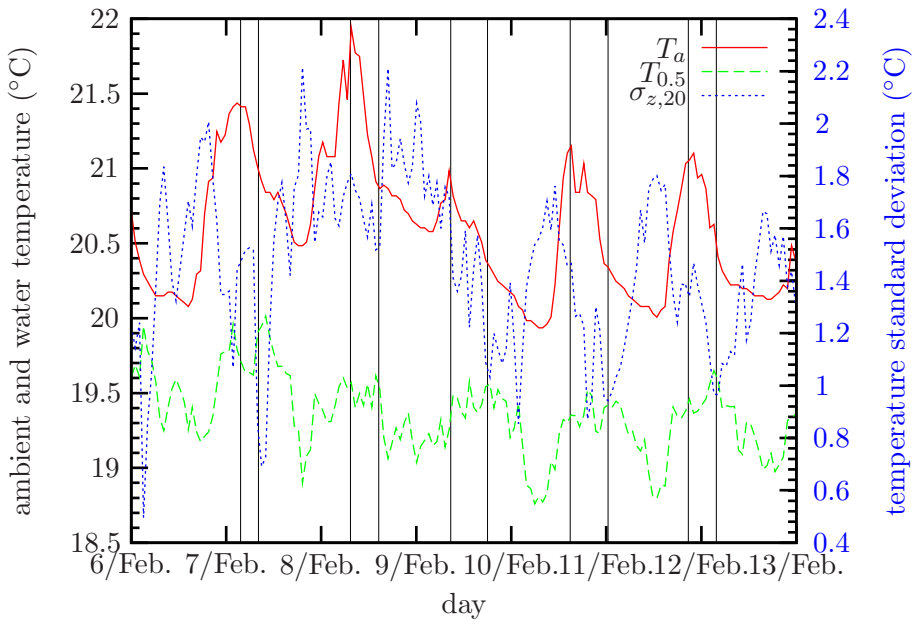

Figure 3.6: Time series for ambient temperature, T_a, temperature measurement at 0.5 m depth, $T_{0.5}$, and standard deviation of temperature over the epilimnion (defined to end at 20 m depth), $\sigma_{z,20}$, for days between 6th and 13th February 2009. Vertical thin lines corresponds to assumed times for start of cooling and onset of mixing. Labels in the x-axis corresponds to noon.

Table 3.4: Resulting dimensional onset times from field data and previous works.

		time (min)		
Date[1]	R	model	field	ratio
7/02	4.0×10^5	27.1	220	8.14
8/02	5.7×10^5	24.6	345	14.04
9/02	4.3×10^5	26.6	450	16.92
10-11/02	4.9×10^5	25.6	465	18.14
11-12/02	4.3×10^5	26.6	345	12.97
J03[2]	1.2×10^5	38	360	9.47
Average				13.27
Std. dev.				3.97

within a time-dependent, growing thermal boundary layer. Following the concepts of propagation theory, values for such proportionality constant as a function of the Prandtl number are proposed.

Although the large difference observed between predicted and available field data, even considering the various sources of error that comes out from them, along with the obvious uncertainties regarding the existence of a background flow prior to the start of surface cooling, the model seems to capture the essential features of the intended prediction. Time and length scales are on the same order of magnitude for values observed both in large systems as lakes, wherein $(\kappa/\omega)^{1/2} \sim 1$ m, and the present laboratory setup, with a length scale for disturbances on the order of the centimetre. Results were compared to experimental analysis and field measurements. Both for the field measurement campaign in lake Villarrica, Chile (Rozas, 2009) and the virtually windless case of lake Sopensee, Switzerland (Jonas *et al.*, 2003), there is a factor on the order of 10 between measured onset times and those determined using the proposed model. Interestingly, this trend was even found using rough approximations for eddy viscosity, thermal diffusivity and surface temperature pattern, thus suggesting opportunity for model improvement.

Chapter 4

Stability of impulsively-driven natural convection with unsteady base state: implications of an adiabatic boundary

This chapter, authored by Christian Ihle and Yarko Niño, was submitted in the form of research article to *Physics Letters A*.

Abstract

The energy method is used to estimate stability conditions of a horizontally infinite fluid layer with adiabatic bottom while the top is impulsively cooled. The effect of different kinematic boundary conditions is studied. This analysis, which takes into account that the base state for temperature is unsteady during the whole domain of time, predicts that the induced convection has lower critical Rayleigh numbers for stability than Bénard convection, in agreement with previous theoretical findings. Instability limits for such impulsively-driven convection are also investigated using a frozen time model, finding a very narrow gap between stability and instability thresholds. Critical stability curves for top free-bottom rigid and top rigid-bottom free kinematic boundary conditions exhibit a crossing point, according to both linear and nonlinear approaches. Such crossing concurs, as time increases, with the inset of a stronger influence of the bottom boundary on the balance between stabilizing and destabilizing effects. For large values of time, stability curves resulting from energy and

frozen time approaches exhibit the same temporal growth rate, but no asymptotic convergence, suggesting a bound for the temporal asymptotic behavior of the energy method.

4.1 Introduction

The onset of Rayleigh-Bénard convection in a horizontally infinite Boussinesq fluid layer of height d, subject to a vertical temperature difference, depends solely on the opposing effects of buoyancy and viscous forces in a time scale commensurate to that of temperature diffusion through the whole layer depth. Such balance is commonly expressed in dimensionless form using the Rayleigh number, $R = g\beta\Delta T d^3\nu^{-1}\kappa^{-1}$ (Drazin & Reid, 1981; Rayleigh, 1916), where g is the magnitude of the gravity acceleration vector, β, ν and κ are the coefficient of thermal expansion, kinematic viscosity and thermal diffusivity of the fluid respectively, and $\Delta T > 0$ is the characteristic vertical temperature difference. If the temperature profile that conforms the base state to perturbations is unsteady, time appears through the temperature evolution as a second variable that can play a role on the onset of convection. This sort of problem, referred to herein as URB, resembles many flows found in industry as well as in nature, which makes research on thermal convection to remain attractive, in terms of its application to practical problems, despite its long tradition. Examples can be found in industry (Kerr *et al.*, 1989) as well as in nature (Jonas *et al.*, 2003; Linden, 2001).

In the case of URB, the prediction of onset times for convection have been studied in the past by several authors using "frozen time" approaches, which correspond to an analogy of Rayleigh's analysis, considering time in the base state as a parameter and an exponential growth for disturbances. Alternatively, eigenfunction expansions of the temporal evolution of disturbances can be used to relax the, mathematically non-rigorous, separability assumption imposed upon the linear stability equation that is inherent to frozen time models. Such approach is known as the "amplification model" (see Goldstein & Volino, 1995; Homsy, 1973, and references therein for excellent reviews). The overall effect of unsteady heating have been estimated both using a frozen time model (Gresho & Sani, 1971) and the energy method (Homsy, 1973; Joseph, 1966), the latter being a non-linear approach based upon an energy criterion for stability. This method, has shown that the manner of heating positively affects global stability conditions: in particular, fast heating rates tend to make the system less stable (Neitzel, 1982; Wankat & Homsy, 1977), while the same conclusion have been obtained using an earlier, quasi-static approach (Currie, 1967).

A different and more recent method to predict onset times for convection is propagation theory (Yang & Choi, 2002*b*), a linear analysis technique that relies on the assumption that temperature and velocity disturbances mainly develop in a length scale commensurate with that of the advancing base state temperature front. It is applicable when the temperature base state admits a similarity solution, allowing time to be implicitly included in a

system of similarity linear disturbance equations, posing an eigenvalue problem in this new framework. This approach does not impose exponential growth rates for disturbances. A consequence of such relaxation is that, at difference with frozen time models, results depend on the Prandtl number ν/κ. Propagation theory have been used in a variety of problems involving different step and time-dependent boundary conditions for URB. A key result of such analyses is that theoretical times for the onset of convection have been found to be lower, by a factor of 1/4, than onset times detected experimentally (e.g Choi *et al.*, 2004*a*,*c*; Kim *et al.*, 2002, 2005; Yang & Choi, 2002*b*), and close to such factor when heating binary mixtures, where the Soret effect conditionally induce convection (Kim *et al.*, 2007), except when shear-free boundaries and a temperature step are imposed, where a factor of 1/10 is likely to fit better the data (Ihle & Niño, 2006*b*). In the last couple of years, a new linear stability analysis approach has been developed (Riaz *et al.*, 2006), considering the combination of a similarity space for disturbances (e.g. (Yang & Choi, 2002*b*)), combined with an ad-hoc eigenfunction expansion (Foster, 1965*a*; Robinson, 1976), to find onset time predictions largely independent of the initial conditions, thus improving a major drawback of the amplification model. Although the recently developed methodologies mentioned have been proved to yield good results in the prediction of onset times for highly supercritical systems, for which it is reasonable that layers behave as if they were semi-infinite and often similarity solutions for the temperature base state can be found, they give no information about the effect of the manner of heating in overall stability conditions of URB, where frozen time and energy approaches are applicable.

A similar problem to that posed in URB is the flow that results from imposing a temperature step on one side of the horizontally infinite fluid layer without letting heat flow through the opposite boundary. The study of the stability of this kind of system is the matter of the present paper. This configuration resembles that of nonpenetrative convection (Adrian, 1986), and for convenience, the acronym NPC will be used hereafter to refer to it. A key feature of NPC is that the base state never reaches a non-zero steady state, and hence there is not a straightforward steady counterpart to compare critical Rayleigh numbers with, as in the case of URB. For this system and high Rayleigh numbers, propagation theory has been used to predict onset times for convection (Ihle & Niño, 2006*b*), where it was proved that the outer, adiabatic boundary has no effect on convection onset times. On the contrary, this is not necessarily true for Rayleigh numbers slightly larger than critical ones, which is discussed in detail in this paper. Critical Rayleigh numbers for the onset of NPC have not been reported so far in the open literature. In the present paper, theoretical estimations of such values are proposed in the light of a frozen time model and the energy method, using several different kinematic boundary conditions. The energy method yields rigorous bounds for the stability of unsteady evolving systems.

It has been used in the past in the study of URB stability (Homsy, 1973; Neitzel, 1982; Wankat & Homsy, 1977), and very recently to determine reliable critical convective motion onset times and Marangoni numbers for evaporating droplets (Ha & Lai, 2004). Therefore, the energy method is understood as a proper way of assessing frozen time results. Indeed, it is shown here that instability onset times predicted using the frozen time method are consistent and close to those computed using the energy method. Limits for this behavior are proposed by analyzing results for large values of time.

4.2 Problem description

The system is an initially quiescent, horizontally infinite Boussinesq fluid layer of height d, at a constant temperature $T_{\max}$, subject to a sudden temperature drop $\Delta T_{\mathrm{NPC}} = T_{\max} - T_{\min}$ on its upper surface, while the bottom is kept adiabatic. This imposes a transient evolution of the temperature field, which can be merely conductive on the whole domain of time, or driven by the combined effects of conduction and natural convection from a certain time on, provided a minimum imbalance between viscous and buoyant forces exists. Scales for disturbances are d, d^2/κ, κ/d and ΔT_{NPC} for length, time, velocity and temperature, respectively. Notation for dimensionless variables is as follows: x, y denote horizontal coordinates, z denotes a vertical upwards coordinate with origin at the bottom boundary, u, v and w denote disturbance velocity components in the x, y and z directions, respectively, and $\bar{\theta} = (T - T_{\min})/\Delta T_{\mathrm{NPC}}$ is the base state normalized temperature (from now on denoted simply temperature). In the case of the energy method equations, $\mathbf{v} = (u, v, w)^{\mathrm{T}}$ and θ stand for the disturbance dimensionless velocity and temperature, whilst in the frozen time model, $\hat{\mathbf{v}} = (\hat{u}, \hat{v}, \hat{w})^{\mathrm{T}}$ and $\hat{\theta}$ are their analogue definitions.

A Rayleigh number depending on the temperature step ΔT_{NPC} is defined as

$$\mathrm{Ra} = \frac{g\beta\Delta T_{\mathrm{NPC}} d^3}{\nu\kappa}. \tag{4.1}$$

In NPC, in contrast with URB, since the bottom temperature is not fixed, the top and bottom temperature difference is a function of time. Therefore, the analogue to the top-bottom Rayleigh number definition in URB, R (as defined in the Introduction), is time-dependent. As $\bar{\theta}(z = 0, t) = (T_{\mathrm{bottom}} - T_{\min})/(T_{\max} - T_{\min}) = (T_{\mathrm{bottom}} - T_{\mathrm{top}})/\Delta T_{\mathrm{NPC}}$, it follows that a Rayleigh number in NPC based on the top and bottom temperatures can be expressed in terms of $\bar{\theta}$ and Ra as a modified Rayleigh number, $R_m = \mathrm{Ra}\,\bar{\theta}(z = 0, t)$. This parameter will be used to compare URB and NPC stability results. For instance, defining a URB constant top-bottom temperature difference numerically equal to ΔT_{NPC}, identifying $T_{\mathrm{bottom,\ URB}} = T_{\mathrm{max,\ NPC}}$ and $T_{\mathrm{top,\ URB}} = T_{\mathrm{min,\ NPC}}$, then $R_m = \mathrm{Ra}\,\bar{\theta}(z = 0, t) \leq \mathrm{Ra} = R$,

for any fixed value of t, given the same fluid properties, temperature difference and layer depth for URB and NPC problems. Although the control parameters Ra and R can be set to be equal, as in the previous example, this does not mean that the instability conditions associated with URB and NPC problems are the same. In fact, it is shown in this paper that eigenvalues of the respective stability equations are generally different, which in the context of the above example means that the initial temperature step required for the onset of convection in NPC and URB problems can be expected to be different for identical fluid properties and layer thickness.

4.3 Non-linear stability analysis

Limiting conditions for the stability of NPC are analyzed using the energy method. Details about the derivation of equations for this method are given elsewhere (Joseph, 1965; Joseph, 1966), so only some aspects concerning the interest of the present analysis are mentioned here. This approach relies on the definition of an energy functional, based upon a linear combination of kinematic and thermal components: $E = \langle |\mathbf{v}|^2/\mathrm{Pr} + \lambda \mathrm{Ra}\,\theta^2 \rangle$, where $\langle \cdot \rangle$ denotes integration over the fluid volume, with $\lambda > 0$ a coupling parameter.

According to energy theory, NPC convective motion can exist for a certain $t \geq t^*$ (Gumerman & Homsy, 1975) if $\mathrm{Ra} \geq \mathrm{Ra}^*$ (where $\mathrm{Ra}^* = \mathrm{Ra}(t^*)$ is the analogy of the critical Rayleigh number found in the Rayleigh Bénard stability problem with steady base state), provided disturbances exist from the beginning of the base state evolution. Following Homsy (1973), defining $\phi = (\lambda \mathrm{Ra})^{1/2}\theta$, a set of Euler-Lagrange equations can be deduced:

$$\frac{1}{2}\rho_\lambda \left(\frac{1}{\sqrt{\lambda}} - \sqrt{\lambda}\frac{\partial \bar{\theta}}{\partial z} \right) \nabla_h^2 \phi + \nabla^4 w = 0, \tag{4.2a}$$

$$\nabla^2 \phi + \frac{1}{2}\rho_\lambda \left(\frac{1}{\sqrt{\lambda}} - \sqrt{\lambda}\frac{\partial \bar{\theta}}{\partial z} \right) w = 0. \tag{4.2b}$$

Here, ∇^{2n} is the Laplacian operator applied n times and ∇_h^2 its horizontal version.

Initially, the system remains quiescent and $\bar{\theta}(t \leq 0, z) = 1$. For $t > 0$, $\partial\bar{\theta}/\partial z = \partial\phi/\partial z = w = 0$ at $z = 0$, $\bar{\theta} = \phi = w = 0$ at $z = 1$; besides, $\partial w/\partial z = 0$ is imposed on a rigid boundary and $\partial^2 w/\partial z^2 = 0$ on a free one (both types or kinematic boundary conditions are applied alternatively to top and bottom surfaces). ρ_λ is a Lagrange multiplier which is a solution

of the problem:

$$\frac{1}{\rho_\lambda} = \max_h \left\{ \frac{\langle w\phi \rangle}{\sqrt{\lambda}} - \sqrt{\lambda} \left\langle w\phi \frac{\partial \bar{\theta}}{\partial z} \right\rangle \right\} \tag{4.3a}$$

$$\langle \nabla \mathbf{v} : \nabla \mathbf{v} + |\nabla \phi|^2 \rangle = 1, \tag{4.3b}$$

where h is a function space that allows solutions for nonlinear disturbance velocity $\mathbf{v}$ and temperature θ (and hence ϕ) such that they satisfy prescribed kinematic and thermal boundary conditions, as well as $\nabla \cdot \mathbf{v} = 0$ (see (Homsy, 1973) and references therein for a more complete discussion). Noting that (4.2) can be decomposed into horizontal Fourier modes, if α is the dimensionless wavenumber of a horizontal wavevector and ρ_λ is the lowest eigenvalue of (4.2) with appropriate boundary conditions, the goal is to find an optimal solution:

$$\tilde{\rho} = \max_\lambda \min_\alpha \rho_\lambda \tag{4.4}$$

The term $\partial\bar{\theta}/\partial z$ is time-dependent, and so then is $\tilde{\rho}$. If the flow is strongly stable, i.e., if the energy decreases exponentially with time for arbitrary amplitude disturbances, then $\rho_\lambda > \sqrt{\mathrm{Ra}}$ (Joseph, 1965). This corresponds to the decreasing portion of the $\tilde{\rho}(t)$ curve that results from the solution of the problem (4.4) for different values of time (Homsy, 1973). The fluid layer will be globally stable for $\sqrt{\mathrm{Ra}} < \min_t \tilde{\rho}$.

Since λ is chosen to yield the largest eigenvalue of (4.2), it can also be a function of time, but system (4.2) is obtained under the assumption that λ is a constant. Generally, this is not a major obstacle for the analysis, as Homsy (1973) showed that the derivation just outlined still holds if $\mathrm{d}\lambda/\mathrm{d}t < 0$, and that, when ρ_λ^2 varies monotonically with time, the optimal lower bound for stability does not change if $\mathrm{d}\lambda/\mathrm{d}t \geq 0$. In the present case, for each of the kinematic boundary conditions imposed, corresponding minimum is achieved from monotonic curves $\rho(t)$, and consequently, computed optimal lower bounds are considered to be sound.

The shooting method and an optimization routine based on the Newton-Raphson iteration, whose validation has been previously reported (Ihle & Niño, 2006*b*), were used to solve the minimax problem (4.4). Time-dependent $\rho_\lambda(t)$ curves obtained for different boundary conditions are shown in Figure 4.1. Stability results for NPC are summarized in Table 4.1.

To validate the present application of the energy method, the analysis of unsteady URB was chosen, since results of a previous application of such method to that system are available (Neitzel, 1982). Critical stability parameters, i.e., minimum Rayleigh number, corresponding time and wavenumber, obtained with the energy method for the unsteady URB problem, are reported in Table 4.2, together with those obtained by Neitzel (1982),

with the exception of critical wavenumbers, which were not reported by him. Good general agreement between both sets of results was found. However, at difference with Neitzel's results, present computations show the existence of a subcritical minimum for the free-free condition. In the rest of the cases, correspondence among Ra^* values was found within the zero-decimal precision reported by Neitzel (1982). On the other hand, in every case, present results were observed to converge to the well-known steady state Ra^* values as $t \to \infty$ (Drazin & Reid, 1981).

Table 4.1: Critical overall stability bounds $(t^*, \mathrm{Ra}^* = \mathrm{Ra}(t^*))$ and their corresponding optimal wavenumbers α^* for NPC, obtained with the energy method (labeled as EM, in columns 2 to 5), and frozen time model (labeled as FTM, in columns 6 to 9), for different kinematic boundary conditions. $R_m^* = \mathrm{Ra}(t^*)\,\bar{\theta}(z=0,t^*)$. In the first column, the first kinematic condition corresponds to the upper boundary, which is cooled in every case, while the second one corresponds to the bottom boundary.

	EM				FTM			
Condition	t^*	α^*	Ra^*	R_m^*	t^*	α^*	Ra^*	R_m^*
Rigid-rigid	0.101	2.65	1 438.6	1 363.6	0.105	2.64	1 463.1	1 378
Free-rigid	0.087	2.28	825.4	798.1	0.092	2.27	840	806.8
Rigid-free	0.114	2.16	865.8	803.1	0.117	2.15	882.1	813.8
Free-free	0.103	1.8	452.4	427.4	0.106	1.79	460.6	433.1

Table 4.2: Critical overall stability bounds $(t^*, \mathrm{Ra}^* = \mathrm{Ra}(t^*))$ and their corresponding optimal wavenumbers α^* for URB using the energy method. Columns 5 and 6 show corresponding results by Neitzel (1982). The first kinematic condition corresponds to the upper boundary, which is cooled in every case, while the second one corresponds to the bottom boundary. When no critical time is given, curves decrease monotonically toward asymptotes in the (t, Ra) space.

	Present algorithm			Neitzel (1982)	
Condition	t^*	α^*	Ra^*	t^*	Ra^*
Rigid-rigid	0.138	3.12	1 699.4	0.14	1 699
Free-rigid	—	2.68	1 100.6	—	1 101
Rigid-free	0.085	2.69	1 012.9	0.08	1 013
Free-free	0.135	2.23	654.6	—	657.5

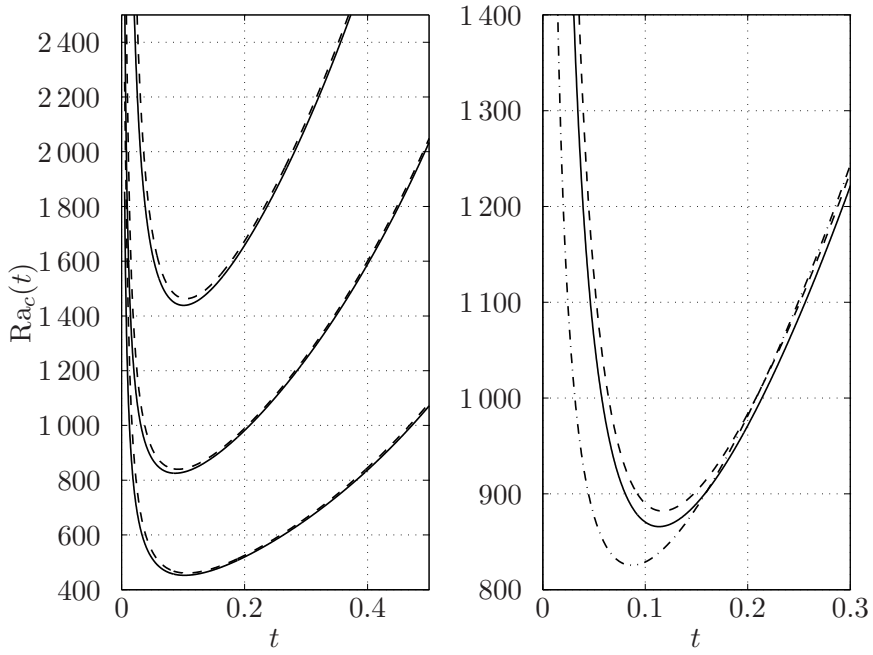

Figure 4.1: Critical NPC stability curves for fixed values of time, obtained from the optimization problem using the energy method, corresponding to system (4.4) (solid lines), and frozen time model, corresponding to equations (4.6) (dashed lines), respectively. Left panel: from top to bottom, curves corresponding to rigid-rigid, free-rigid and free-free kinematic boundary conditions, respectively. Right panel: curves corresponding to the rigid-free boundary condition. The dash-dotted line corresponds to the free-rigid critical curve computed using the energy method. The first kinematic condition applies to the top boundary.

4.4 Linear stability analysis

Limiting conditions for the instability of the NPC system are analyzed using the frozen time model. To derive the equations for this method, it is argued that NPC onset corresponds with the transition between the purely conductive and the conductive-convective states of the system. As the former state is independent of the Prandtl number, it is expected that the instability condition should also be independent of this parameter. The z-component of the linearized momentum and energy disturbance equations in the present system are, respectively:

$$\left(\frac{1}{\mathrm{Pr}}\frac{\partial}{\partial t}+\frac{\partial^2}{\partial z^2}-\alpha^2\right)\left(\frac{\partial^2}{\partial z^2}-\alpha^2\right)\hat{w}-\alpha^2\hat{\theta}=0 \tag{4.5a}$$

$$\frac{\partial\hat{\theta}}{\partial t}+\mathrm{Ra}\,\hat{w}\,\frac{\partial\bar{\theta}}{\partial z}-\left(\frac{\partial^2}{\partial z^2}-\alpha^2\right)\hat{\theta}=0, \tag{4.5b}$$

where $\hat{\theta}(z,t)$ and $\hat{w}(z,t)$ are first order disturbances of temperature and vertical velocity, respectively. Here, α and boundary conditions for disturbances have the same definition as in the energy approach.

In the frozen time model, time is treated as a parameter and hence solutions of the form $(\hat{\theta},\hat{w}) = [\theta_1(z), w_1(z)] \exp \sigma t$ are considered. This assumption turns the PDE system (4.5) into an ODE system that corresponds to an eigenvalue problem, where the latter can be found in spite of the fact that system (4.5) is not separable. The validity of this quasi-static approach requires that disturbances evolve much faster than the base state conductive heat flow, represented by the term $\partial\bar{\theta}/\partial z$. This is generally the case in the present analysis as is discussed next. Indeed, in the case of impulsively-driven URB, it has been shown (Gresho & Sani, 1971) that for supercritical systems (i.e., those with values of the Rayleigh number greater than the critical one for the onset of instabilities), growth rates of disturbances of frozen time model variations converge to those computed using transient analysis (Foster, 1965*a*), where disturbances are written in terms of Fourier series with time-dependent coefficients, turning system (4.5) into an eigenvalue problem subject to certain initial conditions. In their problem, the temporal threshold of validity suggested by Gresho & Sani (1971) is $t \sim 0.01$, such that for larger times the frozen time model would yield similar results as the transient analysis. Following the trend of this result, in the NPC system the quasi-static hypothesis is likely to be reasonable, as in the present analysis estimated values of the onset time of instabilities are on the order of 0.1. These values are computed from marginal stability curves, obtained by solving the optimization problem $\min_{\alpha,t} \mathrm{Ra}$, where

$$\left(\frac{\sigma}{\mathrm{Pr}} + \alpha^2 - \mathrm{D}^2\right)\left(\mathrm{D}^2 - \alpha^2\right) w_1 + \alpha^2 \theta_1 = 0 \tag{4.6a}$$

$$\sigma\theta_1 + \mathrm{Ra}\, w_1 \frac{\partial\bar{\theta}}{\partial z} - \left(\mathrm{D}^2 - \alpha^2\right)\theta_1 = 0 \tag{4.6b}$$

$$\sigma = 0, \tag{4.6c}$$

with $\mathrm{D}(\cdot) \equiv \mathrm{d}(\cdot)/\mathrm{d}z$. The marginal stability curves obtained are shown in Figure 4.1. Onset times, corresponding to the minima of these curves, are indeed of about 0.1. The marginal stability curves appear to be physically meaningful compared with global stability curves obtained with the energy method, as critical Rayleigh numbers and corresponding times are greater and lower, respectively, than those predicted by the energy theory. Nonetheless, although present results are thought to describe well the physics underlying the present problem, further verification with Foster's approach (Foster, 1965*a*), which is beyond the scope of the present paper, would give additional information about this point.

The present numerical algorithm, used for both the linear and non-linear analyses

reported in this paper, was also ckecked in the context of the frozen time model, using results of Gresho & Sani (1971) in the case of unsteady URB. In the rigid-rigid case, the present analysis yields a minimum of $\mathrm{Ra} = 1\,706.41$ at $t = 0.185$, whereas for the same case, Gresho & Sani (1971) computed $\mathrm{Ra} = 1\,706.36$ and $t = 0.186$, respectively.

4.5 Discussion

For small enough values of dimensionless time, when the thermal penetration depth is small compared with the thickness of the fluid layer, the effect of temperature and velocity disturbances is slight in contrast with the rapid evolution of the temperature base state. As a matter of fact, in the light of both of the approaches considered, in this time range the system exhibits critical Rayleigh numbers that are increasingly high as time decreases. On the other hand, in this time range, URB and NPC have the same instability behavior as they are independent of the boundary opposite to the step change in temperature (Ihle & Niño, 2006*b*). Writing a force balance taking into account the effects of viscosity, thermal diffusivity and buoyancy, it can be shown that $\mathrm{Ra}_c \sim t^{-3/2}$ (see also Jhaveri & Homsy (1982)). The validity of this relation relies on the assumption that the thermal boundary layer thickness scales with $\sqrt{t}$, which is true if $t \lessapprox 0.01$. If the dimensionless time is not so small, then the latter scaling is not valid, and the temporal behavior of the stability (as well as instability) of the system saturates to a minimum value of the Rayleigh number, which depends on kinematic boundary conditions on both sides, as shown in Table 4.1. In the present system, for larger values of time, the available heat from which an instability can give rise to thermal convection decays exponentially to zero with time. As it will be shown later, a consequence of this is that corresponding critical Rayleigh numbers must necessarily increase exponentially as time increases, at difference with URB where convergence to the steady state stability limit is obtained.

Data on Table 4.1 indicate that the NPC system becomes unstable before and at lower Rayleigh numbers than URB given the same kinematic boundary conditions. Previously, Joseph & Shir (1966) commented on the destabilizing effect of the Robin boundary condition (i.e., a generalization of that applied in the NPC problem, consisting of an isothermal boundary condition at one boundary and a heat flux boundary condition at the other), showing via manipulations of the set of energy Euler-Lagrange equations that the corresponding stability limit is a monotonically increasing function of the Nusselt number (Nu) on the boundaries. In particular, given kinematic boundary conditions, fixing the upper thermal boundary condition as isothermal and allowing the prescribed heat flux on the bottom to be set through Nu, according to Joseph & Shir (1966), the lowest stability boundary will be found for $\mathrm{Nu} = 0$, that is, for the NPC setup. The lack of heat flow

on the bottom precludes compensation of the buoyant force exerted downwards to fluid parcels due to the cooling on top by other volume forces from the bottom, such as the upwelling force that exists in the URB case, caused by the heating at $z = 0$. Therefore, the numerical results found in the light of the energy method are consistent with present and previous predictions for URB and also thought to be physically appealing.

Experimental data for the minimum Rayleigh number necessary for NPC are available only for the rigid-rigid case (Soberman, 1959), for which a critical time-dependent condition of $R_m = 1\,700$ was found. This is consistent with the theoretical R_m lower bound reported here, equal to 1 363.6 (Table 4.1).

The relationship between critical or onset times predicted by the energy method (i.e., times that minimize the energy functional) in NPC and URB depends on upper and lower boundary conditions. According to results shown in Tables 4.1 and 4.2, dimensionless onset times in NPC (0.101 and 0.103) are lower than those in URB (0.138 and 0.135) for rigid-rigid and free-free cases, respectively. The opposite is true in the rigid-free case, with onset times of 0.114 and 0.085 for NPC and URB, respectively. No comparison of critical times can be done in the free-rigid case, since in URB, monotonic convergence to the steady state critical value was achieved, both in the present work and in Neitzel (1982). Regarding computed results for NPC using both approaches, it is readily apparent from Figure 4.1 that, given fixed boundary conditions and values of time, linear and nonlinear results are similar, being critical Rayleigh numbers yielded by the frozen time model always greater to those produced by the energy method, with relative differences on the order of 0.02.

Stability (and instability) curves corresponding to the free-rigid and rigid-free cases cross each other for times equal to 0.161 and 0.175 according with energy and frozen time computations, respectively (Figure 4.1). In the free-rigid case, the system can experiment convective motion before and with a lower Rayleigh number than in the rigid-free system, due to the lack of restrictions for the generation of a horizontal flow on the top lid. As time goes on, the vertical heat flux space derivative near the bottom, $\partial q/\partial z(z = 0, t) = -\partial\bar{\theta}^2/\partial z^2(z = 0, t)$, departs from zero (Figure 4.2), and an interplay between this evolution and the kinematic boundary condition sets in. It is interesting that the mentioned curve crossing occurs, according to both methods, very close to the maximum of $\partial q/\partial z(z = 0, t)$, found at $t = 0.167$. After this time, rigid-free curves dip slightly below free-rigid ones toward an asymptotic difference, to be analyzed below.

It can be argued whether the increasing portions of the set of marginal stability curves corresponding to Figure 4.1 can be possibly reached experimentally. Although it is quite difficult to suppress experimentally every natural source of disturbance, which would be one way to retain the stability of the system after the critical onset time at a higher Rayleigh number than that corresponding with the global minimum, it may be possible

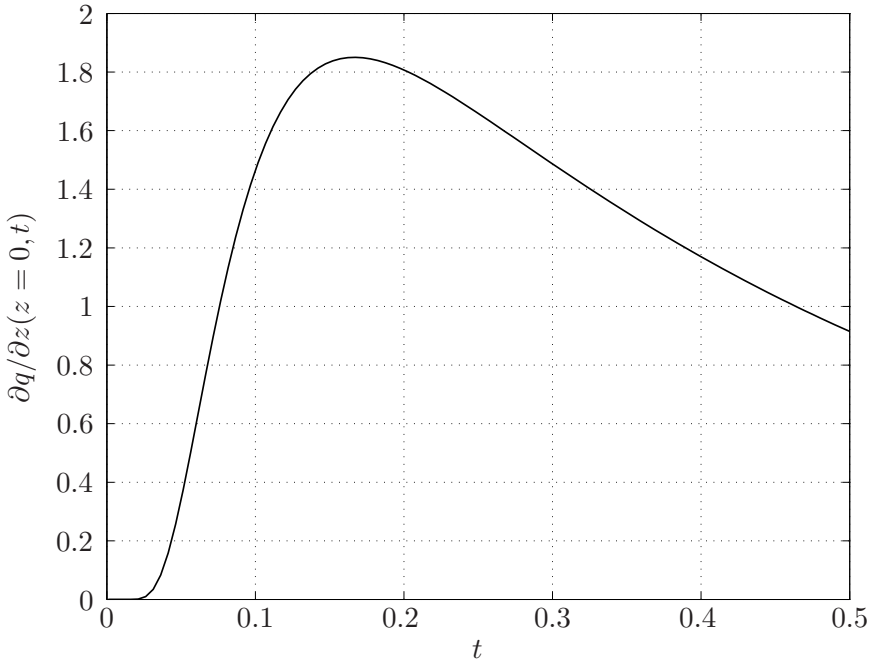

Figure 4.2: Vertical gradient of the base heat flux at $z = 0$, $\partial q/\partial z(z = 0, t) = -\partial\bar{\theta}^2/\partial z^2(z = 0, t)$. The maximum occurs at $t = 0.167$.

to suppress convection through the use of active control systems (see, e.g., Howle, 1997), shifting critical Rayleigh numbers significantly (Tang & Bau, 1993). Thus, the discussion of conditions for stability at large values of time is considered meaningful in physical terms.

It is noted that for large values of time, the base state vertical base heat flux can be approximated as:

$$\frac{\partial\bar{\theta}}{\partial z}(z, t \gg 0) \approx -2\sin\left(\frac{\pi z}{2}\right)\exp\left(-\frac{\pi^2}{4}t\right). \tag{4.7}$$

In particular, this is a very good approximation of $\partial\bar{\theta}/\partial z$ for $t \gtrapprox 0.4$.

Using the energy method, Joseph & Shir (1966) have shown that the value of the coupling parameter, λ^*, that maximizes problem (4.4), thus making $\partial\rho_\lambda/\partial\lambda = 0$, satisfies $\lambda^* = -\langle w\phi\rangle/\langle w\phi(\partial\bar{\theta}/\partial z)\rangle$, where in the present case,

$$\lambda^* \approx \frac{\langle w\phi\rangle}{2\langle w\phi\sin(\pi z/2)\rangle}\exp\left(\frac{\pi^2}{4}t\right) \geq \frac{1}{2}\exp\left(\frac{\pi^2}{4}t\right), \tag{4.8}$$

showing that the critical coupling parameter has an exponential factor (with a dimensionless time constant equal to $4/\pi^2$) for large values of time. Although $w\phi$ is also a function of time, from numerical computations it is evident that the latter dependence vanishes for large enough dimensionless times (in the present case, on the order of 0.5).

Computed prefactors $\langle w\phi\rangle/\langle 2w\phi\sin(\pi z/2)\rangle$, extrapolated for large values of time, are 0.76, 0.72, 0.85 and 0.8 for the rigid-rigid, free-rigid, rigid-free and free-free cases respectively. Critical Rayleigh numbers, $\rho^2_{\lambda^*}$, exhibit the same growth rate, as can be readily checked using (4.3a) for λ^* and (4.8). Corresponding prefactors for such growth rate, Ra_∞, along with their corresponding wavenumbers, α_∞, are shown in Table 4.3.

In the case of the linearized equations, for large values of time, a temporal dependence of eigenvalues can be set to compensate the exponential decrease of the base state gradient. This can be achieved in the present case if $\mathrm{Ra}(t) \sim \exp(\pi^2 t/4)$. Thus, system (4.5) is separable, and the assumption of an exponential growth of disturbances is mathematically consistent. Marginal condition for this case corresponds to $\sigma = 0$ (Pellew & Southwell, 1940), and equations turn to the following eigenvalue problem:

$$(\mathrm{D}^2 - \alpha_\infty^2)^2 w_1 - \alpha_\infty^2 \theta_1 = 0 \tag{4.9a}$$

$$Ra_\infty w_1 f(z) - (\mathrm{D}^2 - \alpha_\infty^2)\theta_1 = 0, \tag{4.9b}$$

with $f(z) = -2\sin(\pi z/2)$. Results for the different boundary conditions considered are shown in Table 4.3, where it is observed that minimum differences between stability and instability are not asymptotically zero, though very small. As the frozen time model becomes progressively better with time, lack of convergence among energy and frozen time approaches, must be due to the bound limitation given by construction of the energy method. For values of dimensionless time greater than about 0.2, the difference between energy and frozen time critical Rayleigh values is nearly constant. Figure 4.3 shows this trend, where the ratio r_f/r_e is plotted as a function of time, with $r_f = \mathrm{Ra}/\mathrm{Ra}_\infty$ using the frozen time model and $r_e = \mathrm{Ra}/\mathrm{Ra}_\infty$ using the energy method (see also Table 4.3). This result supports the validity of computations obtained with the frozen time model, as their difference with asymptotic ones (which are more accurate for larger values of dimensionless time) are slight.

4.6 Conclusions

The onset of Rayleigh-Bénard convection depends on two aspects, namely, the relative importance of the overall temperature difference, fluid properties and layer depth and, on the other hand, the influence of the manner of heating both in time and in the existence of subcritical stability thresholds. The first topic has been covered early in the 20th century, while the latter more recently, motivated by the large number of applications in industry and environment. Related to this family of problems is that of the stability of an infinite Boussinesq fluid layer with one side kept adiabatic while the other is subject to a

Table 4.3: Wavenumbers and prefactors for Rayleigh numbers, given by $\mathrm{Ra}_\infty = \mathrm{Ra}(t)\exp[-\pi^2 t/4]$, valid for large values of time ($t \gtrsim 0.5$), obtained with the energy method (labeled as EM, in columns 2 and 3), and frozen time model (labeled as FTM, in columns 4 and 5), for different kinematic boundary conditions.

	EM		FTM	
Condition	α_∞	Ra_∞	α_∞	Ra_∞
Rigid-rigid	2.61	995.9	2.61	1 004.4
Free-rigid	2.25	592	2.25	596.2
Rigid-free	2.14	580.8	2.13	587.5
Free-free	1.78	311.9	1.78	314.9

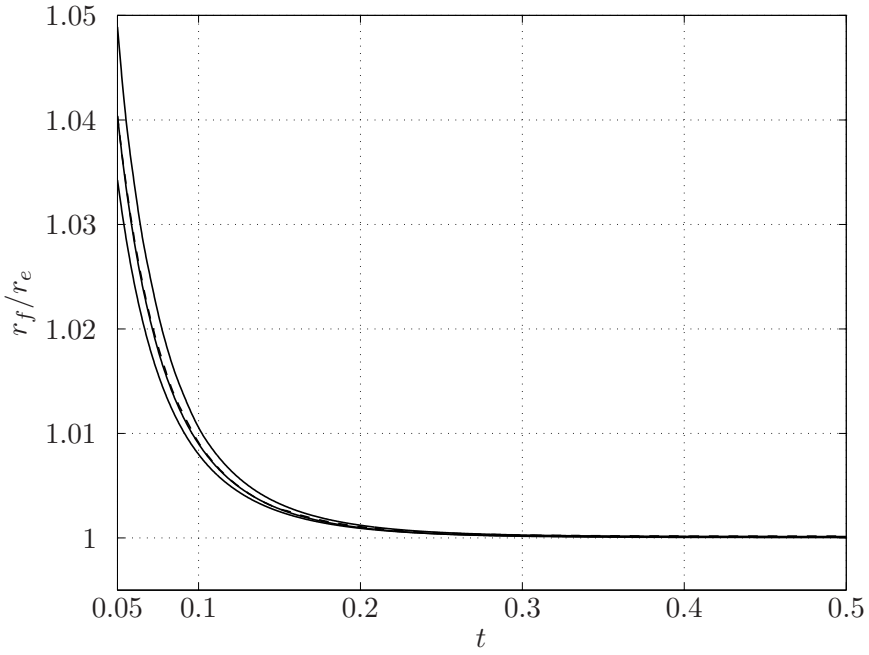

Figure 4.3: Temporal evolution of the quotient r_f/r_e, where $r_f = \mathrm{Ra}/\mathrm{Ra}_\infty$ using the frozen time model and $r_e = \mathrm{Ra}/\mathrm{Ra}_\infty$ using the energy method (see Table 4.3 for corresponding values and definitions). Upper and lowermost curves represent the rigid-free and free-rigid cases, respectively. The dashed, central curve corresponds to the free-free case and the remaining one, the rigid-rigid condition. The first condition applies to the top boundary.

temperature step, labeled herein as NPC. Onset times for such system were recently studied with both theoretical and experimental approaches (Ihle & Niño, 2006*a*,*b*). However, the basic question regarding the minimal control parameter values and maximal expected times

to observe convective patterns remained unanswered. This paper fills such gap.

Nonlinear and linear stability analyses of NPC, obtained from the application of energy theory and the frozen time model, respectively, were presented and discussed in this paper. Given the thermal boundary conditions imposed, the base state of the system is unsteady on the whole domain of time. Overall stability and instability thresholds, expressed in terms of critical onset times and Rayleigh numbers, were presented for different kinematic boundary conditions, including rigid or free top and bottom surfaces. The marginal stability curves obtained from both linear and nonlinear approaches are very close to each other and considered to be physically meaningful, as critical Rayleigh numbers and corresponding times obtained with the frozen time model (representing the instability limit) are greater and lower, respectively, than those predicted by the energy theory (representing the stability limit). Results show that the present system becomes unstable before and with lower Rayleigh numbers than Rayleigh-Bénard convection, in agreement with previous theoretical findings for the type of thermal boundary conditions associated with both systems. Critical stability curves (i.e., critical Rayleigh number versus time) for free-rigid and rigid-free cases exhibit a crossing point, according to both linear and nonlinear approaches. It is suggested that such crossing represents a transitional stage at which the influence of the bottom boundary becomes stronger than that of the top one, on the balance between stabilizing and destabilizing effects. Using both the energy method and the frozen time model, the latter was found to occur near the maximum value of the gradient of the base state vertical heat flux at the bottom of the fluid layer. At difference with unsteady Rayleigh-Bénard convection, an exponential growth of eigenvalues was found at large values of time, using both the energy method and the frozen time model. In both cases, the time constant for such growth is the same. However, prefactors do not converge, but slightly and consistently differ. Since as time increases the frozen time approach becomes increasingly more accurate, this result suggests a bound for the temporal asymptotic accuracy of the nonlinear energy method.

Acknowledgements

The authors gratefully acknowledge support from the Chilean National Commission for Scientific and Technological Research, CONICYT, the Department of Civil Engineering of the University of Chile, and Fondecyt Project No. 1040494.

Chapter 5

Simultaneous particle image velocimetry and synthetic schlieren measurements of an erupting thermal plume

This chapter is published as research paper, authored by Christian Ihle, Stuart Dalziel and Yarko Niño, in *Measurement Science and Technology*, volume 20 (2009), p. 125402.

Abstract

A technique to simultaneously extract Particle Image Velocimetry (PIV) and Synthetic Schlieren (SS) information from a two-dimensional flow field is proposed and exemplified with simultaneous velocity and density measurements of the eruption of a laminar thermal line plume. The proposed experimental method employs colour separation in conjunction with two video cameras in order to unambiguously separate the conflicting requirements of both measurement techniques, PIV and SS. This allows true simultaneous measurements, in contrast to previously published approaches. In the present experiments, a precision better than 10^{-3} K and 0.02 mm s^{-1} was obtained for temperature perturbations and velocity, respectively. The measured temperature field shows perturbations of less than 0.1 K as the induced plume first erupts, driving a vortical structure with velocities of around 2 mm s^{-1} that propagates out in front of the developing thermal structure. The present application of the experimental technique has provided an estimation of the critical Rayleigh number for plume eruption, with excellent agreement with previous works.

Keywords: PIV, synthetic schlieren, thermal convection, velocity measurement, density measurement

5.1 Introduction

Particle Image Velocimetry (PIV; Adrian, 1991; Sveen & Cowen, 2004) has become the most widely used, non-intrusive technique for extracting velocity information from experimental flows. More recently, the pattern matching ideas on which PIV are based were extended to develop Synthetic Schlieren (SS; Dalziel *et al.*, 2007, 1998, 2000; Sutherland *et al.*, 1999) which provides whole-field density measurements. An almost identical approach (known as Background Oriented Schlieren) was developed slightly later by Richard & Raffel (2001). Researchers studying fluids with varying density (whether due to changes in the composition or temperature) typically desire both velocity and density measurements, making the simultaneous use of PIV and SS an attractive proposition. Whereas PIV typically requires a sheet of light illuminating suspended particles, the background 'texture' required for SS must be strongly illuminated to give sufficient depth of field for the optical system. Various approaches have been used for quasi-simultaneous measurements, typically interleaving PIV and SS images. Richard & Raffel (2001) (see also Meier, 2002) used stroboscopic illumination of the background in a study of the compressible vortices shed behind a cylinder. In a study of two-dimensional internal gravity waves, Sveen & Dalziel (2005) back-illuminated their PIV particles using an LCD monitor that alternated between displaying a uniform illumination for PIV and a textured image for SS, using a single camera to capture both diagnostic images. The SS processing took account of the PIV particles, that otherwise contaminated the SS image.

An alternative approach was proposed in Dalziel *et al.* (2007) and exemplified with a study to determine the gradient Richardson number in an internal solitary wave. They removed some of the limitations of the earlier technique in this two-dimensional flow. In particular, they used two cameras, one of them dedicated to PIV and the other to SS. Also, they used two different light sources: one for PIV and the other for SS. The first provided a light sheet and was kept on all the time, while the second, as in the earlier study by Sveen & Dalziel (2005), was pulsed using a fast response LCD monitor to generate an interleaved image sequence.

A further approach to simultaneous PIV and SS is proposed herein. As in Dalziel *et al.* (2007), two cameras and two light sources are used, one each for velocity and density fields. However, in contrast to the previous approach, a separation in colour is used rather than interleaving images in time. This colour separation permits both light sources to be maintained continuously, thus allowing true simultaneous measurement. We illustrate this new approach by considering a starting thermal plume erupting from a line heat source. For the present study a separate computer is used for each camera, although with newer framegrabbers both cameras could have been handled by the same computer.

5.2 Experimental set-up

A tank, with internal dimensions of $370 \times 165 \times 250$ mm (length×width×height) comprising 15 mm acrylic walls and a 0.5 mm copper base, was filled with water. The heat source, consisting of a linear array of eight single stage, square Peltier devices, with sides of size $d_+ = 15$ mm, working as heaters (inducing fluid temperature changes on the order of 0.1 K), was installed across the width of the tank (midway along its length) and attached to the outside of the base. Their position was fixed using an aluminium block that connected them thermally to a heat exchanger held at room temperature by a constant temperature circulator. To either side of the Peltier devices, 20 mm polystyrene foam was used to insulate the gap beneath the copper base. The tank was fitted with a 50 mm polystyrene lid to minimise the influence of evaporative cooling.

The experiments were simultaneously visualised over a 50×30 mm region, by the two synchronised video cameras (Fig. 5.1). The SS texture (consisting of 0.4 mm diameter clear dots randomly distributed on a black background printed on overhead transparency film) was located 167 mm behind the tank and viewed by a Jai CVM4+CL digital video camera (with a resolution of 1320×1024 pixels, here recorded at 8 bits) located 3 m from the tank and fitted with a 2× adapter on an Olympus 135 mm telephoto lens. Backlight for SS is provided using a 5 W cyan Luxeon V power LED from a stabilised constant-current power supply. A second, identical video camera, this time fitted with a 25 mm f0.95 Vortex lens and a red dichroic filter, was used for imaging the PIV particles. The light source for the PIV particles, a 300 W Cermax arc lamp with a parabolic reflector, illuminated 63–71 μm Pliolite S5E tracer particles with a mean concentration in the images of 78 particles/cm^2. The red filter on the PIV camera blocked the cyan light illuminating the SS texture while permitting the tracer particles to be imaged.

The PIV camera CCD was aligned vertically with that of the SS camera. However, it was located at 54.5 cm from the plane of the light sheet, 70 mm to the right of the optical axis of the SS camera. This 7.3° misalignment of the cameras was the minimum necessary to prevent the PIV camera from interfering with the view of the SS camera. (It is worth noting that the misalignment at the central plane of the tank is reduced to around 5.5° taking into account refractive index effects.) The PIV camera distance was chosen to maximise resolution while keeping particles focused. As a result from this setup, the SS field of view magnification was 1.87 times that of the PIV. The processed measurements from both fields of view were mapped to world coordinates using a reference grid immersed in water. The positional error in our mapping procedure is estimated at less than 0.14 mm, or about 0.3% of the width of the field of view.

If no precautions were taken, ambient thermal noise in the laboratory would have ren-

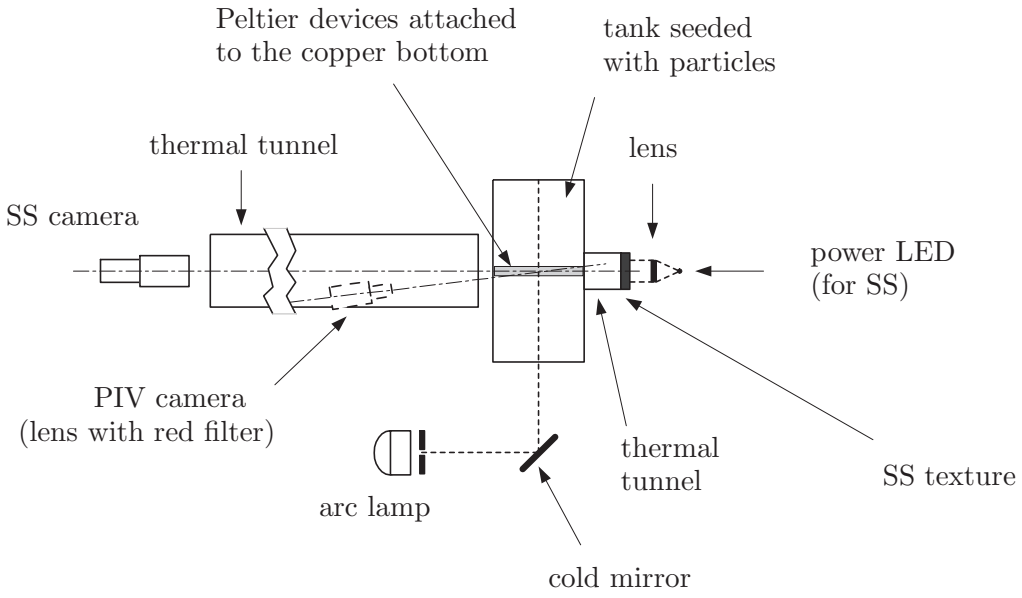

Figure 5.1: Plan view of the optical setup. The width and depth of the tank are 400 and 200 mm, respectively.

dered signal-to-noise ratio levels from the SS experimental data unacceptable. In addition to the installation of physical shielding and insulation, the experiments were automated and run overnight when the laboratory's thermal environment was most quiescent and no personnel were present to disturb the conditions.

Each set of experimental runs was conducted as follows. A LabView routine retrieved the control parameters, then requested DigiFlow (Dalziel, 2007) on the master computer to start the video capture. DigiFlow relayed this onto the instance of DigiFlow on the slave computer, synchronising the start of the capture, then informed LabView it was ready to start the experiment. Complementary temperature information was measured above and below the bottom plate of the tank using thermocouples. LabView logged temperature and power supply current information while an experiment was in progress. Given the relatively low Reynolds number of the flow, all of the present experiments were recorded at a sampling rate of 8 frames per second for video and 2 samples per second for voltage, current and temperature. Monitoring of the flow features and signals was done remotely and thus did not disrupt the course of experiments. Between each run the system was cooled and mixed for 5 minutes with the help of a peristaltic pump that recirculated the water inside the tank, then allowed to settle for 40 minutes before the next experiment was started.

Inevitably, despite our efforts to achieve homogeneous, quiescent initial conditions in the tank, there was some, although slight, residual thermal stratification and motion in most of the experiments. As our SS was only able to measure the perturbation relative to this initial density gradient, and our thermocouples were only accurate to 0.5 K, we cannot be sure of the precise initial thermal stratification. However, based on our SS measurements after the start of the experiment, we believe that at $t = 0$ the stratification was stable with temperature differences of less than 0.03 K with a bulk temperature of 295.5 K, comparable with the ambient temperature in the laboratory. This weak stable stratification is consistent with our measurements of a weak essentially horizontal drift to the right (~ 3 pixels/s $= 0.15$ mm s^{-1}) prior to the commencement of heating.

PIV and SS processing was completed using DigiFlow. For PIV, an adaptive, multipass algorithm was used in conjunction with interrogation windows 25×25 pixels at a spacing of 12 pixels. Estimates of the precision of the velocity measurements exceed 0.3 pixels/s $=$ 0.02 mm s^{-1}. The pattern matching algorithm, evolved from that presented in Dalziel *et al.* (2000) and Sveen & Dalziel (2005), largely avoids the problems of peak-locking seen in traditional PIV algorithms.

Similar pattern matching algorithms optimised for SS were employed on 21×21 pixel windows at a 12 pixel spacing for the density measurements. Here the precision is estimated as better than 0.02 pixels (the precision of $\nabla\rho'/\rho_0$ is better than 5×10^{-5} mm^{-1}, where ρ' and ρ_0 are the perturbation and reference densities, respectively), based on measurements of the constant temperature prior to the start of the experiments. The precision estimate is consistent with that found in an earlier test using a translated static pattern (Dalziel *et al.*, 2000). (The improvement in accuracy for SS measurements over those for PIV arise largely due to the effect of PIV particles entering and leaving the light sheet within the time interval used in the analysis, a problem that is absent in SS.) The corresponding precision achieved for the line-of-sight averaged temperature is better than 10^{-3} K.

Based on the analysis by Dalziel *et al.* (2007) applied to the present geometry, the apparent displacement of the particles due to refractive index gradients in the flow is around 6% of the apparent displacement of the texture, which is itself less than around 2 pixels, giving a maximum error in the position of a vector of less than around 1% of the spacing between the vectors. As the rate of change of the density gradient is itself small compared to the frame rate, the error in the velocity due to refractive index effects is much lower again and substantially less than other sources of error. We may, therefore, safely overlook any correction of the PIV results (Dalziel *et al.*, 2007; Elsinga *et al.*, 2005) for refractive index variation.

5.3 Results

Fig. 5.2 shows a sequence of simultaneous measurements of velocity and temperature for a plume driven by a heat flux of $q = 0.67$ W m^{-1}. The dashed box shows the spatial extent of the SS measurements, which is smaller than the region in which PIV was performed. Within a few seconds after switching on the heater, a boundary layer begins to grow, both vertically above and at the same time horizontally away from the heater. Horizontal thermal boundary layer growth is driven primarily by the rapid thermal diffusion through the 0.5 mm copper base, effectively increasing the width of the heat source as $(\kappa_b t)^{1/2}$ for early times, where κ_b is the effective thermal diffusivity of the base. The vertical growth continues until the boundary layer reaches a critical thickness. This critical thickness marks the plume eruption, a phenomenon that has been related to a critical Rayleigh number (Howard, 1966), with the flow assuming a length scale commensurate with the thickness of the thermal boundary layer. The beginning of the eruption is shown in Fig. 5.2a. Surprisingly, the temperature above the heater seems to be lower than that of the ambient fluid. This is due to the relatively weak stable stratification existing initially at the base of the tank, which is forced upwards as the fluid warmed by the heater begins to swell away from the lower boundary. Fluid at this relatively cool temperature continues to exist, almost undisturbed apart from a slight movement towards the heater, close to the base to either side of the heater.

The circulation visible above the heater in Fig. 5.2a becomes more pronounced by $t = 75$ s (Fig. 5.2b), where the positive temperature perturbation is beginning to be visible a few millimetres above the base of the tank. It is clear that this circulation, which must arise due to baroclinic generation of vorticity, moves out in front of the emerging thermal signature, but the core of this circulation is not marked by a stronger temperature perturbation. The measurements suggest that most of the initial 0.5 s^{-1} vorticity is deposited near the base of the tank. It is possible that entrainment of the slightly cooler, stably stratified fluid near the base of the tank has reduced the buoyancy. It could be argued that, as the PIV measurements are for a single plane whereas the SS measurements are line-of-sight averages, the lack of a strong temperature perturbation at the core of the vorticies could be due to three-dimensional motions in the plume. However, based on the subsequent development in this experiment, and on similar observations in a set of preliminary experiments, we believe this vortical structure is essentially two-dimensional and driven by inertia resulting from earlier baroclinic vorticity generation.

By $t = 95$ s (Fig. 5.2c), the rising thermal plume is clearly visible, carrying warm fluid (with temperatures elevated by around 0.1 K) away from the boundary above the heater. The circulation seen at earlier times is now outside the region in which we have

SS measurements (indicated by the dashed box in Fig. 5.2), but it appears likely that the temperature of this circulation remains essentially that of the ambient.

Due to its sensitivity, SS proves an interesting approach to measure this kind of flow, induced by subtle changes in density. Some explanation of our method for integration of the SS gradient fields to obtain the temperature perturbation is required in order to better understand the limitations of the results given by the method. The vector field of apparent displacements measured by SS, in general, have both an irrotational and a rotational component, although the density gradient itself is irrotational, by definition. We make the projection of the measured apparent displacement field onto an irrotational space unique by minimising the root mean square value of the rotational contribution. The solution of this least squares problem, solved using a multigrid algorithm similar to that often employed for the Poisson equation (Hazewinkel *et al.*, 2010), then leads naturally to the density perturbation, although there is a single arbitrary constant of integration that is left unresolved. For the present results, we impose the average value of the density perturbation in a region towards the top-left corner of the SS measurement domain to remain equal to zero. We justify this by noting that the density perturbation and the flow in this region should remain small for all times with an only weak velocity from the left due to the imperfect initial condition. However, we recognise that there may be a net change in the temperature of this region as the flow develops, and such a change will offset the temperature perturbation shown here. As the background motion is much weaker than that induced by heating, such a temperature change is not expected to significantly alter the temperature gradients that are ultimately driving the flow.

Previous authors have characterised the eruption of an axisymmetric thermal plume in terms of a critical Rayleigh number based on the total heat flux Q from the source of radius R, the thermal conductivity k of the fluid and a thermal boundary layer width δ. Moses *et al.* (1993), and references therein, defined a temperature scale $Q\delta[kR(R+\delta)]^{-1} \approx Q\delta/kR^2$ and found a critical Rayleigh number Ra_c of 130 ± 30, where $Ra_c = g\alpha Q\delta^4[R(R+\delta)C_p\rho_0\nu\kappa^2]^{-1}$. Here g, α, ν, C_p and $\kappa = k\rho_0^{-1}C_p^{-1}$ are the acceleration due to gravity, coefficient of thermal expansion, kinematic viscosity, specific heat and thermal diffusivity of the fluid, respectively. By analogy, for the present line plume with heat flux q per unit length, we define a temperature scale $q\delta/kd$ and form a Rayleigh number $Ra_\ell = g\alpha q\delta^4[dC_p\rho_0\nu\kappa^2]^{-1}$. A thermal boundary layer thickness δ of about 2.6 mm, was observed when the plume begins to form (Fig. 5.2b). This yields a critical $Ra_\ell \approx 128$, in excellent agreement with Moses *et al.* (1993) (see also Castaing *et al.*, 1989; Zocchi *et al.*, 1990). The corresponding temperature scale $q\delta/kd \approx 0.2$ K is slightly higher than the temperatures observed in the plume in Fig. 5.2. The relatively high thermal conductivity of the 0.5 mm copper base causes the effective width of the heat source to increase beyond

the $d = 15$ mm width of the Peltier devices (this is particularly noticeable in Fig. 5.2a), and thus to decrease the induced temperature of the fluid. Of course, the total buoyancy input is unchanged by this, explaining why the critical Rayleigh number remains comparable.

5.4 Conclusions

The colour separation approach to simultaneous PIV and SS used in this study has some advantages over the interleaving approach of previous authors. Perhaps the greatest of these are the truly simultaneous sampling and avoiding the need to phase lock the capture system with the illumination. While the limited temporal response of the LCD monitors used in the earlier studies (Dalziel *et al.*, 2007; Sveen & Dalziel, 2005) posed fairly stringent restrictions, for the present study we could easily have strobed the LED we used for illuminating the SS pattern. However, timing and stability issues derived from the latter approach are avoided using the present colour separation application.

Our selected set-up here is only one of many possibilities using the same basic idea. In the simplest variants, we could have employed a red LED with perhaps an argon-ion laser, placing suitable red and (optionally) cyan filters over the SS and PIV cameras, respectively. The present cyan LED would of course work equally well with a helium-neon or diode laser.

Other technologies are available for simultaneous measurements of velocity and density in buoyancy-driven flows. For instance, laser induced fluorescence (LIF) is widely used in conjunction with PIV (e.g. Westerweel *et al.*, 2002). However, LIF is unsuitable in the present thermally stratified case, as there is no method of introducing dye that will mark temperature, even before considering the differences in their relative diffusivities. Thermochromatic liquid crystals, on the other hand, have proven useful in thermally convective flows in liquids (e.g. Ciofalo *et al.*, 2003; Zocchi *et al.*, 1990) and their use is not limited to two-dimensional flows, although there are difficulties in working at the small scale of the present experiments and the cost of the encapsulated liquid crystals is relatively high.

Although adding slightly to the complexity, the use of two video cameras substantially improves the accuracy and flexibility of the present measurements. This is mainly due to the ability to set appropriate lens apertures for both PIV (large) and SS (small).

The new approach to combining PIV and synthetic schlieren techniques using colour separation has proven a convenient and effective way of obtaining true simultaneous velocity and density measurements in this two-dimensional flow. Although this technology relies on two cameras (and here we used two computers), its simplicity and the relatively low cost of the camera make it a very attractive solution. In the present experiments, a precision of better than 10^{-3} K and 0.02 mm s^{-1} was obtained for temperature perturbations and velocity, respectively, in a 50×30 mm region. Finally, the present application of the

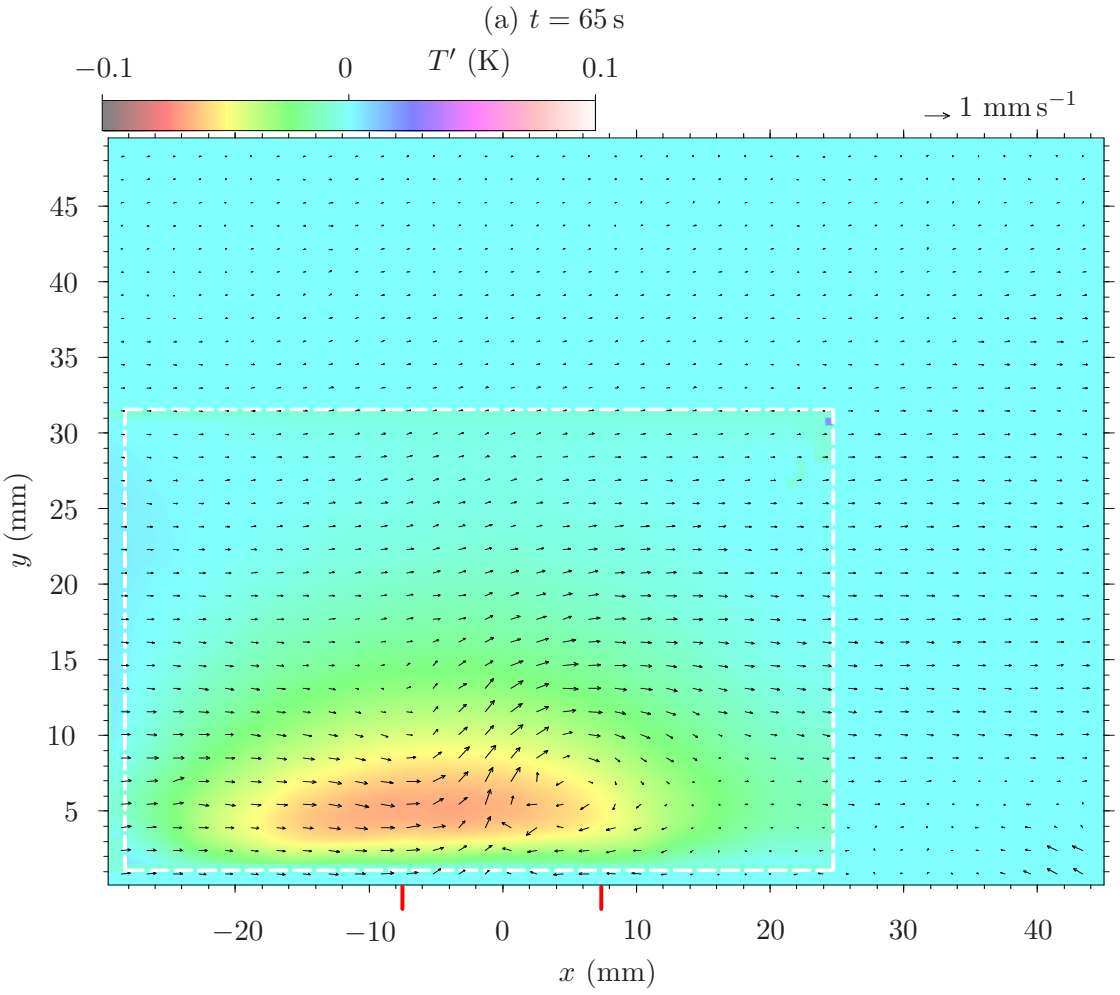

Figure 5.2: Sequence of velocity vectors and temperature perturbation field (inside the white, dashed rectangle) showing the starting plume for (a) $t = 65$ s, (b) $t = 75$ s and (c) $t = 95$ s. The origin on the horizontal axis represents the centreline of the heater ($q = 0.67$ W m^{-1}), whose boundary is marked by the red vertical lines placed below the bottom axis. The region between $y = 0$ and $y = 1.5$ mm contains no information.

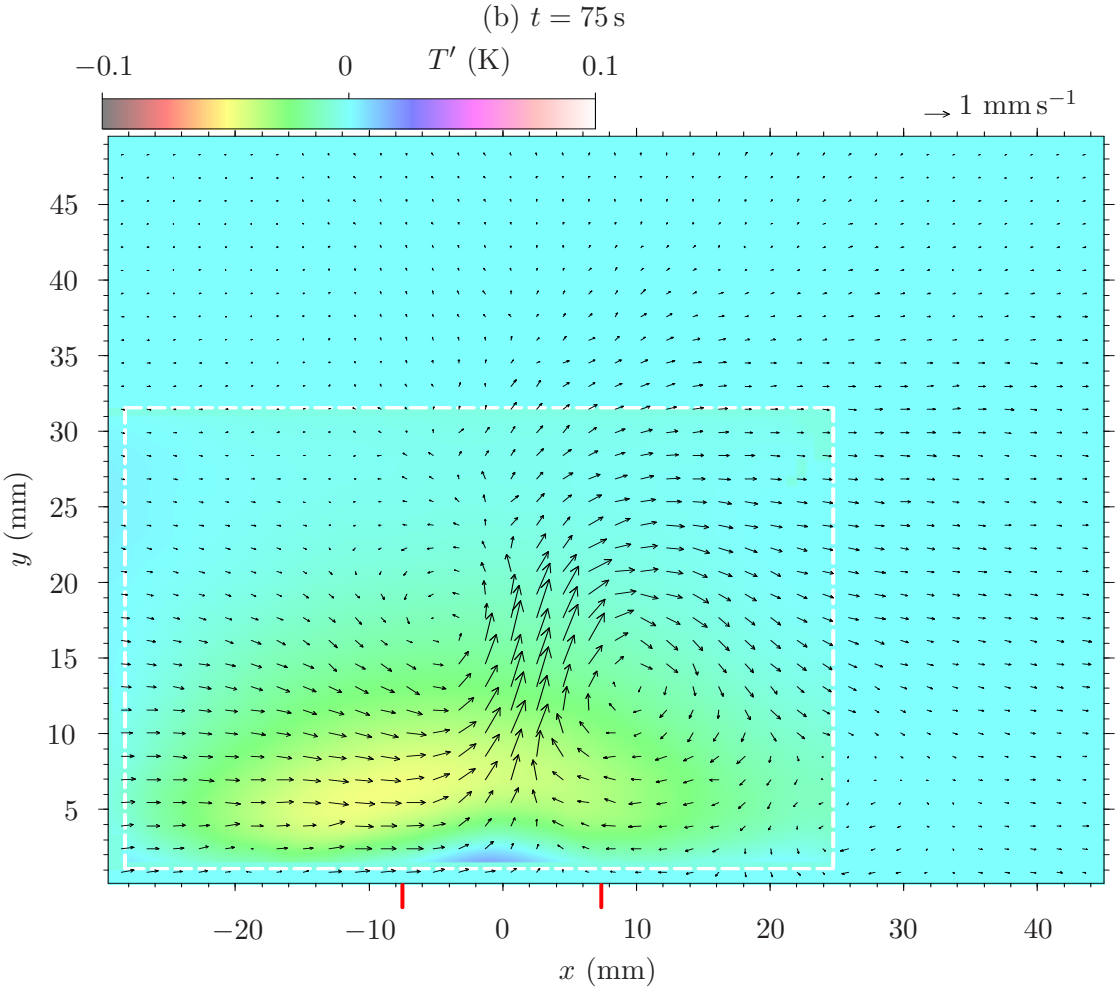

Figure 5.2: Continued

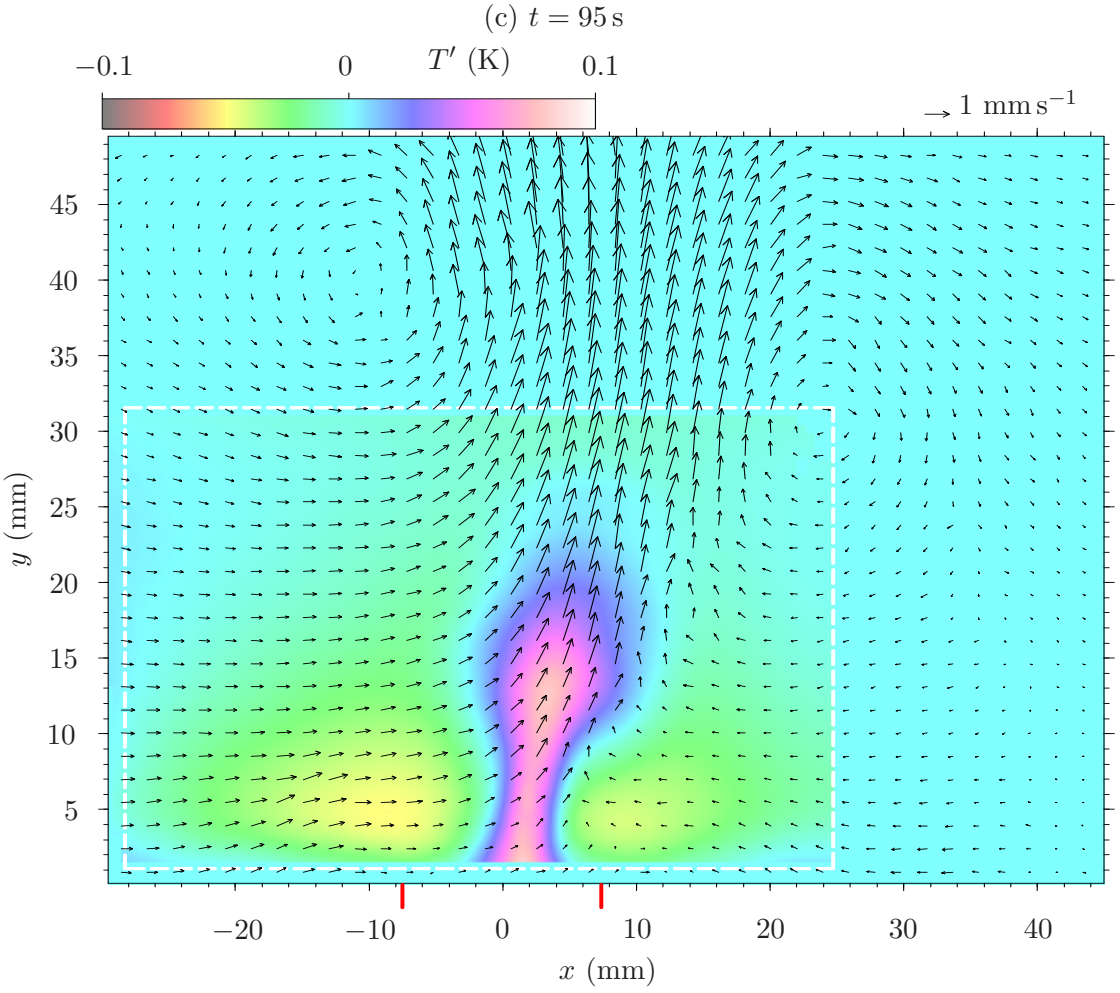

Figure 5.2: Continued

experimental technique has provided an estimation of the critical Rayleigh number for plume eruption, using the critical thermal boundary layer thickness as a length scale, with excellent agreement with previous works.

Acknowledgements

The authors gratefully acknowledge support from the Chilean National Commission for Scientific and Technological Research, CONICYT and Fondecyt Project No. 1080617.

Chapter 6

Effect of surface temperature inhomogeneities on turbulent plume dynamics

This chapter is published as research paper, authored by Christian Ihle, Stuart Dalziel and Yarko Niño, in the Proceedings of the Seventh International Symposium on Environmental Hydraulics, Tempe, Arizona (2007). An extended version of this paper is in preparation.

Abstract

Experimental observations on the dynamics of plumes generated by spatial inhomogeneities of positive and negative line buoyancy sources are reported. A novel experimental technique is applied, allowing for simultaneous measurement of 2D density and velocity fields. Localized heating and cooling at the bottom of a tank produces different flow regimes, ranging from the horizontal displacement of a plume rising from a heat source, to the disappearance of the plume when the rate of cooling is sufficiently high. For a single plume release and high cooling, theoretical considerations show that plume offset scales with the cubic root of the cooling power, a result that agrees with experimental results.

6.1 Introduction

Non-uniform thermal conditions in the vicinity of otherwise steady plumes can trigger small-scale, unsteady dynamics. In contrast with large scale flows driven by horizontal temperature gradients in comparatively wide geometries, such as the meridional overturning circulation (or "thermohaline circulation"; see (Stommel, 1962)), the class of flows of interest here appear in nature at micro- and meso-scales. The phenomena we are interested in are essentially local and affect otherwise stationary systems. An interesting example of such dynamics is the atmospheric boundary layer where there is intermittent low-altitude cloud cover. The distribution of the clouds, and its associated impact on solar heating of the ground, can induce a feedback process resulting on a scattered cloud distribution (Schumann *et al.*, 2002).

6.2 Problem description

Consider a large reservoir containing a Boussinesq fluid that is simultaneously cooled by a line sink and heated by a line source, separated by a distance L at the bottom of the reservoir. The strengths (per unit length) of the sink and source are q_- and q_+, respectively, with corresponding widths d_- and d_+. When used in isolation, the heat sink will cool the fluid immediately above it, generating a dense gravity current that propagates along the bottom. In contrast, the source will generate a buoyant plume or puff that rises from the base, eventually becoming turbulent. Transitions between a single plume to a series of puffs above the heat source are possible and depend on the ratio of thermal properties of the solid base of the reservoir and those of the fluid (see Hunt *et al.* (2003) for the case of a uniformly heated from below tank). The presence of simultaneous cooling in the vicinity of the heat source modifies this transition. In the simplest case, the gravity current from the heat sink causes the plume rising from the heat source to be displaced away from the heat sink. However, more complex behaviours can be also observed, as it is shown in this paper.

6.3 Experimental technique

To study the interaction between the gravity current and the plume, a new experimental technique that combines Particle Image Velocimetry (PIV) and synthetic schlieren was developed. Two light sources are used, one backlighting the dotted mask for synthetic schlieren (Sutherland *et al.*, 1999), while the other illuminates the suspended PIV particles. Two cameras are also used, one for each of the techniques. Whereas previous studies

have used a liquid crystal monitor to switch on and off the pattern for the synthetic schlieren (Dalziel *et al.*, 2007), here we use a 5 W cyan LED to illuminate the synthetic schlieren mask. Placing a red dichroic filter in front of the PIV camera effectively renders the backlighting invisible. While the white light sheet used for the PIV is sufficiently powerful for the PIV camera to image the particles through the dichroic filter, the light sheet is much less bright than the cyan backlighting, allowing the synthetic schlieren camera to image the mask without significant interference. With this arrangement we are able to make truly simultaneous 2D measurements of the density and velocity fields.

In the present set of experiments we filled a 400×150×200 mm Perspex tank was filled with salt water. The observation window corresponds to a 50×50 mm region near the heat source and sink. The synthetic schlieren mask (consisting of 0.4 mm clear dots randomly distributed on a black background printed on overhead transparency film) was located 167 mm behind the tank and viewed by a Jai CVM4+CL digital video camera (1320×1024 pixels, here recorded at 8 bits) located 3Â m from the tank and fitted with a ×2 adapter on an Olympus 135 mm telephoto lens. A second CVM4+CL video camera, this time fitted with a 25 mm f0.95 Vortex lens (fitted with a red dichroic filter) was used for imaging the PIV particles. A 300 W Cermax arc lamp with a parabolic reflector was used to illuminate the particles. The light sheet was formed with a simple 3 mm slit on the side of the tank. The light path was directed via a cold mirror to eliminate most of the heat from the light sheet. Pliolite S5E particles, sieved to 63-71 μm diameter, were rendered approximately neutrally buoyant through the addition of salt to the water in the tank. A schematic of the optical setup is shown in 6.1.

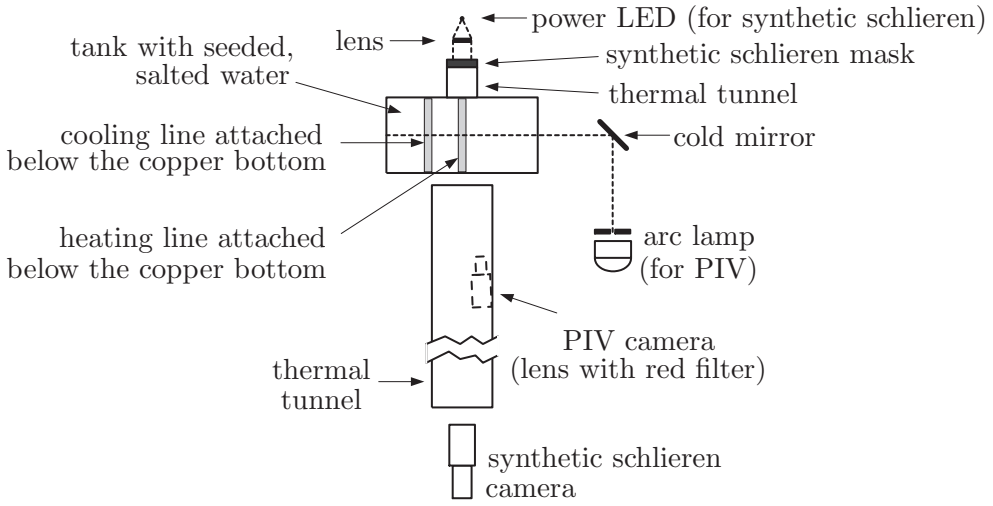

Figure 6.1: Plan view of the optical setup

Both the heating and cooling were provided by arrays of $d_+ = d_- = 15$ mm Peltier devices attached to a thin copper sheet used as the bottom of the tank. Here we present results with two lines of devices located $L = 100$ mm apart.

To minimise thermal noise, most of the experiments were conducted overnight using an automated system. A simple protocol operating over the local network was developed to coordinate the two computers running DigiFlow (Dalziel, 2007) (one for each of the cameras) along with the Peltier elements. The resulting image sequences were synchronised to better than 10 ms, substantially faster than the fastest time scale in the flow or the spacing between the images captured. A stirring device was used to help recover isothermal initial conditions between experiments. This was also controlled automatically together with the experiments.

6.4 Results and discussion

Figure 6.2 shows typical flow features resulting from the interaction between the cold gravity current (generated by the heat sink) and the hot plume (generated by the heat source). Figure 6.2a shows the structure of the plume prior to the arrival of the gravity current, and Figure 6.2b the structure after. In both cases, the upper panel shows the velocity and horizontal density gradient, while the lower panel shows the velocity and vertical density gradient. As the current collides with the plume, it nudges it away from its initial location directly over the heat source. The cooler fluid of the current contrasts with the warm fluid in the plume, enhancing the horizontal density gradient on the left-hand side of the base of the plume as it pushes it to the right. Some of this cool fluid is entrained into the plume, as is seen from the velocity field. The distinct vertical density gradient of the plume prior to the collision (Figure 6.2a) is overrun by the dense fluid of the gravity current, forming a region of statically unstable fluid over the heat source. The incoming gravity current above continues to deflect the warm fluid below to the right into the displaced plume. Such behaviour has a certain resemblance to salt wedge dynamics, as can be seen in Figure 6.2b (bottom). For strong enough cooling, the plume has been observed to disappear altogether.

Different flow regimes depend on the ratio $R = q_-/q_+$, along with heating rate, q_+, the thermal diffusivity of the base, κ_b and fluid properties such as its thermal diffusivity, κ. If the heating rate is sufficiently high (close to ${q_+}^* = 0.67$ W/m, a single starting plume is replaced by the superposition of a number of departing plumes and puffs. This transition is distinct from that found by Hunt *et al.* (2003) where the quotient played a critical role. Examples of different behaviour observed here are shown in Figure 3 as time series of the horizontal density gradient at a fixed height over the tank base. Figure 6.3a

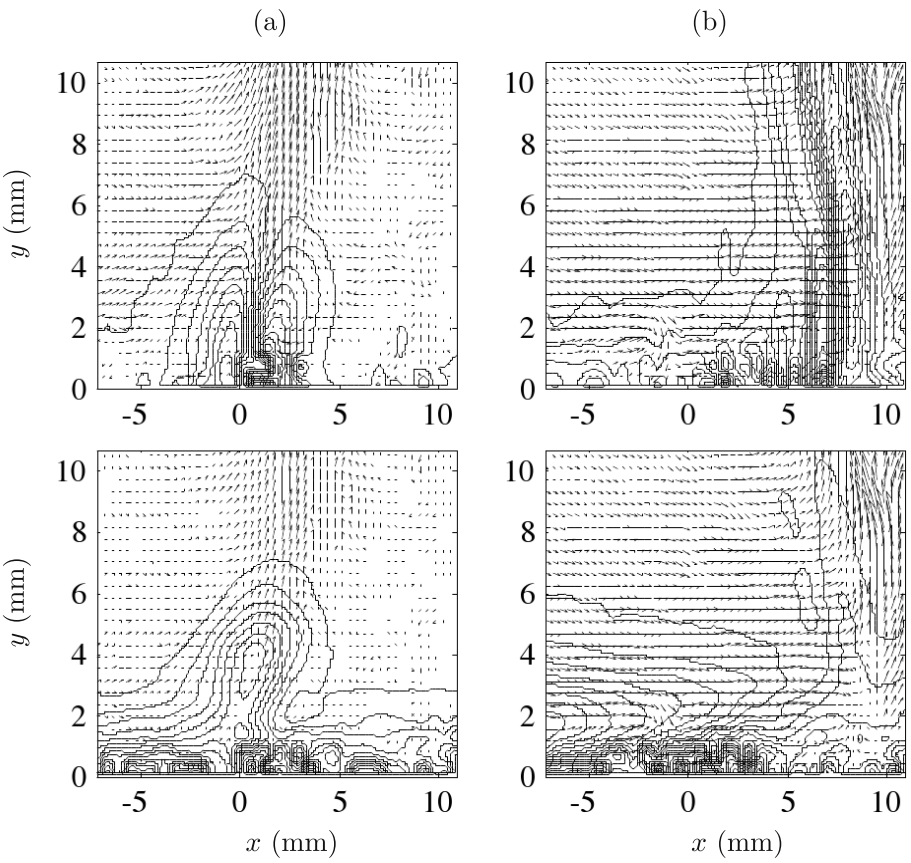

Figure 6.2: Recorded sequence of velocity vectors over horizontal (upper row) and vertical (lower row) density gradient lines. (a) 86.5 s and (b) 155 s after the start of the experiment, for a single plume release, $q_-/q_+ = 112$ and $q_+ = 0.78$ W/m. The heater is centred on $x = 0$.

shows a case where a continuous plume is produced, although it is displaced to the right by the impinging cold current. In contrast, Figure 6.3b shows how the horizontal gradient isolines converge for a high heating rate case when puffs are released.

As found by previous authors (e.g. Härtel *et al.*, 2000), the Grashof number characterises the relative importance of molecular and inertial forces for a gravity current. Here we define the Grashof number for the cold gravity current as $\mathrm{Gr} = g\alpha L^4/\rho_0 C_p \nu^3 d_- \mathrm{Pr}$, where α, C_p and ν are the coefficient of thermal expansion, specific heat and kinematic viscosity of the fluid, respectively. Here ρ_0 is a reference density and $\mathrm{Pr} = \nu/\kappa$ is the Prandtl number of the fluid.

As noted previously, for weak heat sources we find a regime where a single plume is displaced laterally by the advancing gravity current. Even a weak cool gravity current can

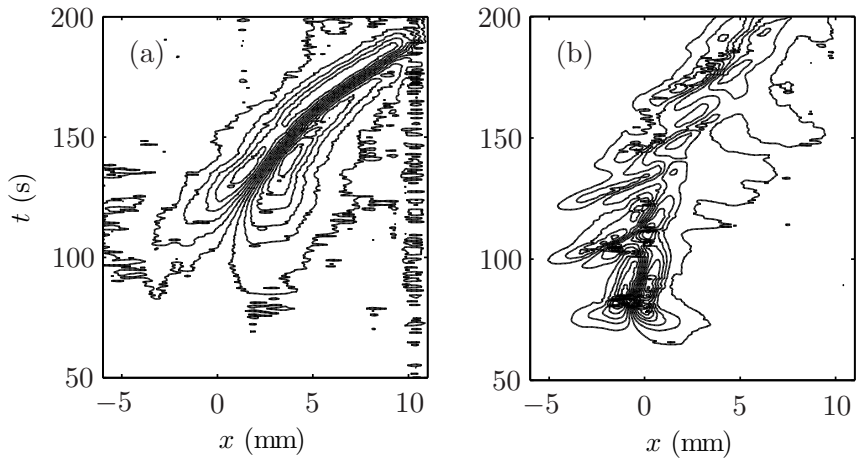

Figure 6.3: Time series for horizontal density gradient, for a vertical distance of 2 mm above the tank base. (a) A single plume release, without puffs. $R = 871$, $q_+ = 0.22$ W/m. (b) Single plume with puffs. $R = 6.6$, $q_+ = 3.22$ W/m. The origin in the abscissa represents the centre of the heater.

lead to a substantial thickening of the bottom boundary layer on the left-hand side, closer to the heat sink; in contrast, the boundary layer on the right-hand side remains essentially unchanged. In this regime, at least for the time periods explored in these experiments (between 100 s and 300 s each), the plume displacement was observed to vary nearly linearly with time. (Here we determined the plume displacement from the definition of a threshold for the horizontal density gradient, approximately 2 mm above the base of the tank.) Using the viscous scaling L/ν to normalize the constant plume displacement velocity u, we find a simple relationship with the Grashof number. Figure 4 shows the experimental relation between the plume displacement velocity u and the Grashof number, where $uL/\nu \approx 0.062\,\mathrm{Gr} - 2.96$, for $100 \leq \mathrm{Gr} \leq 500$.

6.5 Conclusions

Spatially non-uniform thermal forcing has been studied to asses the influence of a heat sink placed near a heat source on the dynamics of buoyant plumes. Using simultaneous measurements of density and velocity fields we found that the gravity current generated by the heat sink displaces the thermal plume horizontally, forming persistent inverse temperature stratification above the source. With weak sources, a single plume is generated, but multiple plumes and puffs are found at higher heating rates. The horizontal displacement of a single heat plume created by a nearby heat sink depends strongly on the gravity current dynamics, with the displacement velocity proportional to the cooling rate $q_-^{1/3}$.

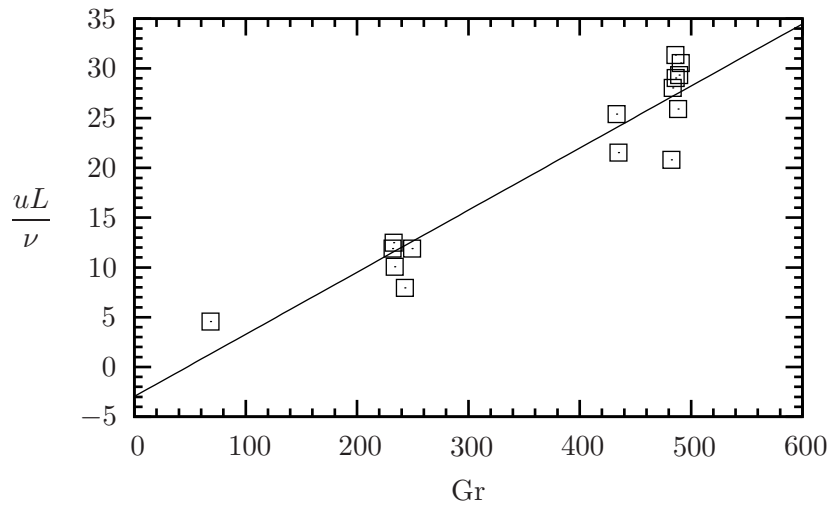

Figure 6.4: Non-dimensional plume displacement as a function of the Grashof number.

Acknowledgments

The authors would like to thank Prof. M.G. Worster and Dr. C.P. Caulfield for useful discussions regarding this research.

Chapter 7

Conclusions

The present thesis has been successfully addressed a set of spatiotemporal effects related to penetrative convection. Using linear and non-linear stability analysis, the appearance of thermal convection was quantitatively linked with the beginning of surface cooling in large-scale water bodies, as it is the case of some middle-sized lakes. This problem can be directly related with the well-known Rayleigh-Bénard for unsteady thermal forcing. For the extreme case of sudden cooling, present results are consistent with those made at laboratory scale. It was shown that the thermal boundary condition at the bottom of the reservoir is unimportant compared to the surface one, where the cooling is applied. Observations show that observed times for the onset of natural convection can be (in first order) modelled to be proportional to theoretical times coming from linear stability analysis. At difference with other works, here it is suggested that such a proportionality constant depends on the kinematic boundary condition where the thermal forcing is applied. Free-surface (or stress-free) boundary condition yields earlier theoretical onset times while differences with observed times are larger. This work has been complemented with the identification of global conditions for the existence of thermal convection in fluid layers where the side opposite to that where the thermal forcing is applied is adiabatic. Computed critical Rayleigh numbers complement those reported for the case of the unsteady Rayleigh-Bénard problem, showing that fluid enclosures cooled at the surface with no heat exchange at the bottom are more prone to mixing (or, observe convection to appear before) than the case where temperature is imposed at the bottom. In the case of sinusoidal cooling, field results from published literature and a recent field campaign in Chile were compared to those obtained using the same theoretical base than that with a step change in temperature. In this case, the complexity introduced by the length scale of the reservoir and the combined effect of wind are evident. Initial temperature and passive scalar concentration stratification plays an important role on the prediction of the beginning of mixing. Interestingly, the studied

case suggests the impact of temperature on mixing is more important that that of wind, even when relatively strong wind events occur. For the initially unstratified case, a relation for the prediction of the onset of convection is proposed. Nonetheless, a larger dataset is required to give an accurate quantitative assessment of the effect of evening and night cooling in the mixing dynamics of lakes and reservoirs.

Finally, an experimental study about the spatiotemporal dynamics relating two-dimensional laminar, thermally induced plumes and gravity currents was done. To study this problem a novel experimental technique, based on colour separation was developed to simultaneously obtain velocity and density gradient vector fields. It was found that under certain plume/gravity current intensity combinations plume can still keep the most of their flow characteristic, though nudged away from their original position by the gravity current. Plume displacement generation times can be significant compared to plume departure or gravity horizontal displacement time scales. An interesting potential was identified on this topic as it can bring further insights on the explanation of local flow phenomena where thermal sinks and sources are found.

Bibliography

Abramowitz, Milton & Stegun, Irene A., ed. 1965 *Handbook of Mathematical Functions*. New York: Dover.

Adrian, R. J. 1986 Turbulent thermal convection in wide horizontal fluid layers. *Exp. Fluids* **4**, 121.

Adrian, R. J. 1991 Particle-imaging techniques for experimental fluid mechanics. *Annu. Rev. Fluid Mech.* **23**, 261–304.

Airey, J. R. & Webb, H. A. 1918 The practical importance of the Confluent Hypergeometric function. *Philos. Mag.* **36**, 129–141.

Bénard, H. 1900 Les tourbillons cellulaires dans une nappe liquide. *Revue Gen. Sci. Pur. Appl.* **11**, 1261–1271 and 1309–1328.

Benjamin, T. B. 1968 Gravity currents and related phenomena. *J. Fluid Mech.* **31**, 209–248.

Blair, L. M. & Quinn, J. A. 1969 Onset of cellular convection in a fluid layer with time-dependent density gradients, the. *J. Fluid Mech.* **36**, 385–400.

Busse, F. H. 1978 Non-linear properties of thermal convection. *Rep. Prog. Phys.* **41**, 1930–1965.

Campos, H., Steffen, W., Román, C., Zúñiga, L. & Agüero, G. 1983 Limnological studies in Lake Villarrica: Morphometric, physical, chemical, planktonical factors and primary productivity. *Arch. Hidrobiologie* **4**, 371–406.

Castaing, B., Gunaratne, G., Kadanoff, L., Libchaber, A. & Heslot, F. 1989 Scaling of hard thermal turbulence in Rayleigh-Benard convection. *J. Fluid Mech.* **204**, 1–30.

Chandrasekhar, S. 1961 *Hydrodynamic and Hydromagnetic Stability*, 1st edn. Oxford: Clarendon.

Chavanne, X., Chillá, F., Chabaud, B., Castaing, B. & Hébral, B. 2001 Turbulent Rayleigh Bénard convection in gaseous and liquid He. *Phys. Fluids* **13** (5), 1300–1320.

Chen, K., Chen, M. M. & Sohn, C. W. 1983 Thermal instability of two-dimensional stagnation-point boundary layers. *J. Fluid Mech.* **132**, 49–63.

Ching, C. Y., Fernando, H. J. S., Mofor, L. A. & Davies, P. A. 1996 Interaction between multiple plumes: a model study with application to leads. *J. Phys. Oceanogr.* **26**, 525–540.

Choi, C. K., Lee, J. D., Hwang, S. T. & Yoo, J. S. 1988 Analysis of thermal instability and heat transfer prediction in a horizontal fluid layer heated from below, the. *Proceedings of the International Conference On Fluid Mechanics* pp. 1193–1198.

Choi, C. K., Park, J. H. & Kim, M. C. 2004*a* The onset of buoyancy-driven convection in a horizontal fluid layer subjected to evaporative cooling. *Heat Mass Transfer* **41**, 155–162.

Choi, C. K., Park, J. H., Kim, M. C., Lee, J. D., Kim, J. J. & Davis, E. J. 2004*b* The onset of convective instability in a horizontal fluid layer subjected to a constant heat flux from below. *Int. J. Heat Mass Transfer* **47**, 4377–4384.

Choi, C. K., Park, J. H., Kim, M. C., Lee, J. D., Kim, J. K. & Davis, E. J. 2004*c* The onset of convective instability in a horizontal fluid layer subjected to a constant heat flux from below. *Int. J. Heat Mass Transfer* **47**, 4377–4384.

Choi, C. K., Park, J. H., Park, H. K., Cho, H. J., Chung, T. J. & Kim, M. C. 2004*d* Temporal evolution of thermal convection in an initially stably-stratified horizontal fluid layer. *Int. J. Therm. Sci.* **43**, 817–823.

Chung, T. J., Kim, M. C. & Choi, C. K. 2004 Temporal evolution of thermal instability in fluid layers isothermally heated from below, the. *Korean J. Chem. Eng.* **21**, 41–47.

Ciofalo, M., Signorino, M. & Simiano, M. 2003 Tomographic particle-image velocimetry and thermography in Rayleigh-Bénard convection using suspended thermochromic liquid crystals and digital image processing. *Exp. Fluids* **34**, 156–172.

Currie, I. G. 1967 The effect of heating rate on the stability of stationary fluids. *J. Fluid Mech.* **29**, 337–347.

Dalziel, S. B. 2007 *DigiFlow User Guide, version 2.0*.

Dalziel, S. B., Carr, M., Sveen, J. K. & Davies, P. A. 2007 Simultaneous synthetic schlieren and PIV measurements for internal solitary waves. *Meas. Sci. Technol.* **18**, 533–547.

Dalziel, S. B., Hughes, G. O. & Sutherland, B. R. 1998 Synthetic schlieren. In *8th International Symposium on Flow Visualization*.

Dalziel, S. B., Hughes, G. O. & Sutherland, B. R. 2000 Whole-field interaction measurements by 'synthetic schlieren'. *Exp. Fluids* **28**, 322–335.

Davenport, I. F. & King, C. J. 1974 The onset of natural convection from time-dependent profiles. *Int. J. Heat Mass Transfer* **17**, 69–76.

Davis, S. H. 1976 The stability of time-periodic flows. *Annu. Rev. Fluid Mech.* **8**, 57–74.

Dowden, J. 1981 The stability of a periodically heated layer of fluid. *J. Fluid Mech.* **110**, 149–159.

Drazin, P. G. & Reid, W. H. 1981 *Hydrodynamic Stability*. Cambridge University Press.

Elder, J. W. 1969 The temporal development of a model of high Rayleigh number convection. *J. Fluid Mech.* **35**, 417–437.

Elsinga, G. E., van Oudheusden, B. W. & Scarano, F. 2005 Evaluation of aero-optical distortion effects in PIV. *Exp. Fluids* **39**, 246–256.

Fernando, H. J. S. 1991 Turbulent mixing in stratified fluids. *Annu. Rev. Fluid Mech.* **23**, 455–493.

Foster, T. D. 1965*a* Onset of convection in a layer of fluid cooled from above. *Phys. Fluids* **8**, 1770–3.

Foster, T. D. 1965*b* Stability of homogeneous fluid cooled from above. *Phys. Fluids* (8), 1249–1257.

Foster, T. D. 1968 Effect of boundary conditions on the onset of convection. *Phys. Fluids* **11**, 1257.

Foster, T. D. 1969 Onset of manifest convection in a layer of fluid with a time-dependent surface temperature. *Phys. Fluids* **12**, 2482–2487.

Gal, G., Imberger, J., Zohary, T., Antenucci, J., Anis, A. & Rosenberg, T. 2003 Simulating the thermal dynamics of Lake Kinneret. *Ecol. Model.* **162**, 69–86.

Gebhart, B., Jaluria, Y., Mahajan, R. L. & Sammakia, B. 1988 *Buoyancy-induced Flows and Transport*, 1st edn. Hemisphere.

Goldstein, A. W. 1959 Stability of a horizontal fluid layer with unsteady heating from below and time dependent body forces. *Nasa Tech. Rep.* (R-4).

Goldstein, R. J. & Volino, R. J. 1995 Onset and development of natural convection above a suddenly heated surface. *J. Heat Trans.-T. ASME* **117**, 808, .

Gresho, P. M. & Sani, R. L. 1971 Stability of a fluid layer subjected to a step change in temperature: Transient vs. frozen time analysis, the. *Int. J. Heat Mass Transfer* **14**, 207–221.

Griffiths, R. W. 2000 The dynamics of lava flows. *Annu. Rev. Fluid Mech.* **32**, 477–518.

Grossman, R. L., Yates, D., LeMone, M., Wesely, M. L. & Song, J. 2004 Observed effects of horizontal surface temperature variations on the atmosphere over a midwest watershed during CASES-97. *J. Geophys. Res.* **110**, DO6117.

Grossmann, S. & Lohse, D. 2000 Scaling in thermal convection: a unifying theory. *J. Fluid Mech.* **407**, 27–56.

Gumerman, R.J. & Homsy, G.M. 1975 The stability of uniformly accelerated flows with application to convection driven by surface tension. *J. Fluid Mech.* **68**, 191–207.

Ha, V. M. & Lai, C. L. 2004 Theoretical analysis of marangoni instability of an evaporating droplet by energy method. *Int. J. Heat Mass Transfer* **47**, 3811–3823.

Härtel, C., Meiburg, E. & Necker, F. 2000 Analysis and direct numerical simulation of the flow at a gravity-current head. part 1. flow topology and front speed for slip and non-slip boundaries. *J. Fluid Mech.* **418**, 189–212.

Hazewinkel, J., Grisouard, N. & Dalziel, S. B. 2010 Comparison of laboratory and numerically observed scalar fields of an internal wave attractor. *To appear in J. Eur. J. Mech. B/Fluids* .

Homsy, G. M. 1973 Global stability of time-dependent flows: impulsively heated or cooled fluid layers. *J. Fluid Mech.* **60**, 129.

Howard, L. N. 1966 Convection at high Rayleigh number. In *Applied Mechanics, Proc. 11th Congr. of Appl. Mech.* (ed. H. Görtler), pp. 1109–1115. Springer.

Howle, L. E. 1997 Active control of Rayleigh-Bénard convection. *Phys. Fluids* **9** (7), 1861–1863.

Hunt, J. C. R., Vrieling, A. J., Nieuwstadt, F. T. M. & Fernando, H. J. S. 2003 The influence of the thermal diffusivity of the lower boundary on eddy motion in convection. *J. Fluid Mech.* **491**, 183–205.

Hutchinson, G. E. 1957 *A treatise on limnology. Vol. 1. Geography*. John Wiley and Sons.

Ihle, C. F. & Niño, Y. 2005 Global stability of nonpenetrative convection. *In preparation* .

Ihle, C. F. & Niño, Y. 2006*a* Onset of modulated penetrative convection: a theoretical and experimental analysis. In *Proceedings of the Sixth International Symposium on Stratified Flows, Perth, Australia*, , vol. 1, pp. 557–562.

Ihle, C. F. & Niño, Y. 2006*b* The onset of nonpenetrative convection on a suddenly cooled layer of fluid. *Int. J. Heat Mass Transfer* **49**, 1442–1451.

Imberger, J. & Patterson, J. C. 1990 Physical limnology. *Adv. Applied Mech.* **27**, 303–475.

Jeffreys, H. 1928 Some cases of instability of fluid motion. *Proc. Roy. Soc. A* **118**, 195–208.

Jhaveri, B. S. & Homsy, G. M. 1982 Onset of convection in fluid layers heated rapidly in a time- dependent manner, the. *J. Fluid Mech.* **114**, 251–260.

Jonas, T., Stips, A., Eugster, W. & Wüest, A. 2003 Observations of a quasi shear-free lacustrine convective boundary layer: Stratification and its implications on turbulence. *J. Geophys. Res.* **108**, 26/1–26/15.

Joseph, D. D. 1965 On the stability of the Boussinesq equations. *Arch. Rat. Mech. Anal.* **20** (1), 59–71.

Joseph, D. D. 1966 Nonlinear stability of the boussinesq equations by the method of energy. *Arch. Rat. Mech. Anal.* **22**, 163–184.

Joseph, D. D. & Shir, C. C. 1966 Subcritical convective instability, part 1. fluid layers. *J. Fluid Mech.* **26**, 753–768.

Kadanoff, L. 2001 Turbulent heat flow: structures and scaling. *Physics Today* **54** (8), 34–39.

Kang, K. H. & Choi, C. K. 1997 A theoretical analysis of the onset of surface-tension-driven convection in a horizontal liquid layer cooled suddenly from above. *Phys. Fluids* **9**, 7–15.

Kerr, R. C., Woods, A. W., Worster, M. G. & Huppert, H. E. 1989 Disequilibrium and macrosegregation during solidification of a binary melt. *Nature* **340** (6232), 357–362.

Kim, K. H. & Kim, M. U. 1986 Onset of natural convection in a fluid layer suddenly heated from below, the. *Int. J. Heat Mass Transfer* **29**, 193–201.

Kim, M.C., Choi, K.H. & Choi, C.K. 1999 The onset of thermal convection in an initially, stably stratified fluid layer. *Int. J. Heat Mass Transfer* **42**, 4253–4258.

Kim, M. C., Choi, C. K. & Yeo, J.-K. 2007 The onset of Soret-driven convection in a binary mixture heated from above. *Phys. Fluids* **19** (8), 084103.

Kim, M. C., Choi, C. K. & Yoon, D. Y. 2008 Relaxation of the energy method for the transient Rayleigh-Bénard convection. *Phys. Lett. A* **372**, 4709–4713.

Kim, M. C., Park, H. K. & Choi, C. K. 2002 Stability of an initially stably stratified fluid subjected to a step change in temperature. *Theoret. Comp. Fluid Dyn.* **16**, 49–57, .

Kim, M. C., Park, J. H. & Choi, C. K. 2005 Onset of buoyancy-driven convection in the horizontal fluid layer subjected to ramp heating from below. *Chem. Eng. Sci.* **60**, 5363–5371.

Kim, M. C., Yoon, D. Y. & Choi, C. K. 1996 Buoyancy-driven convection in a horizontal fluid layer under uniform volumetric heat sources. *Korean J. Chem. Eng.* **13**, 165–171.

Liaqat, A. & Baytas, A. C. 2001 Cooling of molten core material within a pressurised water reactor vessel lower head: interaction of surface radiation and wall conduction with free convection. *Int. J. Eng. Sci.* **39**, 2089–2102.

Lick, W. 1965 The instability of a fluid layer with time-dependent heating. *J. Fluid Mech.* **21**, 565–576.

Linden, P. F. 1999 The fluid mechanics of natural ventilation. *Annu. Rev. Fluid Mech.* **31**, 201–238.

Linden, P. F. 2001 *Perspectives in Fluid Dynamics: A Collective Introduction to Current Research*, chap. 6, pp. 289–345. Cambridge University Press.

Low, A. R. 1929 On the criterion for stability of a layer of viscous fluid heated from below. *Proc. Roy. Soc. A* **125** (796), 180–195.

Mahler, E. G., Schechter, R. S. & Wissler, E. H. 1968 Stability of a fluid layer with time-dependent density gradients. *Phys. Fluids* **11**, 1901–1912.

Majumder, C. A. H. & Yuen, D. A. 2004 Four dynamical regimes for a starting plume model. *Phys. Fluids* **16** (5), 1516–1530.

Marshall, J. & Schott, F. 1999 Open-ocean convection: Observations, theory, and models. *Rev. Geophys.* **37** (1), 1–64.

Martin, J. L., McCutcheon, S. C. & Schottman, R. W. 1999 *Hydrodynamics and transport for water quality modeling*. Lewis Publishers.

Maxworthy, T. 1997 Convection into domains with open boundaries. *Annu. Rev. Fluid Mech.* **29**, 327–371.

Meier, G. E. A. 2002 Computerized background-oriented schlieren. *Exp. Fluids* **33**, 181–187.

Meruane, C. & Garreaud, R. 2005 Simulation of phytoplankton response to strong wind events in Lake Villarrica, Chile. In *Proceedings of the XXXI IAHR Congress*.

Mizushima, J. 1995 Onset of convection in a finite two-dimensional box. *J. Phys. Soc. Jpn.* **64** (7), 2420–2432.

Moin, P. & Mahesh, K. 1998 Direct numerical simulation: a tool in turbulence research. *Annu. Rev. Fluid Mech.* **30**, 539–578.

Morison, J. H., McPhee, M. G., Curtin, T. B. & Paulson, C. A. 1992 The oceanography of winter leads. *J. Geophys. Res. C* **97** (7), 11199–11218.

Morton, B. R. 1957 On the equilibrium of a stratified fluid layer. *J. Mech. Appl. Math.* **10**, 433–447.

Moses, E., Zocchi, G. & Libchaber, A. 1993 An experimental study of laminar plumes. *J. Fluid Mech.* **251**, 581–601.

Neitzel, G. P. 1982 Onset of convection in impulsively heated or cooled fluid layers. *Phys. Fluids* **25**, 210.

Orr, A. C. & Kelly, R. E. 1999 Time-modulated convection with zero mean temperature gradient. *Phys. Rev. E* **60**, 1741–1747.

Pellew, A. & Southwell, R. V. 1940 On maintained convective motion in a fluid heated from below. *Proc. Roy. Soc. A* **176** (966), 312–343.

Plevan, R. E. & Quinn, J. A. 1966 The effect of monomolecular films on the rate of gas absorption into a quiescent liquid. *AIChE J.* **12** (5), 894–902.

Pope, S. 2000 *Turbulent Flows*, 1st edn. Cambridge University Press.

Rayleigh, Lord 1916 On convection currents in a horizontal layer of fluid when the higher temperature in on the under side. *Philos. Mag.* **32**, 529.

Reid, W. H. & Harris, D. L. 1958 Some further results on the bénard problem. *Phys. Fluids* **1**, 102–110.

Riaz, A., Hesse, M., Tchelepi, H. A. & Orr Jr, F. M. 2006 Onset of convection in a gravitationally unstable diffusive boundary layer in porous media. *J. Fluid Mech.* **548**, 87–111.

Richard, H. & Raffel, M. 2001 Principle and applications of the background oriented schlieren (BOS) method. *Meas. Sci. Technol.* **12**, 1576–1585.

Robinson, J. L. 1976 Theoretical analysis of convective instability of a growing thermal boundary layer. *Phys. Fluids* **19**, 778–791.

Rozas, C. 2009 Análisis modal para el estudio de resonancia de ondas internas excitadas por el viento en el lago Villarrica. Master's thesis, Universidad de Chile, in Spanish.

Schumann, U., Dörnbrack, A. & Mayer, B. 2002 Cloud-shadow effects on the structure of the convective boundary layer. *Meteorol. Z.* **11** (4), 285–294.

Siggia, E. D. 1994 High Rayleigh number convection. *Annu. Rev. Fluid Mech.* pp. 137–68.

Simpson, J. E. 1997 *Gravity Currents: In the Environment and the Laboratory*, 1st edn. Cambridge University Press.

Soberman, R. K. 1959 Onset of convection in liquids subjected to transient heating from below. *Phys. Fluids* **2** (2), 131–138.

Spangenberg, W. G. & Rowland, W. R. 1961 Convective circulation in water induced by evaporative convection. *Phys. Fluids* **4**, 743–750.

Sparrow, E. M., Goldstein, R. J. & Jonsson, V. K. 1964 Thermal instability in a horizontal fluid layer: effect of boundary conditions and non-linear temperature profile. *J. Fluid Mech.* **18**, 513–528.

Spigel, R. H. & Imberger, J. 1987 Mixing processes relevant to phytoplankton dynamics in lakes. *New Zeal. J. Mar. Fresh.* **21**, 361–377.

Stommel, H. 1962 On the smallness of sinking regions in the ocean. *Proc. Natl. Acad. Sci.* **48**, 766–772.

Stull, R. B. 1988 *An Introduction to Boundary Layer Meteorology*, 5th edn. Kluwer Academic Publishers.

Sutherland, B. R., Dalziel, S. B., Hughes, G. O. & Linden, P. F. 1999 Visualization and measurement of intertial waves by 'synthetic schlieren'. Part 1. Vertically oscillating cylinder. *J. Fluid Mech.* **390**, 93–126.

Sutton, O. G. 1950 On the stability of a fluid heated from below. *Proc. Roy. Soc. A* **204** (1078), 297–309.

Sveen, J. K. & Cowen, E. A. 2004 Quantitative imaging techniques and their application to wavy flow. Singapore: World Scientific.

Sveen, J. K. & Dalziel, S. B. 2005 A dynamic masking technique for combined measurements of PIV and synthetic schlieren applied to internal gravity waves. *Meas. Sci. Technol.* **16**, 1954–1960.

Svendsen, H. 1997 Physical oceanography and marine ecosystems: some illustrative examples. *Sci. Mar.* **61**, 93–108.

Tan, K. K. & Thorpe, R. B. 1992 Gas diffusion into viscous and non-Newtonian liquids. *Chem. Eng. Sci.* **47** (13/14), 3565–3572.

Tang, J. & Bau, H. H. 1993 Stabilization of the no-motion state in Rayleigh-Bénard convection through the use of feedback control. *Phys. Rev. Lett.* **70**, 1795.

Turner, J. S. 1969 Buoyant plumes and thermals. *Annu. Rev. Fluid Mech.* **1**, 29–44.

Turner, J. S. 1973 *Buoyancy effects in fluids*, 1st edn. Cambridge University Press.

Ueda, H., Komori, S., Miyasaki, S. & Ozoe, H. 1984 Time-dependent thermal convection in a stably stratified fluid layer heated from below. *Phys. Fluids* **27**, 2617–2623.

Ungarish, M. & Huppert, H. E. 2002 On gravity currents propagating at the base of a stratified ambient. *J. Fluid Mech.* **458**, 283–301.

Veronis, G. 1963 Penetrative convection. *Astrophysical Journal* **137**, 641.

Wankat, P. C. & Homsy, G. M. 1977 Lower bounds for the onset time of instability in heated layers. *Phys. Fluids* **20**, 1200.

Wehde, H., Backhaus, J. O. & Hegseth, H. N. 2001 The influence of oceanic convection in primary production. *Ecol. Model.* **138**, 115–126.

Westerweel, J., Hofmann, T., Fukushima, C. & Hunt, J. C. R. 2002 The turbulent/non-turbulent interface at the outer boundary of a self-similar turbulent jet. *Exp. Fluids* **33**, 873–878.

Wetzel, R. G. 2001 *Limnology: Lake and River Ecosystems*, 3rd edn. Academic Press.

Worster, M. G. 2001 *Perspectives in Fluid Dynamics: A Collective Introduction to Current Research*, chap. 8, pp. 393–446. Cambridge University Press.

Wüest, A. & Lorke, A. 2003 Small-scale hydrodynamics in lakes. *Annu. Rev. Fluid Mech.* **35**, 373–412.

Yang, D. J. & Choi, C. K. 2002*a* The onset of thermal convection in a horizontal fluid layer heated from below with time-dependent heat flux. *Phys. Fluids* **14**, 930–937.

Yang, D. J. & Choi, C. K. 2002*b* Onset of thermal convection in a horizontal fluid layer heated from below with time-dependent heat flux, the. *Phys. Fluids* **14**, 930–937.

Zocchi, G., Moses, E. & Libchaber, A. 1990 Coherent structures in turbulent convection, an experimental study. *Physica A: Statistical and Theoretical Physics* (3).

Appendices

Appendix A

Conference papers

A.1 Numerical simulations and linear stability analysis of transient buoyancy-induced flow in a two-dimensional enclosure

This paper is published as a research paper, authored by Christian Ihle, Yarko Niño and Ramón Frederick, in the Proceedings of the Sixth International Symposium on Environmental Hydraulics, Hong Kong, China (2004).

Environmental Hydraulics and Sustainable Water Management – Lee & Lam (eds)

Numerical simulations and linear stability analysis of transient buoyancy-induced flow in a two-dimensional enclosure

C.F. Ihle
Graduate student, Ph.D. Program in Fluid Dynamics, Universidad de Chile, Santiago, Chile

Y. Niño
Departamento de Ingeniería Civil, Universidad de Chile, Santiago, Chile

R.L. Frederick
Departamento de Ingeniería Mecánica, Universidad de Chile, Santiago, Chile

ABSTRACT: Numerical experiments using two-dimensional DNS and a linear stability analysis with an unsteady base state, using propagation theory, were performed to learn about the onset and non-linear dynamics of penetrative convection in lakes and reservoirs. For this purpose, in a first stage of development, some idealized conditions have been considered, namely a step change and constant cool skin temperature imposed onto the surface. Two different horizontal boundary conditions were considered in the stability analysis, seeking for an approximate description of a stratified reservoir. Critical time-dependent Rayleigh numbers were found from the stability analysis, which agree with experimental results for the related Rayleigh-Bénard instability. Non-linear analysis showed the occurrence of periodically self-organized structures of buoyant plumes and iso-Nusselt lines. It was found numerically that boundaries appear to delay the onset of instabilities and to reduce the heat extraction rate.

1 INTRODUCTION

Many numerical and experimental studies in fluid systems subjected to surface cooling or bottom heating have been motivated by problems in several branches of physics, engineering and, particularly, in environmental sciences. Buoyancy driven flows, generated by this kind of phenomenon, are found in many aquatic systems in nature, such as lakes and reservoirs. This kind of instability contributes to strong momentum, heat and concentration transport and complex biological interactions inside the water body.

A particular kind of unstable stratification is found in lakes and reservoirs when the temperature of the surface water drops, due to heat exchange with the atmosphere, below the mean temperature of the water body. This, so called cool skin temperature, may occur on a daily basis in some cases, due to abrupt changes of air temperatures between day and night. The instability generated due to density differences between surface and deep waters drives the water mass to a buoyancy-induced circulation, which eventually evolves to different turbulent patterns, organized according to the depth level, as reviewed by Wüest & Lorke (2003).

The present article summarizes recent research work developed in two aspects relative to this kind of phenomenon: the onset of instability, which can be predicted using linear stability analysis, and a preliminary study of non-linear behaviour solving a DNS two-dimensional model for prescribed conditions.

2 EQUATIONS AND GENERAL CONDITIONS

2.1 *General equations*

Using tensor notation, the governing equations for the *i*th component of flow momentum and temperature field for an incompressible Boussinesq fluid are:

$$\frac{\partial u_i^*}{\partial x_i^*} = 0 \tag{1}$$

$$\frac{\partial u_i^*}{\partial t^*} + u_j^* \frac{\partial u_i^*}{\partial x_j^*} = -\frac{1}{\rho_0}\frac{\partial \tilde{p}}{\partial x_i^*} + \delta_{i3}\beta(T^* - T_0) + \nu \frac{\partial^2 u_i^*}{\partial x_j^* \partial x_j^*} \tag{2}$$

$$\frac{\partial T^*}{\partial t^*} + u_j^* \frac{\partial T^*}{\partial x_j^*} = \alpha \frac{\partial^2 T^*}{\partial x_j^* \partial x_j^*} \tag{3}$$

For convenience, the z axis ($i = 3$) is considered positive downwards. In eq. (2): $\tilde{p} = p^* - \rho_0 g x_3^*$. In eq. (3) the viscous dissipation term is neglected, which would act as a source term in this equation. On the other hand, $\alpha = k\rho_0^{-1}C^{-1}$ denotes thermal diffusivity and δ_{pq} is the Kronecker-delta function. Density changes are modelled as a linear function of temperature: $\rho = \rho_0(1 - \beta(T_c - T_0))$, with $\beta = -(1/\rho_0)\partial\rho/\partial T^*|_0$ denoting the coefficient of thermal expansion.

In the case of lakes, the water body exchanges heat with the atmosphere, inflows, outflows and bed sediments. Reasonable assumptions are to consider that no heat is exchanged between the water body and the bed and that no inflows or outflows are present. However, a way must be considered to model the interaction between the lake and the atmosphere. We could use, for instance, the equilibrium temperature concept, such that the heat flux exchange from the atmosphere to the lake can be estimated as: $H_n = c_e(T_e - T_s)$, where T_e denotes the equilibrium temperature for given meteorological conditions over the lake, T_s denotes the water body surface temperature and c_e a heat exchange coefficient, also depending on meteorological conditions. H_n is continuously modified by weather conditions, via c_e and T_e, which also modifies T_s as it tends to follow T_e. Both H_n and T_s are continuously changing, so constant flux and constant surface temperature hypotheses are not exact but widely used, as reviewed by Maxworthy (1997). In this problem we propose the second case as an approximation for this condition, that is, a step change in surface temperature, which is kept for $t > 0$ at a value equal to T_c. The stability of a similar problem with these initial and boundary conditions have been treated recently (Kim et al., 2002). We aim to implement in the near future a more realistic time varying boundary condition scheme, along with consideration of an initial density stratification, having learned previously from the dynamics offered by the approximated model reported herein.

2.2 *Equations and conditions for linear stability analysis*

Equations (1) to (3) are the starting point for the linear stability system. The enclosure to be considered is the deep pool system, defined by Foster (1969) as a fluid body where no total penetration of the thermal disturbance is observed throughout its depth. Keeping the temperature step hypothesis at the upper surface, we impose the rigid-rigid and free-free boundary conditions, alternatively. The latter reflects the situation of the surface layer in a thermally strongly stratified water body having an idealized thermocline, (whose structure is discussed in the review by Imberger & Patterson, 1990) subjected to a sudden surface cooling. In deep pool systems, the free-rigid case yields the same result as the free-free case, as every perturbation variable vanishes provided x_3^* is large enough. Non-dimensional stability equations for temperature and vertical velocity, deduced from (1) to (3) are:

$$\left(\frac{1}{\mathrm{Pr}}\frac{\partial}{\partial\tau} - \Delta\right)\Delta u_3' = \Delta_1\theta' \tag{4}$$

$$\frac{\partial \theta'}{\partial \tau} + \mathrm{Ra}\, u_3{}' \frac{\partial \Theta'}{\partial x_3} = \Delta \theta', \tag{5}$$

where Δ denotes the three dimensional Laplacian and Δ_1 the horizontal one. $x_3 = x_3^*/L$, $\tau = t^*\alpha/L^2$, $T = (T^* - T_0)/(T_c - T_0) = \Theta' + \theta'$ and $u_3 = u_3^* L/\alpha = U + u_3' = u_3'$, as the fluid is quiescent on its base state. $\mathrm{O}(\theta') = \mathrm{O}(u_3') = \varepsilon$. $\mathrm{Pr} = \nu/\alpha$ is the Prandtl number and $\mathrm{Ra} = g\beta(T_0 - T_c)L^3/(\alpha\nu)$ is the Rayleigh number, based on the length scale L. The unsteady base state $\Theta'(x_3, \tau)$ corresponds to the solution of the well known heat equation subjected to the boundary and initial conditions considered herein. Horizontal modes of the form $\exp(\mathrm{i}(a_1^* x_1 + a_2^* x_2))$ are supposed.

Due to the time dependency of Θ', it is not possible to assume a priori an exponential growth for the amplitude functions, as in the case of systems with a steady base state. This case was treated by Hadji & Jin (1996), and more recently by Kato et al. (2003). According to the propagation theory developed by Kang & Choi (1997) and Yang & Choi (2002), using dimensional reasoning and assuming an early onset (small τ), the dimensionless amplitude functions may have the form: $\left[u_3'(\tau, x_3), \theta'(\tau, x_3)\right] = [\tau u_3(\zeta), \theta(\zeta)]$, with $\zeta = x_3/\sqrt{\tau}$. Propagation theory can be applied if it is possible to find a self-similar solution for the base temperature state. If that is the case, from Eqs. (4) and (5) explicit space and time dependence can be transformed into ζ-only dependence, defining an implicit time-dependent wave number $a_\tau = \tau^{1/2}\sqrt{(a_1^*)^2 + (a_2^*)^2}$ and an implicit time-dependent Rayleigh number $\mathrm{Ra}_\tau = \tau^{3/2}\,\mathrm{Ra}$. Now, the onset of the instability is ruled by the conjunction of the following three parameters: the Prandtl number, which depends solely on the fluid properties, Ra_τ and τ, that depend on the system being studied.

The critical Ra_τ number can be found by using a shooting method to solve (4) and (5) for Ra_τ and the unknown boundary conditions at $\zeta = 0$. For the rigid-rigid case, it was considered that on $\zeta = 0$, $u_3 = Du_3 = \theta = 0$, with $D^n(\cdot) \equiv d^n(\cdot)/d\zeta^n$, and on $\zeta \to \infty$, $u_3 = Du_3 = D\theta = 0$. For the free-free case, equivalent conditions are on $\zeta = 0$, $u_3 = D^2u_3 = \theta = 0$ and on $\zeta \to \infty$, $u_3 = D^2u_3 = D\theta = 0$.

2.3 *Conditions for non-linear analysis*

The results reported here correspond to a two-dimensional flow situation in a rectangular domain with height 1 and width $A = 2$. The region contains water, with $\mathrm{Pr} = 7$. Both side-walls and bottom are considered adiabatic, so heat transfer is allowed only through the air-water interface. Fluid properties (except density as stated) are assumed to be constant. Density inversion below 4°C is not considered.

Initial and boundary conditions are: $T = 0$ in $x_3 = 0$, always, $T(\tau = 0) = 1$ everywhere, $\partial T/\partial x_1(x_1 = 0, x_1 = 2) = 0$, always, and $\partial T/\partial x_3(x_3 = 1) = 0$, always. No-slip is imposed on every boundary.

The time-dependent solution field was found numerically using the finite volume method. To solve the pressure gradient field, the simpler scheme was chosen in an orthogonal staggered grid of 182×92 nodes. Temperature field was computed using the power law scheme (Patankar, 1980). Tolerances for dimensionless values of pressure, pressure correction, temperature and continuity equation residue were set to 10^{-9}. The dimensionless time step used was 10^{-6}. Rayleigh number chosen was 10^6, because of the good balance found between the time for instability onset and computational cost.

A relevant feature of the two-dimensional problem is that it delivers information, from the numerical simulation point of view, of the onset of the instability, provided its origin lies on the x_3 axis.

3 RESULTS AND DISCUSSION

For the deep pool systems studied, a suitable self-similar solution for the base temperature field is $\Theta = \mathrm{erf}(\zeta/2)$, where $\mathrm{erf}(\cdot)$ stands for the error function. For the deep pool Rayleigh-Bénard problem, with an initially uniform temperature in the whole water body, rigid-rigid boundaries, $\mathrm{Pr} = 7$ and $\mathrm{Ra} = 10^6$, Kim et al. (2002) found a critical Rayleigh number $\mathrm{Ra}_\tau = 27.07 \pm 1.35$,

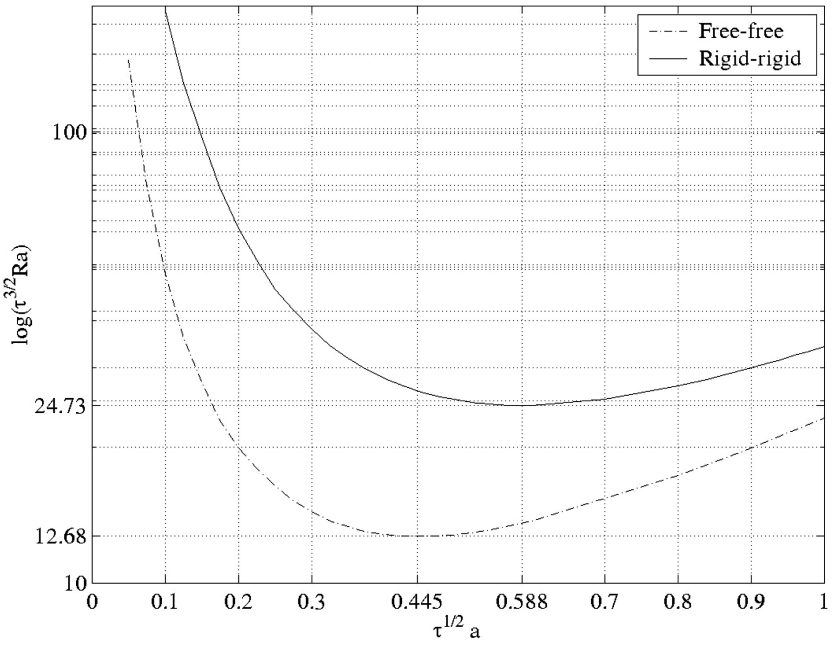

Figure 1. Marginal stability curves for the deep pool system with small onset critical time, τ_c. The rigid-rigid case exhibits a critical value of $\mathrm{Ra}_\tau = 24.73$. In the free-free case the critical value found was 12.68.

slightly higher than the critical value found for the rigid-rigid case in the present study (Figure 1). These results do not consider the existence of vertical side-walls.

For the Rayleigh-Bénard problem, Foster (1969) reported that the time for incipient growth of instabilities, obtained from the linear stability analysis, differs from the experimental observation time (τ_m) by a factor close to 4. In the present numerical simulation, for $\mathrm{Ra} = 10^6$, the onset time found (using both the present numerical model along with a 10 aspect ratio prototype program) was $\tau_m \approx 0.01$. This result comes from the observation of a computed dimensionless velocity field on the order of 10^{-2}. On the other hand, using the results from the stability curve (Figure 1), a critical time τ_c can be found by using the critical Rayleigh number: $\tau_c = \mathrm{Ra}_\tau / \mathrm{Ra}^{2/3} = 0.002473$. With this value, the time for the observed growth of instabilities in the numerical simulations differs from the critical time calculated from the linear stability analysis by a factor $\tau_m/\tau_c = 4.04$, in close agreement with Foster's factor of 4. Further analyses must be done, using other Rayleigh numbers and experimental evidence, to generalize this result for the present problem.

Non-linear evolution after the onset of the fastest growing modes exhibits a spatially-periodic behavior, as vertical plumes tend to organize in nearly fixed places. The downwelling of these thermal plumes generate circulation rolls, and patterns of horizontal motion, where the most active places of heat exchange with the atmosphere lie in between the thermal plumes. This can be observed on Figure 2, which shows the temperature field and the Nusselt number on the upper lid, defined as $Nu_0 = -\partial T/\partial x_3|_{x_3=0}$. Although the mean temperature in the cavity tends to decay throughout the simulation because of the heat extraction with no balancing source terms, the dynamics of the phenomenon keeps its shape and also the mean distance and positions of the convecting rolls, whose motion tends to decay asymptotically. The corresponding organization pattern is shown on Figure 3. Another interesting feature of the phenomenon is the less active (but not null) heat release close to the boundaries, showing the relative importance of the velocity field on the overall cooling process, whose magnitude near the walls is about 40% lower than near the center. It would be interesting to know the relationship between heat extraction efficiency of the system and aspect ratio. This will be addressed in a future stage of the present research project.

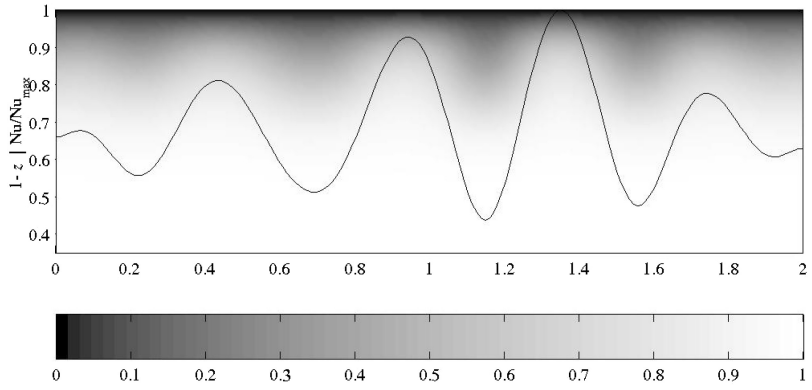

Figure 2. Temperature field for the non-linear model, $\tau = 0.0172$. The black line corresponds to the Nusselt number onto the upper lid, normalized by its maximum. The latter shows that most of the heat exchange with the atmosphere occurs in between the thermal plumes.

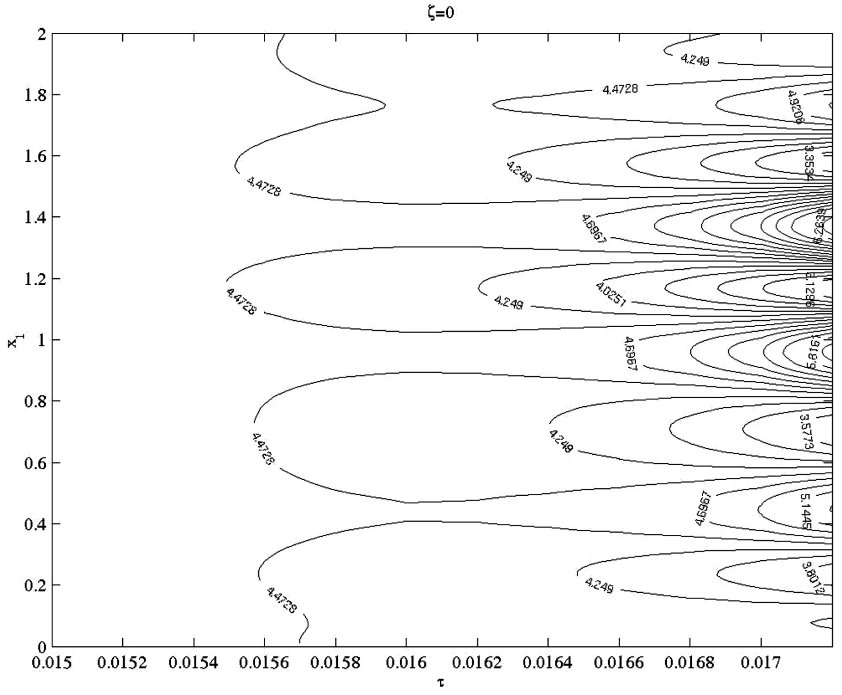

Figure 3. Iso-Nusselt number curves onto the upper lid for the two-dimensional non-linear simulation. Both thermal plumes and the highest heat extraction zones tend to maintain their original positions, given by the kinematic, thermal and geometric conditions imposed.

4 CONCLUDING REMARKS

A relatively novel linear stability technique for non-steady base states was applied to predict the onset of the penetrative convection problem with constant surface temperature. Theoretically predicted onset time is about 4 times lower than the time at which the instability is detected in the numerical non-linear simulations. Similar results have been reported for the Rayleigh-Bénard

problem using experimental observations instead of numerical simulations. The deep pool rigid-rigid 2-D system appears to be slightly less stable than the classical Rayleigh-Bénard problem with transient base state, as concluded from comparison with results by Kim et al. (2002). Non-linear dynamics of the penetrative convection flow is characterized by a spatially periodic self-organization of the system on alternating zones with high and low surface heat transfer rates, along with persistent buoyant plumes that create circulation as they fall through the water column. Numerical simulations also show the importance of the vertical boundaries on the heat extraction efficiency, at least for the studied aspect ratio of 2.

ACKNOWLEDGEMENTS

The authors thank financial support by CONICYT, Chile, through a graduate scholarship for the main author and FONDECYT Project No. 1040494.

REFERENCES

Foster, T. D. 1969. Onset of manifest convection in a layer of fluid with a time-dependent surface temperature. *Phys. Fluids*, 12: 2482–2487, 1969.

Hadji, L. & Jin, X. 1996. Penetrative convection induced by the freezing of seawater. *Int. J. Heat Mass Transfer*, 38(18): 3823–3834.

Imberger, J. & Patterson, J. C. 1990. Physical limnology. *Adv. in Applied Mechanics*, 27: 303–475.

Kang, K. H. & Choi, C. K. 1997. A theoretical analysis of the onset of surface-tension-driven convection in a horizontal liquid layer cooled suddenly from above. *Phys. Fluids*, 9: 7–15.

Kato, R., Hashiba, M. & Fujimura, K. 2003. The onset of penetrative double-diffusive convection. *Fluid Dyn. Res.*, 32: 295–316.

Kim, M. C., Park, H. K. & Choi, C. K. 2002. Stability of an initially stably stratified fluid subjected to a step change in temperature. *Theoret. Comput. Fluid Dynamics*, 16: 49–57.

Maxworthy, T. 1997. Convection into domains with open boundaries. *Annu. Rev. Fluid Mech.*, 29: 327–371, 1997.

Patankar, S. V. 1980. Numerical Heat Transfer and Fluid Flow. Mc Graw Hill, 1980.

Wüest, A. & Lorke, A. 2003. Small-Scale hydrodynamics in lakes. *Annu. Rev. Fluid Mech.*, 35: 373–412.

Yang, D. J. & Choi, C. K. 2002. The onset of thermal convection in a horizontal fluid layer heated from below with time-dependent heat flux. *Phys. Fluids*, 14(3): 930–937.

A.2 Onset of modulated penetrative convection: a theoretical and experimental analysis

This paper is published as a research paper, authored by Christian Ihle and Yarko Niño, in the Proceedings of the Sixth International Conference on Stratified Flows, Perth, Australia (2006).

Onset of modulated penetrative convection: a theoretical and experimental analysis

Christian F. Ihle and Yarko Niño

Program in Fluid Dynamics and Department of Civil Engineering
Universidad de Chile
cihle@ing.uchile.cl

Abstract

A simple model to study the onset of modulated penetrative convection induced by surface cooling of lakes and large reservoirs is proposed. It is based on linear analysis of the Boussinesq Navier-Stokes and energy equations, and considers the effect of time-dependent surface temperature forcing, initial thermal stratification, and variable eddy viscosity and thermal diffusivity along the depth. A set of dimensionless parameters that govern the onset of convection is defined. It is found that the ratio between the thickness of the mixed layer and a length scale built upon a reference eddy diffusivity value and the forcing period, are much more important than the strength of the initial stratification. These results are consistent with laboratory experiments.

1. Introduction

Convection plays an important role on vertical mixing in lakes and reservoirs, contributing to the effect of wind-induced surface stress, inflows and outflows. It occurs in certain water bodies, either when the ambient temperature dips below the water surface temperature or due to evaporative cooling. The intensity and temporal variation of the latter turbulence sources depend on local climate phenomena. In particular, daily temperature oscillations appear to both induce and suppress turbulence in the epilimnion, as shown by field studies in lakes (see, for instance, Jonas et al., 2003). The present paper focuses on the development of a simple model for the prediction of the onset time of daily convection induced by surface cooling in a temperature (and hence density) stratified Boussinesq water layer, given a sinusoidal temperature forcing function in one of the horizontal boundaries.

Since the early 1960s, several one-dimensional models have been developed in order to predict the thermal structure of the ocean due to the effects of solar heating and surface cooling in a seasonal basis (see Turner, 1973, and references therein). In those cases, the daily fluctuations of mean surface temperature and radiation were not considered. The first important contribution to the study of the daily response of the ocean to the daily effect of radiation and convection is due to Foster (1971), who developed a model based on the Fourier expansion of the Navier-Stokes equations under the Boussinesq approximation, considering the effect of radiation (along with the effect of the water turbidity) in a full-forcing period. Two strong assumptions were considered in his model: The first is the use of an infinite turbulent Prandtl number, that is, that the eddy coefficient of viscosity is much larger than the eddy coefficient of thermal diffusivity. Although this statement prevented his analysis from yielding quantitative results, it is claimed that the essential features of the phenomenon were preserved. The second assumption is that the surface cooling is constant, thus allowing for a daily energy balance to be considered in the analysis. Actually, as the surface temperature depends on ambient temperature, which is also a periodic function of time, a better approximation to the real effect of surface cooling would be to set it as a periodic function of time.

In the present work, a simplified model, based on the linearised Navier-Stokes and energy

equations in a Boussinesq fluid layer, is proposed to predict the onset of thermal convection. Alongside, experiments consisting of the measurement of onset times in a sinusoidally thermally forced water tank were conducted to validate and adjust the model.

2. Problem description and methodology

2.1. Analytical model

Consider an initially stratified, zero-mean-flow, horizontally infinite isothermal Boussinesq well-mixed fluid layer of height d on top of a large reservoir (see Figure 1). The initial stratification and depth-dependent eddy viscosity and thermal diffusivity are essential features in the present model of this system. The initial stratification represents the diurnal thermocline, whereas the diffusion is allowed to evolve from molecular (in the hypolimnion) to turbulent (in the epilimnion). Among other effects, the present model excludes the onset of turbulent patches.

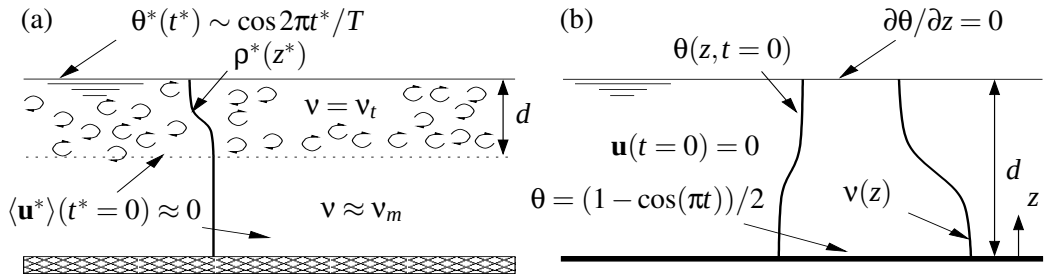

Figure 1: Schematic representation of the model. (a) Real situation to be modelled: a well-mixed layer on top of a density interface. Surface temperature dips beneath the water body temperature in a sinusoidal fashion. Initially a null mean velocity field is assumed. (b) Assumed model and experiment configuration: a bottom plate is heated sinusoidally in an initially quiescent reservoir. In the case of the experiment, the whole layer has a molecular viscosity, but not in the analytical model, where functions of the initial temperature field and viscosity are considered.

The forcing temperature, $\theta_0^*(z^* = 0, t^*) = \theta_{\max}^* + (\theta_{\min}^* - \theta_{\max}^*)\cos(\pi t^*/T)$, acts at the bottom of the layer. The forcing period, T, is on the order of 24 h for the case of climate forcing. As the aim of the present work is the study of the onset of convection due to surface cooling, assumed in the absence of radiation, on a daily basis, $t^* \in [0, T/2]$. The problem of convection suppression due to positive heat conduction and radiation, although interesting, is beyond of the scope of the present paper. The semi-period $T/2$ will be assumed as a characteristic time scale for the present problem. Length, velocity and temperature scales are d, $2d/T$ and $\theta_{\max}^* - \theta_{\min}^*$, respectively. Scales for kinematic viscosity and thermal diffusivity are $\hat{\nu}$ and $\hat{\kappa}$, respectively.

The dimensionless parameters of interest for a Boussinesq, Reynolds Averaged Navier Stokes (RANS) description of the flow are:

$$P_\kappa = \frac{2d^2}{\hat{\kappa}T}; \qquad P_\nu = \frac{2d^2}{\hat{\nu}T}; \qquad G = \frac{\alpha g(\theta_{\max}^* - \theta_{\min}^*)Td}{2\hat{\nu}}, \tag{1}$$

where α is the coefficient of thermal expansion of the fluid and g the magnitude of the gravity acceleration vector. Considering the vertical component of the expression resulting from taking twice the curl of the linearised, three dimensional momentum equation in cartesian coordinates, provided depth-dependent eddy viscosity and diffusivity, leads to a differential equation for the vertical disturbance velocity and temperature. Decomposing the resulting equations into

horizontal Fourier modes of wavenumbers a_x and a_y, and assuming an exponential growth rate of disturbances, an eigenvalue problem for G, given $a^2 = a_x^2 + a_y^2$ and t is set:

$$\left[\left(P_\nu s + \frac{\mathrm{d}^2\nu}{\mathrm{d}z^2} - \nu(\mathrm{D}^2 - a^2) - 2\frac{\mathrm{d}\nu}{\mathrm{d}z}\mathrm{D}\right)(\mathrm{D}^2 - a^2) - 2\frac{\mathrm{d}^2\nu}{\mathrm{d}z^2}\mathrm{D}^2\right] w = -a^2 G\theta \tag{2a}$$

$$\left[P_\kappa s - \kappa(\mathrm{D}^2 - a^2) - \frac{\mathrm{d}\kappa}{\mathrm{d}z}\mathrm{D}\right]\theta = -P_\kappa w\frac{\partial\bar{\theta}(z,t)}{\partial z}, \tag{2b}$$

where $\mathrm{D}(\cdot) \equiv \mathrm{d}(\cdot)/\mathrm{d}z$ and the integration domain is $[0,1]$ (i.e., it is required for the instability to develop in the layer of thickness d and to have completely decayed outside of it, as depicted in Figure 1). In the present set of calculations it is assumed that the lower boundary is a rigid heated surface whereas the upper is shear-free, resulting in the kinematic boundary conditions: $w(z=0) = \mathrm{D}w(z=0) = w(z=1) = \mathrm{D}^2 w(z=1) = 0$. The base state corresponds to the solution of a dimensionless diffusion equation

$$\frac{\partial\bar{\theta}}{\partial t} = \frac{1}{P_\kappa}\frac{\partial}{\partial z}\left(\kappa\frac{\partial\bar{\theta}}{\partial z}\right), \tag{3}$$

with time-dependent forcing, $\theta(z=0,t) = (1-\cos\pi t)/2$, and variable thermal diffusivity $\kappa(z)$. The following initial dimensionless condition is assumed:

$$\bar{\theta}(z,t=0) = \frac{\lambda_0}{2}\left\{1 + \tanh\left[\gamma(z-\lambda)\right]\right\}, \tag{4}$$

where $\lambda_0 = \Delta\theta_0^*/(\theta_{\max}^* - \theta_{\min}^*)$ stands for the maximum dimensionless initial temperature difference attainable in the fluid layer at the beginning of the cycle. A typical value for the latter is $\lambda_0 \approx 0.05$; this value was used throughout the present calculations. On the other hand, λ is set to $1/2$, implying a symmetry condition for the initial temperature, namely one with respect to the point $(\lambda_0/2, 1/2)$. The coefficient γ is a measure of the strength of the initial temperature stratification and is large enough to set the initial temperature gradient virtually zero at $z = 0$ and 1. This is consistent with the assumption that disturbances should decay in the limit with the outer region, at $z = 1$. In Figure 2a, a set of curves generated with some values of γ for a fixed value of λ and P_κ are depicted. The viscosity function is consistent with (4) in the sense that higher density gradients should have corresponding lower eddy viscosities. The matching was made in a linear fashion. In particular, it is assumed that

$$\kappa(z) = \nu(z) = 1 - \frac{\bar{\theta}(z,t=0)}{\lambda_0}(1-r), \tag{5}$$

where r is the ratio between molecular and eddy viscosities, set here to 10^{-2}, representative of the type of fluid layers considered in the model. Further, it has been assumed that both molecular and turbulent thermal diffusivity are equal to the corresponding molecular and turbulent viscosity, effectively stating that both the turbulent Prandtl number, $\sigma = \hat{\nu}/\hat{\kappa}$, and the Prandtl number, remain on the order of unity. The eigenvalue problem (2) is solved for a set of wavenumbers. For each value of time, the critical wavenumber is that which minimises the eigenvalue G. The computation of (3) was done using a finite difference scheme. A description and the validation of the numerical technique used to solve the eigenvalue problem is presented elsewhere (Ihle and Niño, 2006).

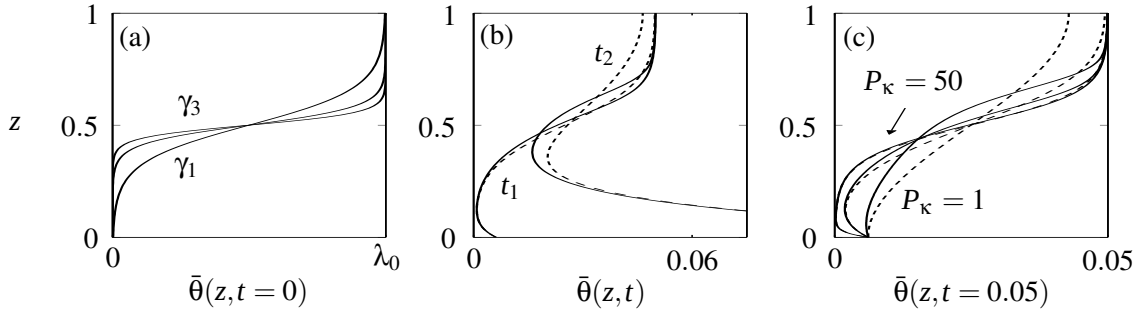

Figure 2: (a) Initial temperature stratification used to solve (3). Three different values for γ are depicted, namely, 6, corresponding to γ_1, 12 and 18, the latter corresponding to γ_3 in the figure. (b) Base state solutions for two values of dimensionless time, namely $t_1 = 0.05$ and $t_2 = 0.3$, considering variable thermal diffusivity, corresponding to (5) (solid lines) and the solution using the constant, thermal diffusivity scale, $\kappa_0 = \kappa/\hat{\kappa} = 1$, corresponding to dashed lines, with $\lambda_0 = 0.05$. In both cases, $\gamma = 7$ and $P_\kappa = 10$. (c) Base state solutions considering variable (solid lines) and constant (dashed lines) thermal diffusivities, for $t = 0.05$ and three different values of P_κ: 1 (right), 5 (centre) and 50 (left), with λ_0=0.05 and $\gamma = 7$.

2.2. Experimental setup

A heated $40 \times 15 \times 20$ cm perspex tank filled with water, initially at 19.5 °C, was used to account for a preliminary experimental verification of the onset time for convection predicted by the model. The heater was a brass plate connected to a Haake C heat bath. The latter has a built-in controller that allows the setting of the brass plate temperature at a time scale much faster to that of the experiment. Temperature of the plate was modified sinusoidally, fixing a semi-period of 55 min and an overall temperature difference of 6.8 °C. The tank bottom temperature was measured using a K-type thermocouple. The flow was seeded with 90–110 μm Pliolite particles (Figure 3a). Convective motion was exposed using a 4 mm thick light sheet generated with a 1 kW photographic lamp and captured using a Jai CVM4+CL digital video camera with a 50 mm f0.95 Vortex lens mounted, at a refresh rate of 4 frames per second. The criterion employed to decide on the onset time for convection was to detect a rapid increase of the root-mean-square of the computed velocity field using a PIV algorithm (Dalziel et al., 2000). For the present conditions, the rapid increase was found to occur close to 300 s after the start of the experiment, as seen in Figure 3b.

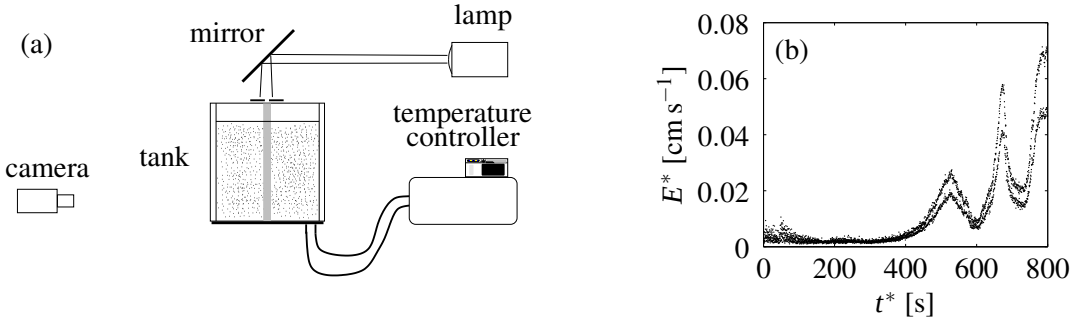

Figure 3: (a) Experimental setup scheme (side view). (b) RMS of the kinetic energy, computed as $E^* = \left(\langle u^{*2}\rangle + \langle v^{*2}\rangle\right)^{1/2}$, as a function of time. The apparently two groups of data are a consequence of the choice of the data sampling frequency, biased towards the detection of onset times for convection instead of an accurate reproduction of the non-linear dynamics of the flow.

3. Results and discussion

The length scale d considered in the present problem is representative of the mixed layer, also referred to as the diurnal thermocline. A dimensionless account for the ratio between the convective layer width and the overall reservoir depth is given by ${P_\kappa}^{-1/2}$. For instance, a typical value for the eddy thermal diffusivity of $10^{-4}\mathrm{m}^2\,\mathrm{s}^{-1}$ (Wüest and Lorke, 2003) and a semiperiod of 12 h leads to a mixed layer scale of 1 m, which is commensurate with field observations. For large reservoirs, normally ${P_\kappa}^{-1/2} < 1$, and in most of the cases for small and medium-sized reservoirs, ${P_\kappa}^{-1/2} > 1/10$.

The effect of variable viscosity in the heat transfer characteristics of the system can be seen in Figure 2b, where a comparison with the constant diffusivity case is presented. For t_1, which is approximately the time when convection starts, it is observed that for a low value of P_κ, heat transfer up to about half the layer height is more efficient than in the constant diffusivity case, as expected. However, a zone exists near the outer boundary where this trend is reversed. Interestingly, for medium to large values of P_κ, at times on the order of those corresponding to the onset of convection in water, the response of the variable thermal diffusivity system is very close to that with a constant one. For values of P_κ on the order of or larger than 50, this statement holds also for large values of γ, as is shown in Figure 4c. Onset times for a range of values of G, γ and P_κ are shown in Figure 4. Parameters for the experimental verification correspond approximately to $P_\kappa = 85.3$ and $G = 1.1 \times 10^7$. The corresponding dimensionless measured onset time is close to 0.09. For these parameters, solving the eigenvalue problem (2) with its corresponding boundary conditions yields an onset time close to 0.03, commensurate with the experimental one. From Figure 4, it is apparent that onset times for convection are much strongly dependent on the P_κ parameter than on the strength of initial stratification, given by γ. In other words, the thickness of the mixed layer and the forcing temperature amplitude strongly determines the time that marks the increase of eddy motion, in a much greater extent than the initial stratification. However, present results suggest that for low values of the P_κ parameter, corresponding to a high effective thermal diffusivity, stratification plays an important role, as shown in Figure 4a, where the tendency of the critical curves is inverted with respect to cases b and c: the higher γ is, the more stable the system becomes.

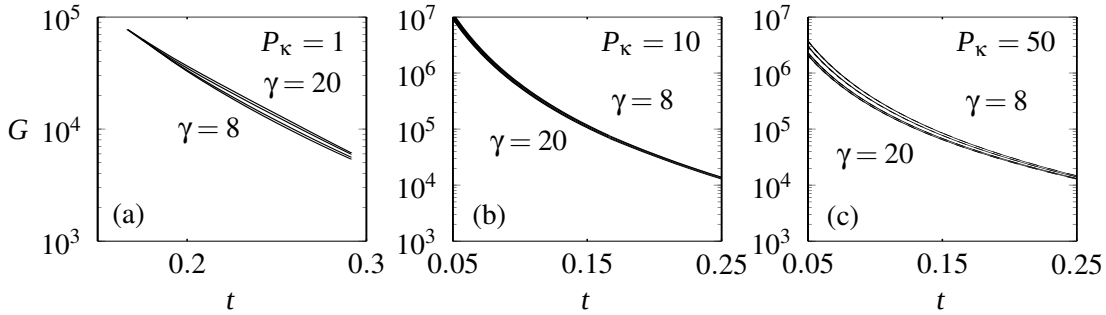

Figure 4: Critical values for G in terms of the dimensionless time t, for $\gamma = 8$, 10, 15 and 20, with $\lambda_0 = 0.05$. (a) $P_\kappa = 1$. (b) $P_\kappa = 10$. (c) $P_\kappa = 50$: solid lines represent results considering variable viscosity, and are practically overlapped with the ones corresponding to constant viscosity, rendered using dashed lines.

4. Conclusions

A simple model to study the onset of penetrative convection in lakes and reservoirs has been proposed and contrasted with experimental results. The effect of periodic heat flow, variable initial temperature field, eddy viscosity, and thermal diffusivity has been considered. A dimensionless number that relates the forcing period with the mixed layer depth and eddy viscosity, appears to strongly influence onset times, in comparison with initial stratification strengths. Experimental evidence gathered so far is consistent with predicted values of onset times.

Acknowledgements

The authors would like to thank Dr. Stuart Dalziel, University of Cambridge, for useful comments regarding the present work along with the grant of experimental and computational facilities from GK Batchelor Laboratory. The first author acknowledges support from the Chilean National Commission for Scientific and Technological Research, Conicyt, and the Chilean Ministry of Education, through the MECE Program for Higher Education. The second author acknowledges support from the Department of Civil Engineering of the University of Chile and Fondecyt Project No. 1040494.

References

Dalziel, S. B., Hughes, G. O., and Sutherland, B. R. (2000). Whole field measurement by 'synthetic schlieren'. *Exp. Fluids*, 28:322–335.

Foster, T. D. (1971). A convective model for the diurnal cycle in the upper ocean. *J. Geophys. Res.*, 76(2):666–675.

Ihle, C. F. and Niño, Y. (2006). The onset of nonpenetrative convection on a suddenly cooled layer of fluid. *Int. J. Heat Mass Transfer*, 49:1442–1451.

Jonas, T., Stips, A., Eugster, W., and Wüest, A. (2003). Observations of a quasi shear-free lacustrine convective boundary layer: Stratification and its implications on turbulence. *J. Geophys. Res.*, 108:26/1–26/15.

Turner, J. (1973). *Buoyancy effects in fluids*. Cambridge University Press.

Wüest, A. and Lorke, A. (2003). Small-Scale hydrodynamics in lakes. *Annu. Rev. Fluid Mech.*, 35:373–412.